SEISMIC PERFORMANCE EVALUATION OF HYFRC BRIDGE PIER BY HYBRID SIMULATION

by

Needhi Kotoky

DEPARTMENT OF CIVIL ENGINEERING
INDIAN INSTITUTE OF TECHNOLOGY GUWAHATI
GUWAHATI-781039, INDIA

August 2017

SEISMIC PERFORMANCE EVALUATION OF HYFRC BRIDGE PIER BY HYBRID SIMULATION

A Thesis Submitted
in Partial Fulfilment of the Requirements
for the Degree of

DOCTOR OF PHILOSOPHY

by

Needhi Kotoky

DEPARTMENT OF CIVIL ENGINEERING
INDIAN INSTITUTE OF TECHNOLOGY GUWAHATI
GUWAHATI-781039, INDIA

August 2017

Dedicated to my loving Parents

DECLARATION

I hereby declare that work which is being presented in this thesis entitled "SEISMIC PERFORMANCE EVALUATION OF HYFRC BRIDGE PIER BY HYBRID SIMULATION", submitted in the fulfilment of the requirements for the award of the degree of DOCTOR OF PHILOSOPHY in CIVIL ENGINEERING, with specialization in STRUCTURAL ENGINEERING, is an authentic record of my own work carried out in the Department of Civil Engineering, Indian Institute of Technology Guwahati under the supervision of Dr. Anjan Dutta and Dr. Sajal K. Deb, Professor, Department of Civil Engineering, IIT Guwahati.

The matter embodied in this thesis work has not been submitted by me for the award of any other degree or diploma of this Institute or any other University/Institute.

Date: 14/8/17

Place: Guwahati

Needhi Kotoky
(Needhi Kotoky)

CERTIFICATE

This is to certify that the above statement made by the candidate is correct to the best of our knowledge.

Anjan Dutta

(Dr. Anjan Dutta)
Professor
Department of Civil Engineering
Indian Institute of Technology Guwahati,
Guwahati-781039

(Dr. Sajal K. Deb)
Professor
Department of Civil Engineering
Indian Institute of Technology Guwahati,
Guwahati-781039

ACKNOWLEDGEMENT

Though only my name appears on the cover of this dissertation, a number of people have contributed to its production. I owe my gratitude to all those people who have made this thesis possible and have helped me in years leading up to this.

I would like to express my deep sense of gratitude and indebtedness to my learned and enlightened supervisors Dr. Anjan Dutta and Dr. Sajal K. Deb, Professor, Department of Civil Engineering, Indian Institute of Technology, Guwahati for their instinctive and careful guidance and continued encouragement in the completion of this thesis work. Our discussions on thesis and curricular subjects helped me in professional training and confidence building.

I sincerely acknowledge the education and working environment provided to me by IIT Guwahati. I am highly indebted to the entire structural engineering faculty member of IIT Guwahati, as I owe to them whatever I have learned in my five years of stay here. Special thanks to Dr. Hemant B. Kaushik, Dr. Kaustubh Dasgupta and Dr. Arun Ch. Borsaikia for technical enrichment on various subjects. The financial support provided by the Department of Science and Technology, India and M/S D2S Infrastructure Pvt. Ltd., Guwahati, India are gratefully acknowledged. Reliance Industries Limited, India and Bekaert Mukand Wire Industries Pvt. Ltd., India are gratefully acknowledge for their generosity in providing free fibre samples. Technical support provided by Dr. Shawn You of MTS Systems, USA is deeply appreciated.

I am grateful to all my colleagues and batchmates who rendered me support throughout the period I worked on this dissertation and also for the most cherished time we spent together at IIT Guwahati. The continuous support offered by Biswajit and Nishant at the various stages of preparation of thesis is warmly appreciated. I am grateful to all other members of the civil department including seniors and staff members, especially Biswajit Debnath for their valuable suggestions and encouragement throughout the completion of this work. I thank my classical dance group and inter IIT table tennis team mates, who made my stay in campus happy and pleasant. I extend my deep appreciation to the entire IITG community, who helped me directly or indirectly in bringing this work to this present form.

My heartiest thank goes to my dearest husband, Shivang, a constant source of love and inspiration who not only encouraged me but also provided guidance and support throughout my thesis work. I am also very grateful to his patience and understanding during my extended stay at IIT Guwahati.

Last but not the least, my father Dilip Kr. Kotoky, mother Dr. Savita Kotoky and brother Abikshit along with my in-laws deserves special mention for their love, affection, care and inseparable support in all my endeavours. I especially thank my father who actually made me who I am today. His encouraging words are constant source of inspiration for me and taught me to look forward and dream for the best.

Finally, I would like to thank everybody who was important to the successful completion of my stay at IIT Guwahati. I will always cherish all the moments I spent in the beautiful campus of IIT Guwahati.

Needhi Kotoky

ABSTRACT

Bridges are important lifeline structures and vital links in land transportation network. The failures of bridges during a seismic event would prevent smooth relief and rehabilitation activity in the neighbourhood, as alternative routes may not be available in the vicinity. Deficiencies in the behaviour of bridges are observed during many earthquakes all over the world. In these failure of bridges, the reinforced concrete piers are mostly observed to be considerably damaged, which implies that clear understanding of non-linear behaviour of these structural elements during intense earthquakes is an important issue.

In order to reduce the extent of damage and avoid any brittle mode of failure, it is felt that improving ductility of bridge pier with appropriate high performance materials like hybrid fibre reinforced concrete (HyFRC) is necessary. Increase in ductility leads to redistribution of stress-resultants to less stressed elements and the piers sustain lower strength degradation. The primary objective of this research is identified as the experimental investigation on performance of HyFRC in bridge pier under the action of earthquake induced excitations. Use of advanced testing procedure is also mooted for more realistic assessment of evaluation of response.

Steel fibres of different sizes and polypropylene fibres are used in HyFRC. Best possible volume fraction of selected fibres for improving ductility of concrete specimens is evaluated. It is also observed from literature that the HyFRC has superior shear resistance as compared to that of conventional concrete. Shear capacity of standard prisms are evaluated with 50% reduction in shear reinforcement for HyFRC specimen. The test results proved that high confinement steel requirement in seismic resistant design procedure may be reduced by the use of HyFRC, without compromising displacement ductility. This would help in reduction of congestion due to reinforcement, particularly at the junction region and would thus reduce the possibility of formation of void and honeycomb in concrete.

An existing bridge is considered for the study. It is known that damage in a bridge pier is mostly localized at the pier-foundation interface region. Post-earthquake rehabilitation works of bridge piers become easier if the damage is distributed and shifts away from the pier-foundation interface zone. This is targeted to be achieved by incorporation of some additional features at pier-foundation interface. Three different detailing strategies are considered at pier-foundation interface region. While normal reinforcement details are followed for specimen type 1, additional reinforcing bars (dowels) are used in the pier-foundation interface region for specimen type 2 and corrugated sheet duct is provided below the interface region in specimen type 3. It is necessary to utilize an advanced level of experimental test in order to evaluate the seismic performance of the bridge with pier made of high performance material.

Experimental methodology plays a vital role in correct estimation of response. Testing of structures under seismic loading is one of the best approaches to evaluate response of structure during a seismic event. This type of testing can check the effectiveness of new and advanced materials in enhancing earthquake resistant characteristics. In the present research, the effect of introduction of HyFRC in bridge piers is investigated by hybrid simulation. Hybrid simulation technique is carried out by physically testing critical elements of a structure (such as bridge piers), while the remaining elements are concurrently simulated computationally. The hybrid testing is carried out by considering both the numerical and physical components and using a step-by-step numerical solution of the governing equations of motion (Schellenberg et al. 2009, Lavorato 2009, Pinto et el. 2004). The numerical model is developed in OpenSees platform and is capable of simulating non-linear behaviour in bridge pier under the action of seismic excitation. The experimental investigation using hybrid simulation is found to be an efficient technique for the evaluation of seismic performance of a complete structural system.

Cyclic tests are also performed after the completion of hybrid simulation to evaluate ultimate capacities. The specimens are subjected to cyclic displacements of gradually increasing amplitudes and thus having different values of drift ratio. Load carrying capacity of HyFRC piers at different drift ratios and its comparison to conventional concrete specimen is evaluated. HyFRC specimens are observed to consistently exhibit improved seismic performances in terms of improvement in parameters like delayed growth of strain, damage tolerance, energy dissipation capacity, stiffness at any drift ratio and improved load carrying capacity.

Past research works on seismic performance of HyFRC beam-column connections indicated that the improved displacement ductility with fibres is also accompanied by reduced strains in the reinforcement (Kheni et al. 2015). Thus, rupture of reinforcement along with overall structural damage and eventual collapse may be delayed due to such reduced strain growth. Longitudinal and transverse reinforcements of the specimens in this research work are instrumented with strain gauges for recording strain values during the experimental program. This data provide sufficient information related to the behaviour of scaled bridge pier under seismic excitation, made of two different materials as well as with different detailing at the pier-foundation interface. Strains in concrete are also measured by embedded strain gauges while deflection along the height of the pier is measured by linear variable differential transducers (LVDT). On the basis of strain measurement, it is established that the growth of strain and hence crack initiation is delayed in HyFRC specimens compared to that of conventional concrete specimens. Further, it is also observed that the presence of additional components like dowel bars, corrugated sheets in the vicinity of pier-foundation interface zone shift the damage zone away from the interface region. This may facilitate ease of rehabilitation, if required after any high intensity earthquake event.

Comparison of results obtained from the numerical model and experimental results indicate the requirement for calibration of the numerical model for improvement in the evaluated response. Numerical simulation using the uncalibrated model is observed to exhibit higher stiffness of the pier as compared to that obtained from the experimental observation. The numerical model is calibrated by using a nonlinear zero length translational spring in bridge pier at the pier-foundation interface. The parameters of the spring are systematically obtained from experimentally obtained hysteresis loops. This use of spring at the pier base is found to be quite effective in terms of attaining equivalent experimental observations.

It is important to determine the level of risk associated with the loss of serviceability, damage or collapse of bridge structure, even though built with advanced materials. The prediction of seismic performance of a bridge structure is very challenging because of randomness associated with seismic loading and the ability of the structure to resist this loading. Fragility curves are widely used to represent the damage that can be expected to the structure under future earthquakes. Damage states in this research work are identified for developing fragility curves of the considered bridge using the experimental results. Fragility curves of the bridge are developed using the identified damage states and the calibrated numerical model. Seismic vulnerabilities are compared for bridges with piers made of HyFRC and conventional concrete and the study clearly establishes that HyFRC piers are less vulnerable as compared to that of conventional concrete piers across all damage states.

✲ ✲ ✲

TABLE OF CONTENTS

Declaration .... **i**
Acknowledgement .... **iii**
Abstract .... **v**
List of Figures .... **xiii**
List of Tables .... **xvii**
List of Symbols .... **xix**

Chapter 1 Introduction **1**
1.1 Background 1
1.2 Overview 2
 1.2.1 Hybrid Fibre Reinforced Concrete 4
 1.2.2 Hybrid Simulation 5
 1.2.3 Bridge Fragility 7
1.3 Objectives of Present Study 8
1.4 Scope of Research 9
 1.4.1 Experimental study 9
 1.4.2 Numerical study 10
1.5 Organisation of Thesis 11

Chapter 2 Review of Literature **13**
2.1 General 13
2.2 Fibre reinforced concrete 13
 2.2.1 Hybrid fibre reinforced concrete 15
 2.2.2 Application of FRC and HyFRC in structural members 21
 2.2.3 Reduction of shear reinforcement 22
2.3 Additional features at pier-foundation interface 24
2.4 Experimental evaluation of seismic performance of structural components 25
 2.4.1 Hybrid simulation 27
 2.4.2 Experimental studies using hybrid simulation 31
2.5 Bridge fragility analysis 34
2.6 Concluding Remarks 38

Chapter 3 Assessment of Mechanical Properties of Constituent Materials **39**

3.1 General 39
3.2 Test program (Part I) -Evaluation of volume fractions of steel and polypropylene fibres in HyFRC 39
3.2.1 Evaluation of compressive strength 45
3.2.2 Evaluation of split cylinder strength 45
3.2.3 Four point bending test 46
3.2.3.1 Loading characteristic and test frame 48
3.2.3.2 Testing procedure 48
3.2.3.3 Results 50
3.3 Test program (Part II) –Evaluation of possible reduction in shear reinforcement in HyFRC specimens 54
3.3.1 Details of test specimen 54
3.3.2 Loading characteristic and test frame 57
3.3.3 Results 57
3.4 Concluding remarks 58

Chapter 4 Numerical Modelling of Bridge 59
4.1 General 59
4.2 Numerical Model of Bridge Structure 60
4.2.1 Modelling of Superstructure 61
4.2.2 Pier modelling 63
4.2.2.1 Material modelling 64
4.2.2.2 Modelling of mass 65
4.2.2.3 Modelling of damping 65
4.3 Results from Numerical Analysis 66
4.3.1 Modal analysis 66
4.3.2 Nonlinear static analysis 67
4.3.3 Nonlinear time history analysis 68
4.4 Concluding Remarks 72

Chapter 5 Testing of Bridge by Hybrid Simulation 75
5.1 General 75
5.2 Testing procedure by hybrid simulation 75
5.2.1 Hybrid simulation framework 76
5.2.2 Integration scheme 77

5.3 Details of test specimen 81
5.3.1 Description of material used in construction 84
5.3.2 Fabrication of specimen 84
5.3.3 Loading characteristic and test frame 87
5.3.4 Instrumentation 88
5.3.4.1 Procedure for fixing strain gauge 92
5.3.5 Selection of earthquake time history 93
5.3.6 Details for cyclic test 94
5.4 Simulation results 95
5.4.1 Observed distribution of damage 95
5.4.2 Force-displacement hysteresis 101
5.4.3 Cumulative energy dissipation 103
5.4.4 Stiffness degradation during cyclic test 104
5.4.5 Displacement ductility 105
5.4.6 Failure Surface of damaged specimen 107
5.4.7 Buckling length of ruptured reinforcement 108
5.4.8 Observation of strain distribution in reinforcement and concrete 109
5.5 Concluding remarks 113

Chapter 6 Calibration of Finite Element Model 115
6.1 General 115
6.2 Modelling Assumption 115
6.3 Comparison of Hybrid Simulation Results with Initial Numerical Model 117
6.4 Model Calibration Procedures and its Results 119
6.4.1 Energy dissipation of calibrated results 124
6.5 Concluding remarks 126

Chapter 7 Seismic Vulnerability Assessment of the Bridge 127
7.1 General 127
7.2 Methodology for Development of Analytical Fragility Curve 128
7.2.1 Fragility analysis using PSDM and regression 129
7.2.2 Fragility analysis using maximum likelihood estimates 131
7.3 Definition of Damage State using Experimental Results 132
7.4 Selection of Ground Motions 135

7.4.1 Normalization method 138
7.4.2 Scaling procedure 139
7.5 Seismic Fragility Curves 141
7.5.1 Comparisons of two fragility analysis methods 141
7.6 Comparisons of fragility curves obtained using calibrated and un-calibrated model for conventional concrete bridge 144
7.6.1 Comparisons of fragility curves for conventional concrete and HyFRC bridge... 146
7.7 Concluding remarks 147

Chapter 8 Conclusions and Recommendation for Future Research 149
8.1 Overview 149
8.2 Summary 149
8.3 Conclusions 152
8.4 Recommendation for future research 154
Appendix A Mix Design According to IS 10262-1982 155
A.1 Material Testing 155
A.2 IS Method of Mix Design 156
Appendix B Design of Beam for Shear Reinforcement Test Program 159
B.1 Load Carrying Capacity of Beam with Four 10 mm ø Longitudinal Reinforcement 159
Appendix C Tensile Test Results of Reinforcement Bar 163
C.1 Steel for Longitudinal Reinforcement 163
C.2 Steel for Transverse Reinforcement 164
Appendix D Response History of Strain Gauges in Longitudinal Reinforcement . 165
References 177
List of Publications 193

LIST OF FIGURES

Figure 1.1. Flexure damage of pier of Hanshin Expressway in 1995 (Picture courtesy: Priestley et al. 1995) 2
Figure 1.2. Key components of hybrid simulation 7
Figure 2.1. Typical fragility curve conditioned on PGA as intensity measure 34
Figure 2.2. Flowchart for development of hybrid fragility curves 37
Figure 3.1. (a) Steel fibre (Dramix) (b) Polypropelene fibre (Recron 3s)....40
Figure 3.2. Mixing procedure of different constituents in HyFRC 44
Figure 3.3. Vee-Bee Consistometer....44
Figure 3.4. Compressive stress-strain curve of concrete 45
Figure 3.5. Tensile stress- strain curve of concrete 46
Figure 3.6. Arrangement for testing of prism specimen....48
Figure 3.7. PCS Technique (Banthia and Trottier, 1995)....49
Figure 3.8. Final damaged state after testing of conventional concrete specimen 50
Figure 3.9. Final damaged state after testing of HyFRC specimen....50
Figure 3.10. Load vs Deformation plots of different prism specimens from four point bending test....53
Figure 3.11. Reinforcement detailing of the prism specimen....56
Figure 3.12. Reinforcement cage for (a) conventional concrete specimen (b) HyFRC specimen 56
Figure 3.13. Casting of prism specimen 56
Figure 3.14. Failure pattern of specimen after test (a) conventional concrete (b) HyFRC....57
Figure 3.15. Load vs deformation curve of reinforced prism specimens 57
Figure 4.1. Elevation of Prototype Bridge (All dimensions are in mm) 60
Figure 4.2. Three dimensional finite element model of the bridge 61
Figure 4.3. Representation of local and global coordinate system and degrees of freedom of the bridge 62
Figure 4.4. Fiber discretization of pier section....63
Figure 4.5. Stress-Strain curve for conventional concrete....64
Figure 4.6. Stress-Strain curve for HyFRC 65

Figure 4.7. Force-deformation curve of bridge pier 68
Figure 4.8. (a) Simulation of scaled El Centro (1940) acceleration time histories for four different intensity levels (b) Simulated response spectra of the four intensity levels 69
Figure 4.9. Force-displacement response from NLTHA 72
Figure 5.1. Flow chart for hybrid simulation procedure 80
Figure 5.2. Reinforcement details of scaled pier model (All dimensions are in mm) 82
Figure 5.3. Mixing of concrete in a mechanical drum type mixer 84
Figure 5.4. Galvanized steel tube used to separate HyFRC from conventional concrete in the footing 85
Figure 5.5. Photograph showing cast of test specimen 85
Figure 5.6. Construction phases (a) foundation and column reinforcement cage (b) close up of top of circular reinforcement cage (c) pouring of foundation concrete (d) vibration with stick vibrator (e) foundation after cast 86
Figure 5.7. Schematic representation of test set up 87
Figure 5.8. Photograph showing the overall view of the test set up 88
Figure 5.9. Expected strain profile along the height of the column 90
Figure 5.10. Location of strain gauges on the (a) longitudinal reinforcement (b) transverse reinforcement. 91
Figure 5.11. Photograph showing strain gauges fixed on rebars 92
Figure 5.12. (a) Location of concrete embedded strain gauge in the specimen (b) photograph showing a sample embedded strain gauge 92
Figure 5.13. Procedure of fixing strain gauge in the reinforcement bar (a) removing ribs of the bar by filing (b) smoothing of the surface by sand paper and cleaning by RMS1 (c) fixing of the strain gauge by Z70 and application of P140 protective coat (d) application of protective coating of Anabond 673 (e) fixing of ABM75 93
Figure 5.14. Cyclic load history 94
Figure 5.15. Damage states of the six test specimens 101
Figure 5.16. Load vs deformation hysteretic response of the six test specimens 103
Figure 5.17. Energy dissipation at different drift ratio in cyclic test 104
Figure 5.18. Stiffness degradation during cyclic test 105
Figure 5.19. Procedure of ductility calculation 106
Figure 5.20. Schematic diagram of damage zone in the pier 107

Figure 5.21. Sample photograph of buckled reinforcement 109
Figure 5.22. Strain profile of longitudinal reinforcement C1 at all levels of excitation ...110
Figure 5.23. Strain history of concrete at 3MCE intensity level 112
Figure 5.24. Strain profile of stirrup at (a) 0.5MCE intensity level and (b) 3MCE intensity level. 113
Figure 6.1. Comparison of the numerical results of conventional concrete bridge pier obtained from uncalibrated model with experimental results for different intensity levels 117
Figure 6.2. Comparison of the numerical results of HyFRC bridge pier obtained from uncalibrated model with experimental results for different intensity levels ..119
Figure 6.3. (a) Sample Hysteretic material model created using OpenSees platform (b) backbone curve developed from experimental force-displacement hysteretic response...122
Figure 6.4. Back-bone curve for all the tested specimens 122
Figure 6.5. Comparison of the numerical results of conventional concrete bridge pier obtained from calibrated model with experimental results for different intensity levels 123
Figure 6.6. Comparison of the numerical results of HyFRC bridge pier obtained from calibrated model with experimental results for different intensity levels 124
Figure 6.7. Comparison of the energy dissipation for all MCE levels for conventional concrete bridge pier 125
Figure 6.8. Comparison of the energy dissipation for all MCE levels for HyFRC bridge pier...126
Figure 7.1. Scaling procedures: (a) target spectra based on PGA (b) target spectra based on S_a(T1) (c) target spectra by minimizing misfit over range of periods 139
Figure 7.2. Comparison between IS 1893 (2002) design spectrum with mean spectrum of 22 selected ground motions 140
Figure 7.3. IDA curves along with limit state capacity for conventional concrete bridge pier...142
Figure 7.4. Comparison of fragility curves obtained using two methods for conventional concrete bridge pier...143
Figure 7.5. Comparison of fragility curves obtained from calibrated and un-calibrated model for conventional concrete bridge pier..145

Figure 7.6. Comparison of fragility curves of bridge piers made of conventional concrete and HyFRC developed using calibrated model 147

LIST OF TABLES

Table 2.1. Key issues and limitations of different methods for development of fragility curves for highway bridges 36
Table 3.1. Details of fibres and their properties 40
Table 3.2. Results of tests on cement 41
Table 3.3. Compressive strength of cement 41
Table 3.4. Result of sieve analysis of sand....42
Table 3.5. Result of sieve analysis of coarse aggregate 42
Table 3.6. Details of different fibre volume fraction....47
Table 3.7. Toughness evaluation of the prisms 54
Table 3.8. Summary of experimental results....58
Table 4.1 Sectional properties of the deck 62
Table 4.2. Modal properties of the bridge 67
Table 4.3. Evaluation of peak responses for all intensity levels....72
Table 5.1. Details of scaled bridge pier model....81
Table 5.2. Details of special features of the test specimens 83
Table 5.3. Displacement ductility of the specimens....106
Table 5.4. Surface failure evaluation....108
Table 7.1. Damage state definition based on hybrid simulations under different intensity levels of excitations 134
Table 7.2. Limit state capacity for each damage state in terms of Drift Ratio (Dr) 135
Table 7.3. Details of selected ground motions 137
Table 7.4. Comparison of PSDM regressed and maximum likelihood fragility method ..144
Table 7.5. Difference in median value and dispersion of the fragility obtained from un-calibrated and calibrated model....146
Table 7.6. Median and dispersion values of fragilities for all damage states for both conventional and HyFRC bridge pier....147

This page is intentionally left blank

LIST OF SYMBOLS

D	Seismic demand of the bridge component
C	Capacity of the bridge component
PGA	Peak ground acceleration
PCS	Post crack strength
f_c	Compressive strength
P_u	Peak load
E	Young's modulus of elasticity
$I_{Z,} I_Y$	Moment of inertia
e_c	Strain at peak compressive strength
e_{cu}	Strain at crushing strength
f_t	Maximum tensile strength
e_t	Ultimate tensile strain
$u(t)$	Current system state
$u(t+\Delta t)$	State at a later time $t+\Delta t$
Δt	Small time increment
M	Assembled mass matrix
C	Assembled viscous damping matrix
$a(t)$	Acceleration vector
$v(t)$	Velocity vector
$r(t)$	Structural restoring force vector
$f(t)$	External force vector applied to the system
u_n	Known displacement vector
v_n	Known velocity vector
a_n	Known acceleration vector
μ	Displacement ductility factor
l_p	Height of the cantilever column
f_{ye}	Yield stress of longitudinal reinforcement
d_{bl}	Diameter of longitudinal reinforcement

Δ_u	Total imposed displacement
Δ_y	Yield displacement
$\Phi[.]$	Standard normal cumulative distribution function
IM	Intensity measure
S_D	Median of log-normally distributed seismic demand
$\beta_{D/IM}$	Dispersion of log-normally distributed seismic demand
S_C	Median of log-normally distributed seismic capacity
β_C	Dispersion of log-normally distributed capacity
a	Regression coefficient
b	Regression coefficient
λ	Median value of the lognormally distributed fragility function
ζ	Dispersion value of the lognormally distributed fragility function
F_r	Fragility function
c_k	Median acceleration capacity
β_R	lognormal standard deviation of the randomness
L	Likelihood function
PGV	Peak ground velocity
γ	Density
W	Weight
f_{ck}	Grade of concrete (Compressive strength)
f_{ck}'	Target mean strength
f_y	Grade of steel (Yield strength)
S	Standard deviation
b	Width of the section
D	Depth of the section
d	Effective depth of the section
x_u	Depth of neutral axis
$x_{u,max}$	Limiting depth of neutral axis
ϕ_s	Diameter of stirrups
ϕ_l	Diameter of longitudinal bars
A_{st}	Area of longitudinal reinforcement
M_{uR}	Ultimate moment of resistance

w	Factored uniformly distributed load
w_1	Factored point load
V_u	Factored shear force
V_{uc}	Shear force resisted by concrete
V_{us}	Shear resistance provided by vertical stirrups
τ_c	Design shear strength of the concrete
A_{sv}	Area of two-legged stirrups
s	Spacing of stirrups

This page is intentionally left blank

Chapter 1
INTRODUCTION

1.1 BACKGROUND

Structures built in seismic prone areas are subjected to the risk of damage from earthquake induced vibrations. Bridges are important lifeline structures and provide vital links in land transportation network. These class of structures are required to remain as functional after a design level earthquake. The failures of bridges during a seismic event would prevent smooth relief and rehabilitation activity in the neighbourhood, as alternative routes may not be available in the vicinity. Bridges may suffer damage, but prevention of structural collapse should be guaranteed after a seismic event. A higher level of seismic protection is therefore essential to bridge structures.

The inertia force generated during an earthquake ground motion is predominantly resulted from the mass of superstructure i.e. the bridge deck. Seismic loading hardly governs the design of bridge decks, which is primarily designed based on the dead and imposed loads. Earthquake induced motion in general impose substantial forces on the piers and foundation. Bridge foundations are usually built sturdier than the piers to prevent substructure failures which are difficult to inspect and restore after any occurrence of seismic induced damage. Thus, piers are the critical elements for bridge structure in seismically active zones. This necessitates further research to improve seismic performance of bridge pier to avoid failures as shown in Figure 1.1.

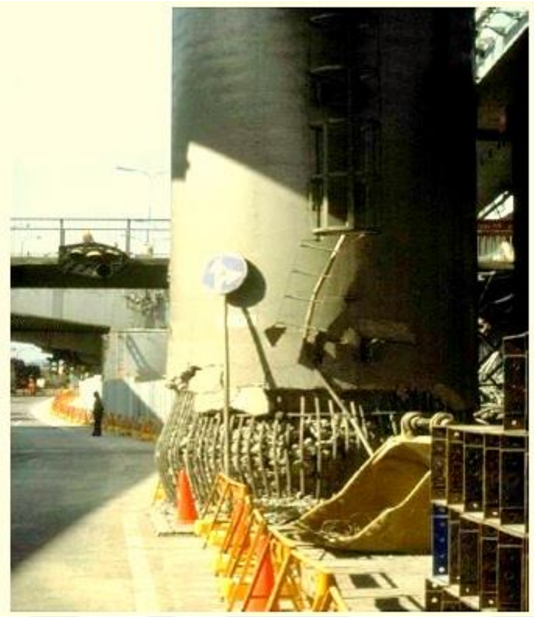

Figure 1.1. Flexure damage of pier of Hanshin Expressway in 1995 (Picture courtesy: Priestley et al. 1995)

1.2 OVERVIEW

Deficiencies in the behaviour of bridges were observed during many earthquakes all over the world. In these failure of bridges, the reinforced concrete piers were mostly observed to be considerably damaged, which implies that clear understanding of non-linear behaviour of these structural elements during intense earthquakes is an important issue. Poor seismic performances of bridges were observed from as early as the 1923 Kanto earthquake (M 8.3) in Japan. Piers supporting bridge spans collapsed during the strong shaking. In 2001, more than 500 bridges were damaged during Bhuj earthquake as per Road and Building Department, Government of Gujarat, India. The piers of some of these bridges showed severe spalling of concrete near the interface of pier and foundation. Based on the damages to highway bridges sustained during the past earthquakes, seismic design procedures of highway bridges were documented in Japan since 1926 and equivalent static *Seismic Coefficient Method* was introduced for the analysis of bridge systems subjected to earthquake loads. The 1971 San Fernando earthquake (M 6.6) served as an eye opener leading to the development of seismic design criteria for bridges in the USA.

Seismic design of concrete bridges are done by taking due consideration of design seismic load. However, in case of exceedance of such considered design load corresponding to a seismic event, damage and eventually failure may occur in the bridges. Though current bridge design codes prevents brittle failure and provide desired level of ductility, any further improvement in ductility can be attained through the use of appropriate advanced materials like fibre reinforced concrete (FRC). Increase in ductility leads to redistribution of stress-resultants to less stressed elements and the piers may sustain relatively lower strength degradation.

Introduction of any kind of new material in structural elements however needs experimental evaluation. Experimental methodology plays a vital role in correct estimation of response. Testing of structures under seismic loading is one of the best approaches to evaluate response of structure during a seismic event. This type of testing can check the effectiveness of new and advanced materials in enhancing earthquake resistant characteristic.

It is important to determine the probability of damage in a bridge for a given ground motion intensity. This is more so when any of the bridge elements are having some new design features or are made up of any new / advanced material. Such seismic vulnerability assessment of bridge is also useful for decision making and retrofit prioritization in both pre and post-earthquake disaster management. Fragility curves are widely used to predict the probability of damage that the structure may experience under any future earthquakes.

1.2.1 Hybrid Fibre Reinforced Concrete

Concrete is the most widely used construction material as it can be used to cast specimen of any desired shape. The main requirements for improving performance of earthquake resistant structures are good ductility and higher energy absorption capacity. It is established that FRC exhibits better performance not only under static and quasi-statically applied loads but also under fatigue, impact, and impulsive loadings (Banthia and Trottier 1995). Specimens with conventional concrete and FRC experiencing an excitation may undergo almost similar displacement. However, specimen with FRC remains more integrated due to the presence of fibres, where developments of macro crack from coalescing of micro cracks are delayed. Existing literature also clearly indicates that there is improvement in displacement ductility in specimen along with reduced level of strains in the reinforcement (Kheni et al. 2015). This results in delay in rupture of reinforcement which in turn leads to delay in development of any damage state and eventual collapse. Reduced damage in a structure helps in post-earthquake rehabilitation works. It is known that the inclusion of steel fibres in the concrete mix is an effective way of reducing macro-cracking, while polymer fibres are very good at arresting micro-cracking as well as enhancing impact strength and toughness (Banthia and Soleimani 2005). Thus, it would be advantageous to use concrete mix with both types of fibre. Hybrid fibre reinforced concrete (HyFRC) containing two or more fibres not only enhances important seismic parameter like toughness and ductility, the overall load carrying capacity of HyFRC specimen is also found to be marginally higher in comparison to conventional concrete specimen (Kheni et al. 2015). The intent is that the performance of these hybrid systems would exceed to that induced by single fibre type. That is, there would be a synergy classified into three groups, depending on the mechanisms involved (Banthia and Soleimani 2005):

- Hybrids based on the fibre constitutive response, in which one fibre is stronger and stiffer and provides strength, while the other is more ductile and provides toughness at high strains.
- Hybrids based on fibre dimensions, where one fibre is very small and provides microcrack control at early stages of loading; the other fibre is larger, to provide a bridging mechanism across macrocracks.
- Hybrids based on fibre function, where one type of fibre provides strength or toughness in the hardened composite, while the second type provides fresh mix properties suitable for processing.

The use of hybrid fibre reinforced concrete (HyFRC) for enhancing toughness and to ensure a more ductile mode of failure of concrete specimens is an active area of research. All over the world, research groups are putting in effort to the investigation of effectiveness of HyFRC which is till date however mostly limited to material characterization using cube / prism specimens and a few limited applications to actual structural elements like beam-column joints. Very few works were done by researchers on influence of fibres in concrete of bridge piers subjected to simultaneous action of high gravity load and lateral loads.

1.2.2 Hybrid Simulation

In large structural systems, a few elements may experience highly non-linear behaviour, which may be difficult to simulate numerically. Force-displacement behaviour of these elements may be captured from a physical test in laboratory. Thereafter, non-linear response of overall system subjected to earthquake excitation is computed. This reduces modelling uncertainties by replacing numerical modelling of highly non-linear element by physical test of the element. Hybrid simulation testing facilitates this type of structural testing and hence is selected for the experimental procedure for current research work. Hybrid testing technique is executed using a step-by-step numerical solution of the governing equations of motion for a model formulated considering both the numerical and physical components of a structural system. Unlike shake-table test, the complete structure need not be tested physically in this testing. The first official publication on hybrid simulation appeared in 1975 when Takanashi (1975) proposed “online test” method as an alternative experimental technique to shaking table tests. Since then a vast number of variations of this experimental method and the accompanying numerical algorithms were developed to improve its efficiency, accuracy and performance. It is easier to observe specimen behaviour to previously recorded earthquake and measure specimen deflection in hybrid simulation as compared to that of test on shake table. Further, when compared to conventional quasi-static tests, the hybrid simulation test method can be considered as a major enhancement that requires only a small incremental investment. Conventional quasi static testing is useful for comparing the performance of different structural design under a standardized load history. Realistic assessment of seismic inertial and damping effect cannot however be evaluated in quasi-static testing. It also suffers from the difficulty of interpreting the results with respect to the structure it represents. Such problems can be resolved with the hybrid simulation method, in which the displacements applied to a structural element are determined from the solution of equation of motion of the structural system. The hybrid simulation method provides scope to subdivide a large structure into subassemblies. The part of the structure where the behaviour is well understood can be modelled reliably using finite element models while the part having uncertainty in numerical simulation can be taken care of through actual physical test of the element(s) in laboratory. Hybrid simulation of structural system consists of numerical simulation module and experimental module along with an interface for effective communication between these two modules as shown in Figure 1.2.

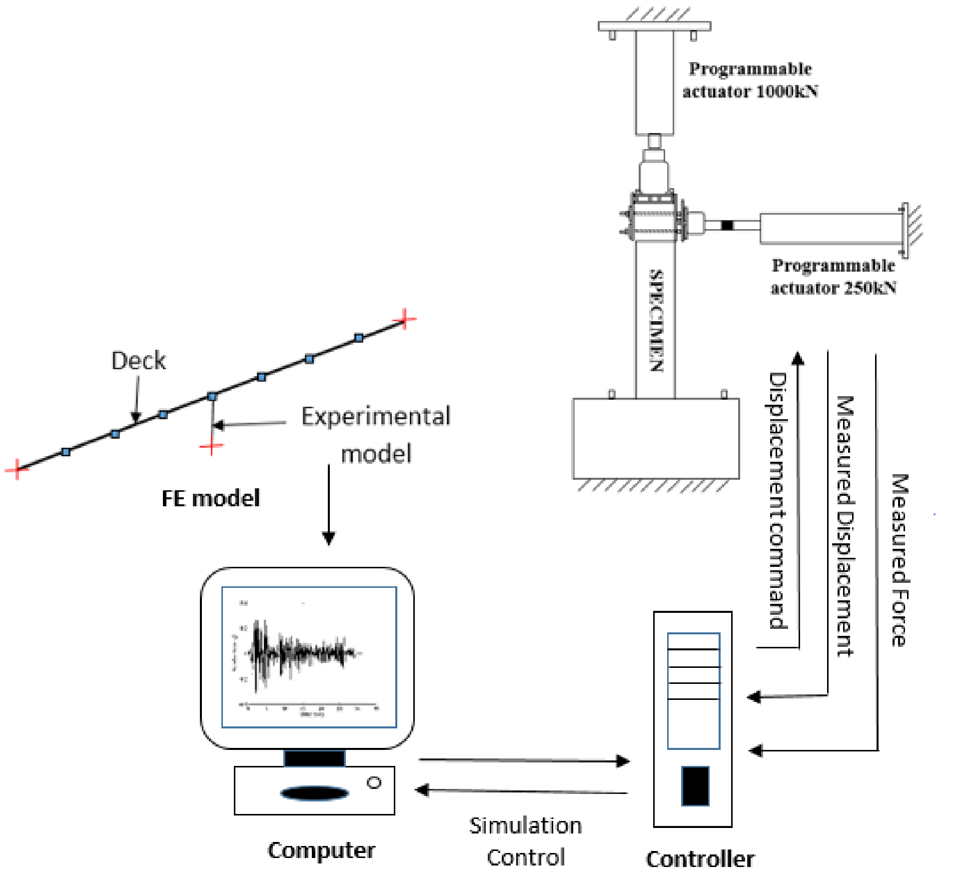

Figure 1.2. Key components of hybrid simulation

1.2.3 Bridge Fragility

Basic objective of using new materials like HyFRC in bridge pier is to reduce seismic risk of the bridge system. For quantification of improvement in seismic performance or reduction in seismic vulnerability of bridge system, comparison of fragility curves, which is an effective tool for seismic vulnerability assessment is popularly undertaken. Thus, fragility curves of HyFRC bridge pier and conventional bridge pier can be compared to evaluate their comparative performances. Earthquake demand on a structure is measured by engineering demand parameters (EDP), which reflect deformation and damage sustained by the structure. Damage states (DS) is a measure of damage sustained by a structural system. The progression of damage of a structure during a seismic loading is described by DS. In recent decades, seismic fragility curves have emerged as a powerful tool to quantify the probability of exceeding a DS for a given the intensity of ground motion. While researchers have focussed on the development of these curves for conventional concrete bridges, very few researches have compared the seismic demand and failure probabilities of HyFRC bridge piers and conventional concrete bridge piers using fragility curves. Several techniques/methodologies for generating seismic fragility curves for bridge structures have been recently developed. They can be broadly classified into three groups: expert opinion based (Applied Technology Council (ATC) 1991), empirically based (Basoz and Kiremidjian 1999, Shinozuka et al. 2000), and analytical procedure based (Nielson and DesRoches 2007, Farsangi et al. 2014). Since there are limitations (e.g. the subjectivity in defining damage states and the requirements of large amount of recorded damage data) inherent in expert-based and empirically based fragility curves, analytical fragility curves have been extensively used to generate fragility curves for bridge structures. However, the results of analytical methods are highly dependent on the definition of damage states and the accuracy of analytical model in predicting bridge seismic response. Hence, a more practical bridge specific fragility should consider damage states derived from experimental results and experimentally calibrated numerical model.

1.3 Objectives of Present Study

The research work reported in this thesis is an effort to study use of high performance material in place of conventional concrete to increase ductility. An existing bridge located in severest seismic zone in India is considered for the detailed study. It is necessary to perform an advanced level of experimental investigation in order to evaluate the seismic performance of the structure with the improved material characteristics. The experimental findings may further be utilized to calibrate numerical model of the structure and the calibrated numerical model can be subsequently used in developing fragility curves of the sample bridge structure.

Major objectives of the research work reported in this thesis are as follows:

- Determination of best possible combinations of fibres (HyFRC) for improving ductility of concrete specimens.
- Hybrid simulation of a bridge with pier made of HyFRC and conventional concrete.
- Evaluation of load carrying capacity of HyFRC as well as conventional concrete piers under the application of cyclic displacement.
- Evaluation of influence of fibres in the growth of strain in reinforcement.
- Investigation of influence of HyFRC on seismic performance and enhancement of damage resistance.
- Calibration of numerical model of the bridge using the detailed experimental output from hybrid simulation.
- Development of fragility curves of the bridge using different identified damage states from hybrid simulations and calibrated numerical model.

1.4 Scope of Research

In the light of the preceding discussion, the primary objective of this research has been identified as the experimental investigation on performance of HyFRC in bridge pier in an earthquake scenario using an advanced testing procedure, namely, hybrid simulation. It is expected that the use of HyFRC in place of conventional concrete would improve seismic performance of the specimen. The scope of study in the present research comprises of both numerical and experimental investigation. The detailed scope of studies are outlined as follows:

1.4.1 Experimental study

- To use HyFRC in any structural specimen, evaluation of best fibre proportion is essential. In this study, combination of steel and polypropylene fibre are proposed for making HyFRC. Evaluation of best fibre proportions (steel and polypropylene fibres) are to be carried out by undertaking experimental program involving testing of standard cubes, cylinder and prism specimens.

- To assess the contribution of HyFRC in improving shear strength of concrete, an experimental program is to be undertaken involving flexural testing of prism specimens with and without reduction in shear reinforcements. This findings may help in reducing shear reinforcement in any RC specimens with HyFRC.
- To shift damage zones away from bridge pier – foundation interface and hence to make post-earthquake rehabilitation works of bridge piers easier, two different strategies are to be tried by incorporating some additional features at the interface zone of the pier-foundation. Dowel bars and corrugated sheets are to be used for such studies.
- To carry out hybrid simulation of bridge structure with both conventional concrete and HyFRC piers under the action of different intensity level of earthquake excitation.
- To carry out cyclic test of the scaled pier specimens for the evaluation of ultimate capacities.

1.4.2 Numerical study

- To carry out FE modelling and analysis of the bridge structure with both conventional concrete and HyFRC piers using open source software OpenSees. The nonlinearity is expected in bridge piers only and hence the modelling strategies are to be appropriately adopted.
- To calibrate the numerical model using the response from hybrid simulation. The updating is achieved through adjustment of pier stiffness and such adjustment in stiffness of numerical model is to be carried out by using appropriate spring elements.

- To develop analytical fragility curves for the bridge with both conventional concrete and HyFRC piers. Different damage states are to be identified from the findings of hybrid simulations and analytical fragility curves to be developed by Incremental dynamic analysis (IDA) of calibrated model of the bridge.

1.5 ORGANISATION OF THESIS

This dissertation mainly focuses on assessing seismic performance of HyFRC bridge piers by hybrid simulation along with development of fragility curves of the considered bridge structure. Following the general introduction along with the objective and scope of the study given in this chapter, Chapter 2 discusses the literature review of previous studies on all the important topics related to this research. These topics includes FRC and HyFRC, experimental investigation using FRC/HYFRC in structures, experimental evaluation of seismic performance of structural components, hybrid simulation, model calibration and fragility analysis.

Chapter 3 gives the details of the experimental program. It also provides the objectives and methodology of the test program. It includes all the relevant information required for a thorough understanding of the program from its commencement to its end.

Chapter 4 describes the numerical environment of the research program. Details of the numerical model required for hybrid simulation is provided in this chapter.

Chapter 5 presents the experimental results obtained from the test program. This chapter has been divided into three parts. The first part presents the results from the tests on prism specimens to evaluate the best possible combination of fibres. The second part consists of hybrid simulation results for all the HyFRC specimens and comparison of their performances with conventional concrete specimens. The third part consists of the cyclic test results to compare the ultimate capacities of all the test specimens, which were already damaged to different extent under hybrid simulations.

Chapter 6 includes a detailed comparison between responses of uncalibrated numerical model and experimental investigation. The suitability of this data set for use in model calibration is discussed. The procedure of model calibration is presented with results from the updated model.

Chapter 7 presents the comparison of probability of failure by developing seismic fragility curves for conventional concrete and HyFRC bridge piers using calibrated numerical model obtained in Chapter 6 and damage states identified using experimental observations.

Chapter 8 concludes with a summary of the results and a set of conclusions that address the significance of the findings in this study. Recommendations for use of these findings in informing future experimental and numerical studies are provided. Finally, scope of future work is identified.

Chapter 2
REVIEW OF LITERATURE

2.1 GENERAL

New developments in the domain of fibre reinforced concrete along with its application in structural elements for enhancing ductility, additional features in bridge pier-foundation interface for relocation of damage zone from the interface region and different seismic testing methods are reported in numerous research papers, proceedings of international conferences/symposia and state-of-the-art reports presented by professional societies. This chapter is a review of some of these documents relevant to the present study. A brief review of fragility analysis of bridges is also reported.

2.2 FIBRE REINFORCED CONCRETE

Concrete is a quasi-brittle type of material, which is weak in tension. Longitudinal reinforcing bars are introduced in the likely tension zone of a structural element to address this weakness in concrete. Similarly, use of lateral confining reinforcement reduces brittle mode of failure by enhancing ductility of member made of conventional concrete. However, use of such lateral reinforcement may lead to congestion of reinforcement at joint region and hence affect the overall quality of concrete. Use of randomly distributed fibres in concrete can effectively increase the ductility of reinforced concrete element, thus reducing the demand on lateral confining reinforcements. Short randomly distributed fibres subside the nucleation and growth of concrete cracks, and bridge them after their formation thereby providing increase in strength, toughness and ductility (Soleimani 2002). Fibres suitable for reinforcing concrete structures are steel, glass, carbon and synthetic (mostly polypropylene/polyester) fibres. Naturally occurring asbestos fibres and vegetable fibres, such as sisal and jute, are also used as reinforcement. During the early 1960's in the United States, the first major investigation was made to evaluate the potential of steel fibres as reinforcement for concrete. Since then, considerable research, development, experimentation and industrial application of fibre reinforced concrete (FRC) are being carried out all over the world.

Most FRC used in practice comprises of only one type of fibre. Under an applied load, pre-existing cracks in concrete, which are of the order of microns, grow gradually. In due course these micro-cracks join together to form macro cracks. A macro-crack propagates steadily until it attains conditions of unstable propagation and causes complete fracture. The different stages of crack development and final fracture of concrete indicate that a given type of fibre can perhaps function only at one level and within a limited range of strains. Therefore, different classes of fibres must be combined for achieving more ductile response from a concrete specimen. This is the foremost goal that has inspired researchers over the past decade to work on Hybrid Fibre Reinforced Concrete (HyFRC).

Research work on use on another class of FRC called Engineered Cementitious Composite (ECC) was carried by some researchers (Li 2003, Fischer and Li 2002, Fukuyama et al. 1999). ECC uses higher volume fraction of polymeric fibre and does not contains any coarse aggregate. It has low permeability and is generally classified as a mortar mix. It contains cement, fly ash, sand, and polyvinyl alcohol microfiber (2% by volume) in order to achieve high ductility. However, due to high initial cost as compared to conventional concrete (Li 2003) and requirement of skilled labour for its construction, ECC is not considered in the current study.

2.2.1 Hybrid fibre reinforced concrete

Depending on the size and volume fraction, fibres can be effective in arresting both micro and macro-levels of cracking. Thus, fibres used for HyFRC are divided into two broad categories: macro fibres and micro fibres. Macro-fibres are large fibres, 30-60 mm in length and between 0.5 to 1.0 mm in diameter, while micro-fibres are fine fibres, typically 5-10 mm long and 20 microns in diameter (Soleimani 2002). With their fine size, micro-fibres reinforce the paste and the mortar phases, thus delaying crack amalgamation. On the other hand, macro-fibres try to bridge a fully formed macro-crack, delay its growth and further widening. HyFRC can be produced by the following three combinations of fibres (Bentur and Mindess 2006):

- ***Hybrids based on fibre constitutive responses:*** One type of fibre being stronger and stiffer provides adequate first crack strength and ultimate strength, while the second type of fibre, being relatively flexible leads to improved toughness and strain capacity in the post-crack zone.
- ***Hybrids based on fibre dimensions:*** One type of fibre is smaller, so that it bridges micro-cracks and therefore controls their growth. This leads to a higher tensile strength of the composite. The second fibre is larger and is intended to arrest the propagation of macro-cracks and therefore brings about a substantial improvement in the fracture toughness of the composite.
- ***Hybrids based on fibre function:*** One type of fibre is intended to improve the fresh and early age properties such as ease of production and plastic shrinkage, while the second fibre leads to improved mechanical properties.

The concept of HyFRC was first introduced by Walton and Majumdar (1975) and demonstrated the benefits of generating suitable composites by hybridizing organic and inorganic fibres. Walton and Majumdar (1975) observed that organic polymer fibres such as nylon and polypropylene improves the impact strength of a cement-based composite, but cannot make a significant contribution towards an increase in the tensile or bending strength of the material because of their low modulus of elasticity. Therefore, it was established that it was essential to consider an addition of a suitable second fibre such as glass, asbestos or carbon to the polymer fibre, for applications where improvements in both tensile strength and resistance against impact are desired. Premixing and spray-suction methods were adopted to produce composites in the form of flat sheets, about 9 mm thick and cut into test specimens 50 mm wide and 152 mm long. It was finally found that organic and inorganic fibres work together to produce improvement in both tensile and impact resistant properties. Strength of the bond between polymer fibres and cement or concrete could also be measured. A poor value bond strength of the order of 1 MN/m^2 was obtained with polypropylene monofilament. This interfacial bond is largely responsible for the excellent impact strength of polypropylene fibre cement composites. Different tests were carried out at selected intervals over a period of one year on composite specimens stored under different conditions. The results showed that it is possible to produce satisfactory composites by using a mixture of organic and inorganic fibres as reinforcements.

The most investigated fibre combinations are that of steel and polypropylene fibres. Steel fibres are used since they possess a high Young's modulus and lead to strong and firm composites. The elongation quality of low modulus fibres such as polypropylene, enables the concrete composites to absorb large amounts of energy and therefore, resist better impact and shock loading. Other combinations, such as steel and carbon, steel and steel, polypropylene and glass, and carbon and polypropylene were also tried by researchers. A brief review of works carried out on HyFRC is presented.

Qian and Stroeven (2000b) investigated the effect of polypropylene on hybrid fibres comprising of polypropylene and three different sizes of steel fibres by four-point bending tests on the notched prisms. Mono-filament polypropylene fibre (length: 12 mm, diameter: 18 µm), two types of hooked steel fibres (lengths: 30 mm and 40 mm, diameter: 0.3 mm) and plain steel fibre (length: 6 mm, diameter: less than 0.1 mm) were used. They observed a positive synergy between large steel fibres and polypropylene fibres on the load-carrying capacity and fracture toughness in the small displacement range. However, this synergy effect was found to disappear in the large displacement range. The steel fibre of length 40mm was better than the other two sizes in the aspect of energy absorption capacity in all displacement range. Volume fraction of 0.15% polypropylene was found to be optimum from the view point of toughness and synergy with steel.

Qian and Stroeven (2000a) presented the optimization of fibre size, fibre content, and fly ash content in hybrid polypropylene-steel fibre concrete with low fibre content based on general mechanical properties. Same sizes of fibres as mentioned in Qian and Stroeven (2000a) was used. It was assumed that a certain content of fine particles such as fly ash is necessary to evenly disperse fibres. It was also found that addition of small steel fibres had a significant influence on the compressive strength, but the splitting tensile strength was only slightly affected. On the other hand, large steel fibres type gave rise to opposite mechanical effects, which led to further optimization of the aspect ratio. A synergy effect in the hybrid fibres system was again noticed. The synergy effect implemented in a hybrid fibres system was found to lead to similar significant improvements that could be realized with a mono-fibre system having a higher total fibre content, provided the different types and sizes of fibres were properly dispersed.

The effect of hybrid fibres and expansive agents on shrinkage and water permeation properties were investigated by Sun et al. (2001). Three different sizes of macro steel fibres, one type of micro polypropylene fibres and one type of micro polyvinyl alcohol (PVA) fibres were used in their hybrid systems. It was observed that for the concrete reinforced with hybrid fibres of different sizes and types were not only better than those with hybrid steel fibres; but also better than those with other monotype fibre. It was also established that the addition of an expansive agent, namely UEA, improved the interfacial strength between aggregate, fibres and hardened cement paste. Main mineral components of UEA include aluminosulphate, aluminium sulphate, potassium aluminium sulphate, and calcium sulphate, etc. The shrinkage strains of the concrete matrix with an expansive agent, especially with the combination of hybrid fibres, decreased significantly. This demonstrated that incorporation of expansive agent improved the interface of fibre-matrix and aggregate-matrix, therefore fibres of different sizes and types could resist shrinkage and cracking at different scales. Different series of HyFRC specimens were tested for permeability. The total volume fractions were kept constant and the relative water permeation coefficients of the concrete incorporated with hybrid steel fibres were lower than that of mono-fibre reinforced and plain concretes. The concrete reinforced with three sizes of steel fibres provided improvement in impermeability compared to those with two sizes of steel fibres or mono size fibre. Therefore, it was concluded that hybrid fibres and expansive agents are beneficial to improvements of concrete in shrinkage and permeability resistance.

Banthia and Nandakumar (2003) studied the influence of different types of fibres in a contoured double cantilever beam specimens on the basis of fundamental fracture tests for characterization of the crack growth resistance curves. The specimens were subjected to vertical loads in addition to the horizontal crack opening load (OL). The crack mouth opening displacement was measured using a clip gauge displacement transducer fixed at the level at which the OL acted on the specimen. The study proved that the use of a secondary fibre like polypropylene micro-fibre even at nominal dosage rates appears to be highly effective in enhancing the efficiency of deformed steel fibres in concrete. The study further emphasized on the desired durability characteristics of these composites and their applications.

Banthia and Sappakittapakorn (2004) performed flexural toughness tests for a very high strength matrix of an average compressive strength of 85 MPa. Single, two-fibre and three fibre hybrid composite specimens were cast using different fibre types such as macro and micro-fibres of steel, polypropylene and carbon. Results were extensively analysed to identify maximum synergy associated with various fibre combinations. Based on various analysis schemes, the paper identified fibre combinations that demonstrate maximum synergy in terms of flexural toughness. It was concluded that the addition of fibres does not enhance the compressive strength of the mix but enhances the modulus of rupture. It was evaluated that the deformed steel macro-fibre provides better toughness than the crimped and self-fibrillating polypropylene macro-fibres for identical volume fractions. Between the two polypropylene macro-fibres, the self-fibrillating fibre performs better than the crimped macro-fibre.

Banthia et al (2007) carried out investigation on the toughness of FRC with hybridization of large diameter crimped fibres with smaller diameter crimped fibres to achieve workability and low cost. The results showed that such hybridization can significantly enhance toughness. Such hybrids resulted deflection-hardening, which is generally not seen in composite with large diameter fibres alone. Although this hybridization gives promising toughness value, the results also showed that such HyFRC fail to reach the toughness levels established by the smaller diameter fibres alone.

Eswari et al. (2008) investigated the influence of fibre content on the ductility of HyFRC prism specimens having different fibre volume fractions. The specimens incorporated 0.0 to 2.0% volume fraction of polyolefin and steel fibres in different proportions. Results showed that addition of 2.0% by volume of hybrid fibres improves the ductility appreciably. The hybrid fibre reinforced concrete specimens exhibit reduced crack width at all load levels, the maximum reduction in crack width was found to be 80% compared to that of plain concrete. An adaptive Neuro Fuzzy based model was proposed to predict the ductility characteristics. A reasonably close agreement was obtained between the experimental and predicted results.

Jiang and Banthia (2010) studied the effect of specimen size on measured flexural toughness of FRC along with investigation on hybrid fibre at different dosage rates. Based on observed results, it was concluded that the specimen size affects not only the toughness properties but also the variability in data as quantified by the coefficient of variation (COV). The COV values are significantly higher for the smaller specimens than the larger specimens. Size effect was more pronounced in the early part of the load-deflection curve and as the load-deflection curve extends to larger deflections, size effect diminishes.

Skazlic (2010) discussed some basic results of investigation which was carried out prior to application of HyFRC comprising of steel and polypropylene fibres and also reported case studies on application of HyFRC for construction of concrete pavement as well as repair of bridge deck overlay. The research indicated that a combination of steel and polypropylene fibres can be effectively used to optimize the behaviour of concrete in fresh and hardened states.

2.2.2 Application of FRC and HyFRC in structural members

It is observed from literature survey that most of the researchers carried out investigation using FRC and HyFRC using standard cube and prism specimens. Limited studies are seen, where these fibres were used for investigations of behaviour of large structural specimens.

Kawashima et al. (2011) presented seismic performance of full size bridge piers made using polypropylene fibre reinforced cementitious composite and steel fibre reinforced concrete. They carried out experiments on shake table using near field ground motion as input. Use of polypropylene fibre reinforced concrete and steel fibre reinforced concrete reduced damage level in cover and core concrete, local buckling of longitudinal bars and strains induced in ties as compared to those in the conventional concrete pier.

Kumar et al. (2011) selected a prototype highway overpass bridge based on previous research which described a number of typical bridge structures designed according to the Caltrans Seismic Design Criteria. Investigation on the seismic performance and post-earthquake damage resistance of two 1:4.5 scaled bridge column specimens made of Self Compacting HyFRC (SC-HyFRC) were carried out. In comparison with conventional RC, SC-HyFRC was found to combine the advantages of self-compaction, resulting in improved constructability, and enhanced material properties compared to conventional fibre reinforced composites, resulting in a more ductile behaviour in both tension and compression.

Kheni et al. (2015) performed an experimental study of beam-column joint using HyFRC. In the first part of the study, prisms made of plain concrete, steel fibre reinforced concrete and HyFRC were tested under quasi-static load to account for variability in fibre specifications. Two types of steel fibres with hooked-ends and two types of polymer fibres, namely, polypropylene and polyester were used. The HyFRC prisms exhibited about 10-15 times enhancement in toughness as compared to similar plain concrete prisms till failure. Subsequently, four types of beam-column connections with FRC in D-region were tested under cyclic loading. Test results established the effectiveness of the addition of hybrid fibre in the joint region of the specimens in enhancing their displacement ductility and energy dissipation capacity. Detailed measurement of strain distributions along the main reinforcement of the specimens showed that there was substantial reduction in their strain levels for the specimen with HyFRC in the joint region.

2.2.3 Reduction of shear reinforcement

FRC and HyFRC are observed to contribute in enhancing shear resistance of concrete. Thus, the possibility of reduction in shear reinforcement in concrete specimens made up of FRC / HyFRC can become helpful in reducing congestions of reinforcements generally observed in joint region. Some of the studies carried out by researchers are presented.

Parra-Montesinos (2006) used deformed steel fibres as an alternative to minimum transverse shear reinforcement for beams subjected to factored shear forces. All slender FRC beams that contained 0.75% volume fraction exhibited a shear stress at failure greater than the conservative lower bound value. The performance criteria can be used for acceptance of steel fibres as minimum shear reinforcement.

Kumar et al. (2011) used reduced transverse reinforcement in bridge columns made of HyFRC. The transverse reinforcements were in fact reduced by factor of two compared to conventional RC Caltrans bridge columns and found to enhance seismic performance in comparison to conventional concrete pier specimen with conventional reinforcement.

Susetyo et al. (2011) evaluated the effectiveness of steel fibres in meeting minimum shear reinforcement requirements for concrete panels tested under in-plane pure-shear monotonic loading conditions. The test results indicated that concrete elements exhibiting ductile behaviour, sufficient shear strength, and good crack control characteristics can be obtained with an adequate addition of steel fibres, meeting or exceeding the level of performance achievable using code prescribed minimum amounts of conventional shear reinforcement. Fibre aspect ratio, fibre length, fibre tensile strength, fibre volume content, and concrete compressive strength are found to influence the shear performance of FRC to varying extents. A fibre volume content of approximately 1.0% was required to achieve satisfactory performance in terms of shear strength, deformation ductility, crack width, and crack spacing. However, minor improvement in above mentioned property was obtained, by increasing the fibre volume content from 1.0 to 1.5%, possibly due to fibre saturation.

Mondo (2011) investigated shear strength of FRC beams without conventional shear reinforcement and analysed the test data against the most appropriate equations available in the literature. The equations investigated were proposed formula in Narayanan and Darwish (1987), formulas given in DafStB (2011), RILEM (2003) and CNR (2010). The results established improvement in shear capacity of the FRC beams and possibility of replacement of the conventional transversal reinforcement.

Jain et al. (2013) investigated that the failure modes of beams with steel fibres as minimum shear reinforcement in reinforced concrete beams were comparable to that of the beams detailed as per the recommended minimum shear reinforcement of ACI 318 (2008) and the IS 456 (2000). Although shear strengths of the fibrous concrete beams is significantly smaller than the measured strengths of the beams detailed with the code-specified shear reinforcement, this value was higher than the predicted values from the design codes. Moreover, service load crack widths in the beams with steel fibres as minimum shear reinforcement were significantly lower than the allowable value of 0.3 mm for normal exposure condition as well as the measured values in the beams detailed with the code-recommended minimum shear reinforcement.

2.3 ADDITIONAL FEATURES AT PIER-FOUNDATION INTERFACE

A few researchers introduced some additional features at pier-foundation and beam-column interface to shift the likely damage zone away from the interface region. This is particularly beneficial from the view point of ease of retrofitting after any seismic event.

Greizic et al. (1996) provided the connection between the pier and the footing with dowel bars and the specimens were tested under cyclic load. The dowel bars were anchored into the thick footing with 90° standard hooks. Such arrangement helped in shifting of damage location away from the pier-foundation interface showing increased ductility, increased strength and significant increase in the energy absorption.

Aviram et al. (2014) used dowel reinforcement at the pier-foundation interface to transfer most of the inelastic deformation to occur within the pier. The specimens were tested under bidirectional displacement loading. The specimen with long dowels developed an extended plastic deformation zone with an approximate length of one column diameter. Presence of dowels at the interface improved ductile behaviour, damage tolerance, and energy dissipation in piers as compared to those of a geometrically identical specimen constructed without dowel as per bridge design specifications. This specimen was subjected to displacement corresponding to 10.7% drift ratio while maintaining a constant gravity load. The specimen with short dowels and debonding of main longitudinal reinforcement were responsible for less deformation capacity as compared with specimen with long dowel bars. The reason for such behaviour was the development of a single major crack at the cut-off point of the dowel bars, resulting in a concentration of rotation and damage at that location and limited spreading of the plastic hinge zone towards the base of the column.

Another possible way to shift the damage zone reported in literature is by embedding a corrugated sheet duct in the foundation. Corrugated sheet duct is a tube with a series of parallel ridges and grooves on its surface. Ghobarah et al. (1996) used corrugated steel to upgrade beam-column joints as it provided both lateral confinement and shear reinforcement. The corrugated jacket adds enhanced lateral confinement and shear strength. The experimental results indicated that specimens with corrugated steel jacket performed satisfactorily under high cyclic load levels. The confinement provided to the joints increased the ductility several times.

Kumar et al. (2011) incorporated corrugated steel duct to prevent crack localization in the vulnerable region at the pier base-foundation interface. Results showed that major crack in the pier specimen was formed at 1.2 inch from the base of piers. Strain profiles also indicated crack re-localization from the pier-foundation interface. Energy dissipation capacity of the specimen also increased due to the spread of plasticity.

2.4 EXPERIMENTAL EVALUATION OF SEISMIC PERFORMANCE OF STRUCTURAL COMPONENTS

There are a number of well-established procedures to conduct laboratory testing for evaluating the seismic response of structural component or system. The most common technique is the quasi-static testing method, where sample structural component or structural system is subjected to a predefined force or displacement loading through actuators. Effect of modifications in material properties, boundary conditions and other issues can be easily identified by this type of testing. These test are relatively easy and economical to execute, but the load imposed on the test specimens are not directly related to the actual demand. Kumar et al. (2011) performed uni-directional cyclic loading test to investigate the seismic performance of two 1:4.5 scaled bridge columns composed of self-compacting HyFRC. The cyclic loading amplitude was increased by 0.15% at each step till 0.6% drift and after that it was increased by 0.6% till 6% drift. They mostly considered 3 cycles for each step of loading. In some loading steps they have also considered 1 and 2 cycles. Kawashima et al. (2011) evaluated seismic performance of scaled bridge columns using polypropylene fibre reinforced cement composite, steel fiber reinforced concrete and reinforced concrete in combination with high strength longitudinal bars. All the columns were subjected to combined axial and bilateral cyclic loading. The amplitude of the loading was increased at 0.5% drift ratio at each loading step. Sasaki et al. (2012) investigated the progress of failure and the ductility capacity of two scaled bridge columns made of polypropylene fibre reinforced cement composites using bilateral cyclic loading with actuator and quasi-dynamic loading with shake table. Cyclic loadings was repeated until failure with an increment of 0.5 % drift. No numerical study was however conducted to verify these experimental findings. From review of these literatures, it is observed that realistic simulation of seismic demand on the structure is not realized by this kind of quasi-static test. This drawback led to queries about whether the specimens were under or over tested. Besides, the applied load protocol are generally insufficient for approximating the randomly changing load history that a structure experiences during an actual seismic event.

Shake table tests are also often used to evaluate seismic performance of structures. Shake table tests provides the most realistic response of the investigated test specimen to seismic excitation. However, the capacity and size of most of the available shake tables in the laboratories impose substantial constraint on the size and weight of a specimen that can be physically tested. As a result, reduced scale or highly simplified specimens are usually tested, which may be considered as unrealistic. Test on shake tables are largely employed by researchers for the evaluation of seismic behaviour of civil engineering structures. Tsai et al. (2007) conducted shaking table tests to verify the effectiveness of the rolling-type bearing (with and without viscous dampers) as a seismic isolation device. No numerical study was conducted for the overall bridge system with the bearings. Okada and Unjoh (2008) conducted shake table test as well as numerical analysis to evaluate seismic response of bridge model using sliding bearings and dampers. Chen et al. (2008) carried out shake table test on two bridge specimens having different numbers of bents to check the stiffness degradation due to earthquake ground motions with increasing amplitude. Johnson et al. (2009) conducted shake table test as well as analytical simulation using SAP 2000 and Drain 3DX to study the linear and nonlinear response of a RC bridge model subjected to transverse earthquake excitations. Saiidi et al. (2010) executed shake table test and analytical study using computer program OpenSEES to show the effectiveness of post-tensioning and use of materials like shape memory alloys (SMA), engineered cementitious composites (ECC) and elastomeric pads embedded into columns in reducing damage and permanent displacements. Saiidi et al. (2012) performed shake table test to check the response of concrete bridge subjected to bidirectional motions in the transverse and longitudinal directions up to failure. Carlos and Saiidi (2013) performed shake table test to assess the performance of the bridge and key response parameters. Saiidi et al. (2013) carried out shake table test to investigate the fault rupture effects on the seismic response of a bridge system crossing an active fault. Thus, while a large number of tests were conducted for the assessment of seismic performance of structural systems, the necessity of an advanced seismic testing methodology comprising both physical and numerical model was realized from the limitations of all those previous tests (Schellenberg et al. 2008).

2.4.1 Hybrid simulation

Compared to the above two testing methods, hybrid simulation is the most advanced seismic testing. In this testing method, a simulation of responses of the sample structure under seismic loading is based on a step-by-step numerical integration of governing equations of motion considering both the numerical and physical components of a structural system.

Contrary to purely numerical simulation, the hybrid simulation method combines the physical testing of a part of the structure i.e. substructures with numerical models of the remainder of the structure. It provides complete picture of how earthquake events can affect large structures such as buildings and bridges without having to physically test the entire structure. This enables structural engineers to accurately and efficiently capture the effects that a substructure has on the overall structure, while subjecting the substructure to the same forces and motions it would experience as part of the prototype structure. During the simulation, the physical model of the overall hybrid model are tested in one or more laboratories using computer controlled actuators, while the numerical model are simultaneously analysed on one or more analytical platforms. Considerable research is being carried out worldwide to extend hybrid simulation to applications where there are complexities in non-linear modelling in numerical techniques. Efforts are in progress to improve potentialities for testing portions of the structure in different laboratories of the world, including techniques to overcome the deficiencies of network quality (Schellenberg and Mahin 2006a). Fundamental studies for hybrid simulation are still in process related to improving approaches used for formulation and solution. Characterization and correction for errors related to numerical modelling and simulation, experimental control, scaling, strain rate effects and latency were also studied by many researchers.

Schellenberg and Mahin (2006b) demonstrated how geometric nonlinearities could be accounted for in the numerical module of hybrid simulation on a simple one-story one-bay portal frame with two ductile columns, wherein large deformation (second-order) effects due to gravity loads were consistently taken into account till collapse state.

Schellenberg et al. (2008) presented extension of the hybrid simulation testing method to model structural collapse. Hybrid simulation test was performed on a one-storey portal frame with two ductile columns until collapse to demonstrate and validate the newly proposed approach based on considering OpenSees and OpenFresco. The physical specimens of the columns were not axially loaded, as an alternative, second-order analytical geometric transformations involving the degrees-of-freedom of the experimental subassemblies were used to affect the actions of the axial load. This eliminated the need for complex active or passive gravity load setups. Comparison of results of the two hybrid simulations- with and without accounting for gravity load effects, showed that the hybrid model with P-Delta effects developed negative post-peak stiffness and thus increasing lateral displacements until collapse occured.

Whyte et al. (2008) evaluated the quality of hybrid simulation using a control-theory concept of reachability analysis of a dynamic system, which predicts the sets of states the systems can attain under uncertain dynamic excitation starting from uncertain initial conditions evaluated using uncertain measurements. This method was used to compute the size of reachable tubes (an ellipsoidal tube of the trajectory envelope of states of the system at any instant during a hybrid simulation) for response of a linear single degree of freedom (SDOF) system responding to dynamic excitation such as free vibration and under earthquake excitations. They investigated propagation of disturbances representing the uncertainty of the initial condition of the system and the uncertainty associated with the application of the dynamic excitation to the system response by computing the size of the ellipsoid approximation of the state of the system at each instant of its dynamic response. They also presented a comparison of trajectory envelopes of the system responding to the same excitation under different magnitudes of disturbance. The results established the success of the proposed methods for evaluating the quality of hybrid simulation.

Yang et al. (2008) proposed an on-line error monitoring method to assess the severity of experimental errors during a hybrid simulation. This method predicts the accuracy of the simulation results during the simulation. Hybrid simulation of seismic response of an innovative lateral load resisting system is used to demonstrate the effectiveness of the proposed on-line error monitoring indicators.

Hung (2010) investigated the seismic behaviour of RC Coupled wall systems (CWSs) in which high performance fibre reinforced concrete is used to replace regular concrete in vulnerable regions of the structure through computational and hybrid simulation techniques. A strategy for estimating the tangent stiffness of structures during hybrid simulation was proposed. It was shown that when the strategy was combined with the widely used Operator Splitting Method (OSM) for hybrid simulation, the simulation accuracy got enhanced compared to the traditional OSM. They developed a new conditionally stable algorithm, called Full Operator Method (FOM). They showed that FOM has enhanced accuracy compared to OSM and that it is possible to modify FOM into an unconditionally stable algorithm for cases where the estimated tangent stiffness is larger than the real tangent stiffness. Hybrid simulation of an 18-story prototype based on FOM indicated that the new technique was able to model seismic behaviour of CWSs accurately.

Yang et al. (2012) proposed an online optimization method to improve the accuracy of numerical–experimental hybrid simulations of bridges subjected to earthquake forces. The online optimization method aimed to solve the problem induced by the inconsistency of the multiple identical bridge piers, where only one or a few of them were simulated experimentally by physical specimens, while the others were numerically simulated within a hybrid framework.

The number of researchers working on hybrid simulation have considerably increased worldwide over the last few years, that resulted increase in numbers of publications as well. However, in India the status of hybrid simulation is still at nascent stage.

2.4.2 Experimental studies using hybrid simulation

Many researchers have used hybrid simulation for seismic performance evaluation of structural systems including bridges and building frames. Brief reviews of these literatures are provided in this section.

Pinto et al. (2004) performed pseudo-dynamic tests on a large-scale model of an existing six-pier bridge at the European Laboratory for Structural Assessment using the sub-structuring technique. Two physical pier models were constructed and tested in the laboratory, while the deck, the abutments and the remaining four piers were numerically modelled. Non-linear sub-structuring allowed the testing of the complete bridge model using the existing laboratory facility and thereby reducing considerably the cost of large test set-up. Two piers, instead of six, were constructed and tested. These tests on a large-scale model of an existing bridge were performed considering non-linear behaviour for the modelled substructure. Asynchronous input motion, generated for the specific bridge site, was used for the abutments and the pier bases. Tests under earthquake loading with increasing intensities were carried out, which was aimed at the assessment of the seismic vulnerability of a typical European motorway bridge designed prior to the modern generation of seismic codes. The experimental results confirmed the poor seismic behaviour of the bridge by irregular distribution of damage, limited deformation capacity and undesirable failure locations.

Carrion et al. (2007) presents an approach for real-time hybrid simulation in which compensation for actuator dynamics is implemented using a model-based feed forward compensator. Experimental results showed good agreement with the predicted numerical responses, demonstrating the effectiveness of hybrid simulation method for performance assessment of structural control system.

Lavorato (2009) presented the experimental results of R.C. bridges with the aim of assessing the effectiveness of innovative materials for repairing and reinforcing of severely damaged piers during previous hybrid tests. A representative 1:6 scaled pier was physically tested in the laboratory, while the rest of the structure was simulated numerically. The tests carried out were of both pseudo-dynamic and cyclic type. The description of the retrofitting of the piers as well as the description of test equipment were presented and finally a comparison between the seismic behaviour of the original and the retrofitted piers were shown in terms of seismic response and final structural damage.

Kim et al. (2011) carried out an experimental study for assessing the effect of vertical earthquake ground motion on reinforced concrete bridge piers. The program comprised of testing of four large scale piers by utilizing the Multi-Axial Full-Scale Sub-Structured Testing and Simulation (MUST-SIM) facility at the University of Illinois. Two hybrid numerical-experimental simulations were used to experimentally investigate the effects of vertical ground motion on pier behaviour. Two additional cyclic tests were conducted to allow direct comparison of pier response under tension to pier response under compression. Details of the experimental framework including a sub-structuring scheme, numerical representation of structure, test specimen design and advanced measurement system were provided. The observations and interpretation of experimental results, including the impact on both global and local behaviour, were discussed. It was concluded that vertical ground motion can significantly impact Reinforced Concrete (RC) pier behaviour and failure mode.

Abdelnaby et al. (2014) studied the influence of reinforced concrete (RC) bridge piers subjected to combined loading conditions resulting from complex earthquake ground motions coupled with asymmetry of the bridge structure. They also studied the influence of the assumptions and simplifications made in modelling irregular and curved bridges on the reliability of their computed response. In this study, a hybrid simulation test was conducted on a curved four-span bridge. This test accounted for the 3D system-level interaction between the three experimental piers in two testing facilities with the numerical models of the deck, restraints and abutments. Prior to the hybrid simulation, a detailed numerical finite element, fibre-based model of the whole bridge system was established. The analytical predictions of this model were then used for comparison with the hybrid simulation test results. The achievement of the hybrid simulation of a curved four-span bridge of different span lengths and unequal pier heights was discussed. A rigorous numerical model calibration procedure was then followed to adjust for the initial modelling assumptions which improved the bridge model's overall response. Model calibration procedures were described, focusing on response of pier during the hybrid test and the inadequacy of the numerical tools in capturing these responses. The validity of the hybrid test results used in the numerical model calibration was highlighted. Model calibration was performed to obtain a high degree of agreement between numerical results and the experimental data set. Corrections for assumptions made in the initial un-calibrated model were adjusted through the inclusion of several nonlinear springs. The disparity between the initial analytical predictions and experimental results revealed that some of the commonly adopted modelling assumptions are required to be revisited for improving the performance of the numerical model.

2.5 Bridge fragility analysis

Fragility curve is a conditional probability that gives the likelihood that a structure will meet or exceed a certain level of damage for a given ground motion intensity measure. These curves are derived based on the comparison between available capacity of the structure and the seismic demand due to the expected future earthquakes. Each point on the fragility curve shows the probability that the response under certain level of ground excitation is larger than the response associated with a particular damage state. These curves are found to be most reliable tool for both before earthquake and after earthquake studies of major structures.

The fragility or conditional probability can be expressed as:

$$Fragility = P\left(D > C \mid PGA\right) \tag{2.1}$$

Where, *D* is the seismic demand of the bridge component or system, *C* is the capacity of the bridge component or system and PGA is the peak ground motion, intensity measure. Figure 2.1 shows the graphical representation of a typical fragility curve conditioned on PGA as intensity measure.

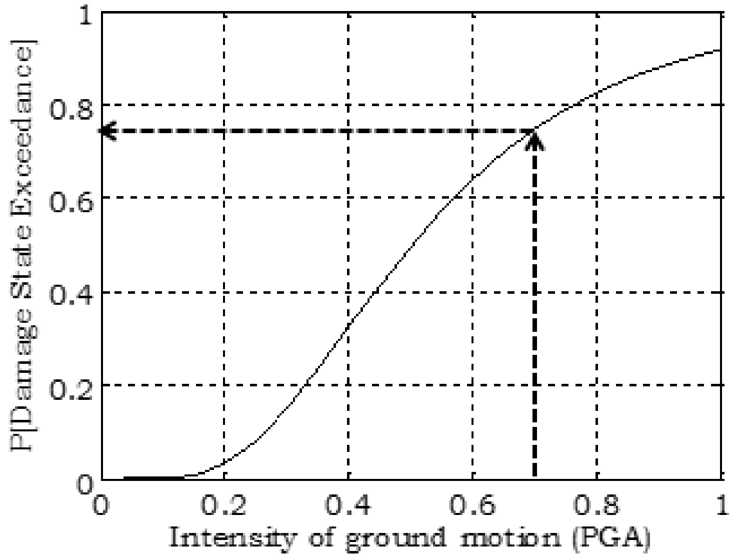

Figure 2.1. Typical fragility curve conditioned on PGA as intensity measure

There are a number of different methodologies that have been employed in the past few decades to develop seismic fragility curves for highway bridges such as expert/judgmental based, empirical, experimental, analytical and hybrid. A brief summary with key features and limitations of various methodologies which is used to develop seismic fragility curves of highway bridges is given in Table 2.1.

It is observed that each method of seismic vulnerability assessment has its share of limitations and among these, fragility curve obtained using hybrid methods i.e. combination of both experimental and analytical environment is best option. Therefore, this study provides an overview of hybrid method for developing fragility curves. As already shown in Table 2.1, this method is developed in order to overcome the drawbacks of other methods such as inadequate damage data from real earthquakes, biasness and subjectivity of judgmental data and uncertainties and modelling) assumption associated with analytical procedures. Following is the brief summary of work done in past to develop fragility curves using hybrid methods for buildings and bridges. Penelis et al. (1988) first employed the hybrid method of developing fragility curves by combining damage data available from Thessaloniki earthquake (1978) with nonlinear dynamic analysis for RC buildings.

Kappos et al. (1998**,** 2006 and 2010) developed fragility curves for RC and unreinforced masonry buildings in Greece. Past damage data of the considered structural typology in Greece is combined with analytical damage statistics obtained using nonlinear analysis of typical structures.

Lin et al. (2012) developed analytical model of 2D frame and tested small scale column in hybrid testing facility. Hybrid fragility curves were developed using the mean peak ground acceleration from hybrid tests and dispersions of peak ground acceleration were taken from the literature.

Table 2.1. Key issues and limitations of different methods for development of fragility curves for highway bridges

Methods	Selected important reference	Key observations
Expert/ Judgemental	ATC-13 (1985)	• Simple method based on post-earthquake survey, therefore more realistic • Depends on panel expertise and are often biased and lack reliability and also involve huge uncertainty
Empirical	Basoz and Kiremidjian (1998); Yamazaki et al. (2000); Shinozuka et al. (2000)	• Based on post-earthquake survey, therefore it shows actual vulnerability • Highly specific to a particular seismo-tectonic and built environment • Lack of adequate data and these are highly clustered in the low damage, low ground motion intensity range • Discrepancy in structure damage classification
Experimental	Vosooghi and Saiidi (2012); Banerjee and Chi (2013)	• Provide actual damage scenario • Large-scale experiments involving entire bridge models or full scale components expensive • Lack of adequate damage data points at all damage states
Analytical	Hwang et al. (2000); Mander and Basoz (1999); Shinozuka et al. (2000a); Mackie and Stojadinovic (2005); Nielson and DesRoches (2007); Pan et al. (2010); Ramanathan et al. (2010); Billah et al. (2012)	• All types of uncertainty can be considered, therefore reliable and less biased • Substantial computational effort is required along with limitation of analytical model • Derived curves depends on type of analysis method (e.g. elastic spectral analysis, Non-linear static analysis, nonlinear time-history analysis), seismic hazard, damage state definition, etc.
Hybrid	Frankie (2013)	• Compensate for the scarcity of damage data, subjectivity of expert opinion and modelling assumption using experimental results and calibrated analytical model • Consideration of multiple data sources is necessary to generate reliable fragility curves

Frankie (2013) developed hybrid fragility curves for a four span curved bridge using results of hybrid simulation and nonlinear dynamic analysis. They tested bridge pier in hybrid testing facility and used the results of simulation for identification of DS. Seismic demand was calculated by carrying NLTHA on calibrated analytical model.

The results of all these studies shows that hybrid fragility curves can be developed either by combining damage states from dynamic analysis of structure subjected to past earthquakes or by conducting hybrid simulation where experiment on scaled model of part of structure is carried out and the results are used to calibrate analytical model and also to identify DS. The calibrated analytical model can be used to evaluate response of the full bridge using nonlinear dynamic time history analysis using a wide range of ground motion. The fragility curves are developed then by assuming lognormal distribution of demand and capacity. Figure 2.2 shows the flow chart of above methodology.

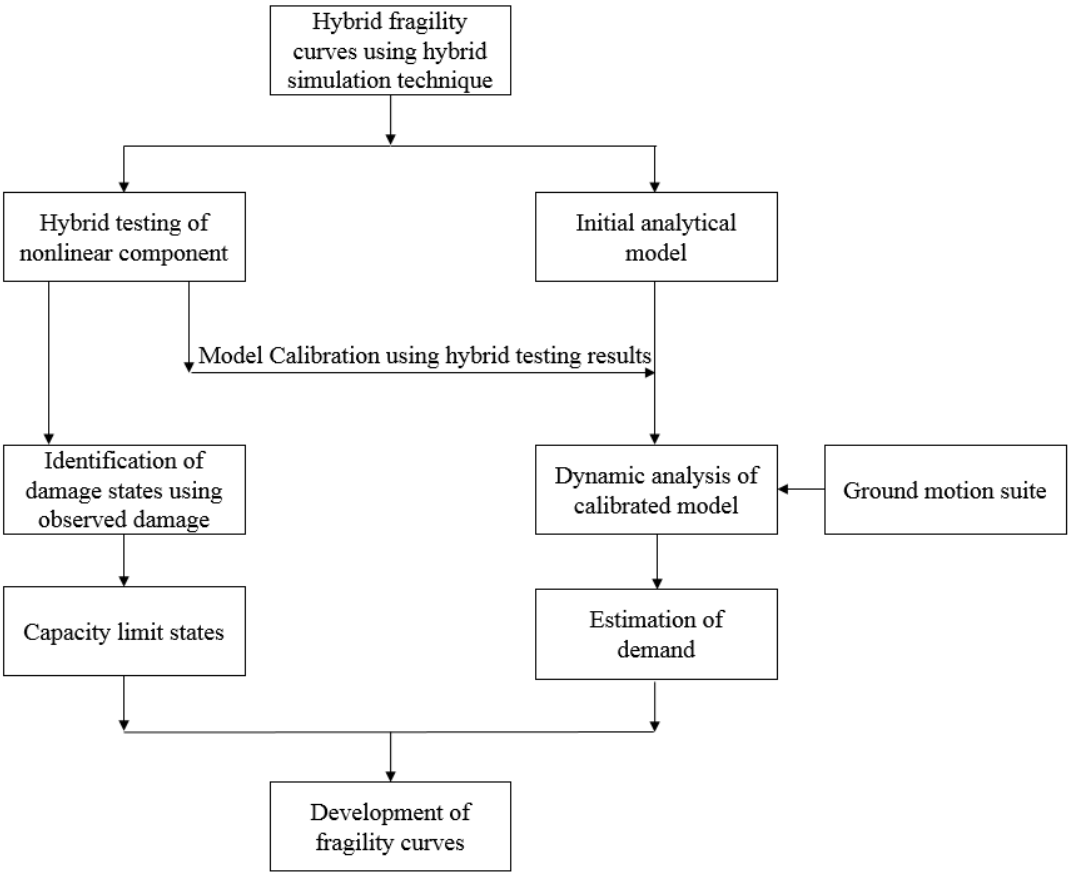

Figure 2.2. Flowchart for development of hybrid fragility curves

2.6 CONCLUDING REMARKS

In the light of the preceding review, the use of HyFRC in place of conventional concrete is found to improve the ductility of structural elements. After concrete reaches the point of rupture, fibres in HyFRC help in providing tensile strength to concrete. This reduces the tensile stress demand in longitudinal reinforcement thus delaying the yielding of reinforcement bars. Different kinds of fibres and volume fractions are used in the different literature. A preliminary study is however essential for arriving at appropriate proportions for the type of fibres to be used in a particular study.

Further, from literature review, it is found that very limited studies were carried out for evaluating seismic performance of HyFRC in bridge structural components like piers. Some experiments were conducted in the past involving bridge structural components, but limited to testing under quasi-static test only. Hybrid simulation technique combines numerical with experimental approaches to investigate a complete structural system which helps to correlate real loading condition and response of the system during a seismic event. Advanced testing technique like hybrid simulation is significant for seismic performance evaluation of bridge piers made of HyFRC.

Available literatures explain the procedures for development of analytical fragility curves of a structure using different methods and highlighted the importance of developing such fragility curves using identified damage states from experimental results and calibrated numerical model for a structure made of fibrous material.

Chapter 3
ASSESSMENT OF MECHANICAL PROPERTIES OF CONSTITUENT MATERIALS

3.1 GENERAL

This chapter details the test program undertaken in the current research program for assessment of mechanical properties of constituent materials. In the present study, steel fibres of two different sizes having different aspect ratio (length/diameter) and polypropylene fibre are used (Figure 3.1). Evaluation of parameters like compressive as well as tensile strength of concrete and HyFRC using prescribed tests according to Indian standard are carried out. All the test programs are however undertaken with two clear objectives and are grouped as Part I and Part II. Test program- Part I is undertaken to finalize the volume fractions of steel and polypropylene fibres in HyFRC on the basis of best possible values of toughness and Part II of the test program is related to the possible reduction in transverse reinforcement in HyFRC specimens without effecting the shear capacity.

3.2 TEST PROGRAM (PART I) -EVALUATION OF VOLUME FRACTIONS OF STEEL AND POLYPROPYLENE FIBRES IN HYFRC

Detailed literature survey clearly showed that the blend of steel and synthetic polymer fibre, namely, polypropylene fibres are best combination for HyFRC. However, evaluation of volume fraction of these fibres are to be carried out with the target of getting best possible values of toughness. In the present study, steel fibres of two different aspect ratios (length/diameter) and polypropylene of two different brands Recron 3s (PP - I) and Bajaj Plast (PP - II) are used and their properties are shown in Table 3.1.

Table 3.1. Details of fibres and their properties

Name of fibre	**Length (mm)**	**Diameter (mm)**	**Geometry**	**Aspect ratio**	**Density (kg/m^3)**	**Tensile strength (MPa)**
SF1 - Steel fibre 1 (Dramix 35)	35	0.55	Hooked end	64	7850	1100
SF2 - Steel fibre 2 (Dramix 60)	60	0.75	Hooked end	80	7850	1225
PP-I: Polypropylene fibre (Recron 3s)	12	0.03	Triangular flat	600	910	450
PP-II: Polypropelene fibre (Bajaj Plast)	10	0.02	Fibrillated (Mesh)	550	910	6700

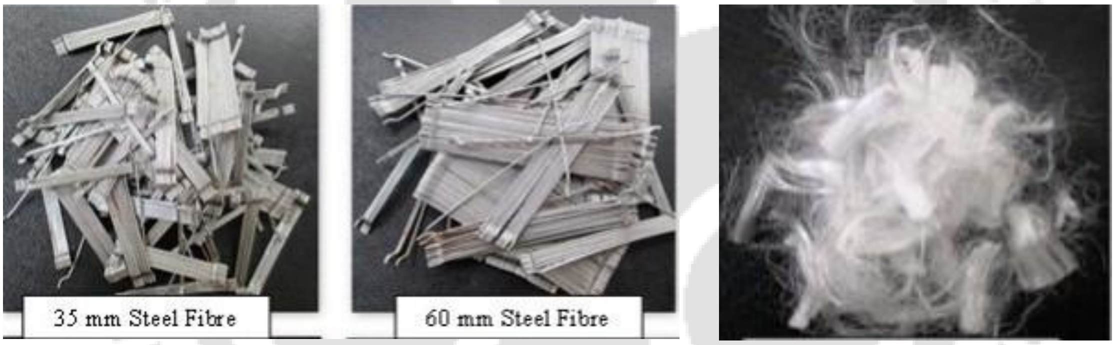

(a) (b)

Figure 3.1. (a) Steel fibre (Dramix) (b) Polypropelene fibre (Recron 3s)

Preciseness to the experimental work depends on to a large extent on proper characterization of the materials to be used for design of concrete mix. The material characterization for the current research work is carried out as per relevant Indian standard codal provisions. The detail results are presented in Table 3.2- Table 3.5. Portland Pozzolana cement used for the research work satisfies all the recommendation mentioned in IS: 4031(4) – 1988. The results of the test are shown in Table 3.2. Compressive strength of cement at 3, 7 and 28 days satisfy IS 1489 (Part 2): 1991 criteria and is shown in Table 3.3.

Table 3.2. Results of tests on cement

Sl. No.	Name of test	Test result
1	Standard consistency	50%
2	Initial setting time	1 Hr 40 minutes
3	Final setting time	6 Hr 10 minutes
4	Specific gravity	2.86

Table 3.3. Compressive strength of cement

No. of days	Compressive strength (MPa)	
	According to IS 1489 (Part 2): 1991	Test Results
3	16	16.5
7	22	22.8
28	33	34.5

Three 150 mm cube specimens are used to determine the compressive strengths and three 150 mm diameter and 300 mm long cylinders are used in order to find out concrete tensile strength. Aggregates used for conventional concrete are also found to be suitable for FRC (Balaguru et al. 1992). The grading requirements for fine aggregates are listed in ASTM specification C-33. The maximum size is limited to 6 mm and at least 80% of the particles should be smaller than 3 mm. Percentage of sand used in this study passing through 2.36 mm sieve size is 95.73% (Table 3.4). The grading requirement for coarse aggregate is recommended by the ACI Committee 544 for Steel fibre reinforced concrete. The maximum size of aggregate should be smaller than-

- 1/5th of the narrowest dimension between form works
- 1/3rd of the depth of the slab
- 3/4th of the clear spacing between reinforcing bars

Table 3.5 shows that the coarse aggregates used for the research work satisfies all the grading requirements. Presence of fibres improve fracture toughness of concrete (Banthia et al. 1998). After mixing of normal concrete constituents, fibres are added gradually to avoid any fibre balling. The mixing procedure is illustrated in Figure 3.2. The mix proportion for conventional concrete are slightly modified to maintain workability, easy fibre mixing and good fibre distribution (Balaguru et al. 1992).

Table 3.4. Result of sieve analysis of sand

IS SIEVE	Wt. Retained (gm)	% Wt. Retained	Cumulative % Retained	Cumulative % passing	As Per IS 383-Table-no.4 for zone III
4.75 mm	26	2.64	2.64	97.36	90-100
2.36 mm	16	1.63	4.27	95.73	85-100
1.18 mm	38	3.86	8.13	91.87	75-100
600 micron	124	12.6	20.73	79.27	60-79
300 micron	530	54.08	74.81	25.19	12-40
150 micron	234	23.78	98.59	1.41	0-10
75 micron	14	-	-	-	-
Pan	2	-	-	-	-
**Specific Gravity = 2.59 as per IS: 12386 (III) - 1963*					

Table 3.5. Result of sieve analysis of coarse aggregate

IS Sieve	Wt. retained (gm)	Cumulative wt. retained	Cumulative % retained	Cumulative % passing	As Per IS 383-Table-no.2 for 12.5mm down
25 mm	-	0	0	-	-
20 mm	12	12	0.6	99.4	100
16 mm	14	26	1.3	-	-
12.5 mm	130	156	7.8	92.2	90-100
10 mm	724	880	44.17	55.83	40-85
4.75 mm	1096	1976	99.2	0.8	0-10
Pan	24	2000	100	-	-
**Specific Gravity = 2.73 as per IS: 12386 (III) – 1963* *Fineness Modulus = 8.02 as per IS: 12386 (I) – 1963*					

Balaguru et al. (1992) also mentioned that FRC requires higher cement and higher fine aggregate content for maintaining the strength and workability. Beside the grading chart of ACI 544, there are details of different proportions used in different literature. A general range of proportion for normal-weight steel fibre reinforced concrete is given in ACI 544. Trial batches of concrete with different fibre proportion are made to arrive at most appropriate proportion. Fibre characteristics such as length, length-diameter ratio and shape play an important role. Workability problem in case of polymeric fibres can be solved by using high range of water reducing admixtures. Aggregate gradation and mixing sequences have to be adjusted to control the amount of entrapped air.

The maximum sized aggregate (MSA) of the concrete for this research is selected as per the guidelines given in ACI 544 (2002), wherein it is mentioned that for steel fibre fraction of 1% in the concrete, the MSA should be 10mm. Design mix for both types of mix are kept same. Cement content and w/c ratio is 372 kg/m^3 and 0.5 respectively. Design mix details are given in Appendix A. Sika Plastocrete super plasticizer (modified naphthalene formaldehyde sulphonate) is mixed with water in dosage of 12 gm per kg cement. Fibres are added to the concrete mix at the end to ensure that proper fibre dispersion is achieved and fibre balling as well as clumping do not occur. The procedure of HyFRC mixing is illustrated in Figure 3.2. Steel fibre used in this research with 45^o hooked ends which are generally deformed slowly during pull-out from concrete ensuring a controlled ductile failure. However, it is seen that adding a large dose of relatively long and stiff steel fibres into concrete may cause workability problems. The polypropylene fibre used in this research prevents the micro cracks, which is developed due to shrinkage during hydration, making the concrete inherently stronger. The post cracking behaviour of concrete continue to absorb energy as fibres pull out.

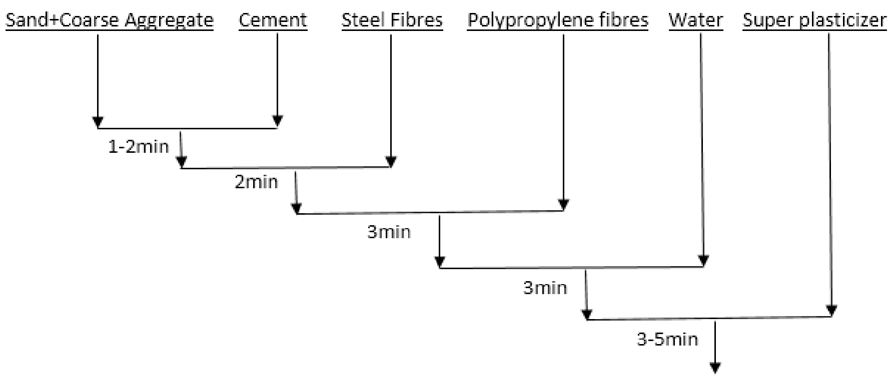

Figure 3.2. Mixing procedure of different constituents in HyFRC

The workability of the HyFRC concrete is tested by Vee-Bee test in accordance with IS 10510:1983, which is a more appropriate test for workability. The freshly mixed concrete is packed into a cone similar to that used for the slump test. The cone stands within a special container on a platform, which is vibrated at a standard rate. After the cone is lifted off the concrete, the time taken for the concrete to be compacted is measured. Vee-Bee time ranges from one second for flowable concrete to more than fifteen second for stiff concrete. Unlike the slump test, the Vee-Bee time test gives useful results for stiff concrete. Figure 3.3 shows a photograph of Vee-Bee test apparatus. Vee-Bee test is carried out for all the mixes considered in the present study and Vee-Bee time is found to lie in the range of 9-12sec.

Figure 3.3. Vee-Bee Consistometer

3.2.1 Evaluation of compressive strength

The average compressive strength of conventional concrete is found to be 34.9 MPa and that of HyFRC is 35.1 MPa. A typical compressive stress-strain curve of both the type of concretes is shown in Figure 3.4. Though compressive strength of HyFRC is not much higher than that of conventional concrete, but the post crack behaviour of HyFRC is far superior to that for conventional concrete.

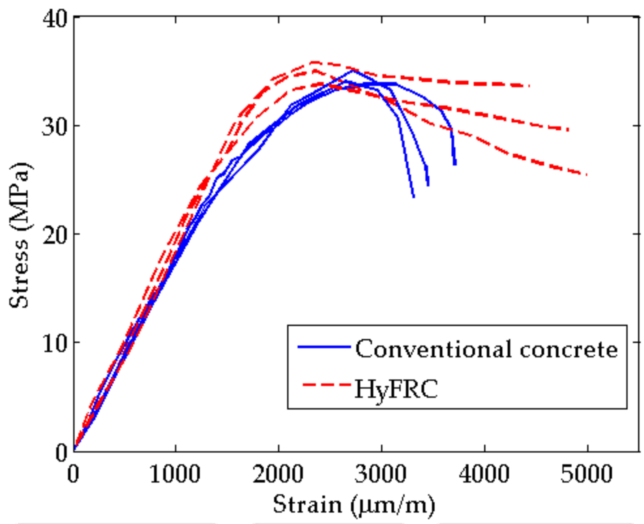

Figure 3.4. Compressive stress-strain curve of concrete

3.2.2 Evaluation of split cylinder strength

Average tensile strength of conventional concrete is found to be 2.6 MPa and that of HyFRC cylinders is 2.83 MPa. A typical tensile stress-strain curve of both the concrete types is shown in Figure 3.5.

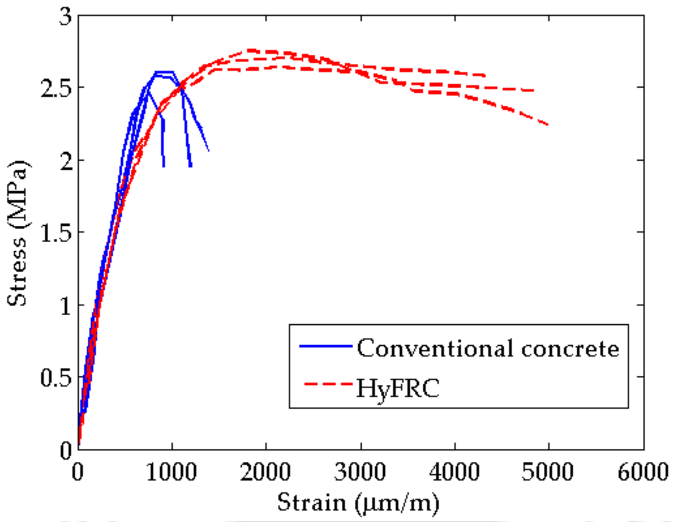

Figure 3.5. Tensile stress- strain curve of concrete

3.2.3 Four point bending test

Tests for the evaluation of flexural toughness of conventional concrete and HyFRC specimens having different combinations of fibres are carried out in accordance with ASTM C1018 (1989). All the specimens are cast without any reinforcement bars. Two prisms (700 mm x 150 mm x 150 mm) are considered for each of the cases and are tested under third point loading.

Available literatures are reviewed for arriving at the best proportion of steel and polypropylene fibres. Qian et al. (2000a) concluded that synthetic fibre proportion should be limited to 0.15% to get increased compressive strength value. Soleimani (2005) reported that FRCs containing 1% macro steel fibres are the best composites for flexural toughness. A limited number of experimental studies are previously conducted on toughness evaluation of HyFRC specimens in India. These tests results from researchers in India are important as the fibres to be used in the current experiments are from local industry. The experimental programs of Sivakumar and Santhanam (2007) and Ganesan et al. (2014) are found to be the most relevant for the present study in arriving at the appropriate volume fraction of HyFRC to be adopted. Sivakumar and Santhanam (2007) carried out an experimental investigation on high strength concrete reinforced with hybrid fibres (combination of hooked steel and a non-metallic fibres – polypropylene, polyester and glass). Among all hybrid fibre combinations, steel of 0.38% volume fraction and polypropylene of 0.12% volume fraction combination performed better in all respects. It is observed that the decrease in toughness is higher when the proportion of non-metallic fibre is increased. Ganesan et al. (2014) carried out an experimental investigation to study the effect of hybrid fibres on the strength of beam column joints subjected to cyclic loads. The combination of 1% volume fraction of steel fibres and 0.15% volume fraction of polypropylene fibres exhibited better performance with respect to energy dissipation capacity and stiffness degradation in comparison to other considered volume fraction combinations. Fibre proportion to be adopted in the subsequent test of bridge pier model is arrived at by carrying out trial tests on 26 prism specimens, where total volume fraction is varied in the range of 0.95% - 1.4%. The details of different volume fraction considered is presented in Table 3.6.

Table 3.6. Details of different fibre volume fraction

Specimen Type	SF1 (%)	SF2 (%)	PP - I (%)	PP - II (%)
PL	-	-	-	-
A1	0.4	0.4	0.15	-
A2	0.4	0.4	0.2	-
A3	0.5	0.5	0.15	-
A4	0.5	0.5	0.2	-
A5	0.6	0.6	0.15	-
A6	0.6	0.6	0.2	-
B1	0.4	0.4	-	0.15
B2	0.4	0.4	-	0.2
B3	0.5	0.5	-	0.15
B4	0.5	0.5	-	0.2
B5	0.6	0.6	-	0.15
B6	0.6	0.6	-	0.2

3.2.3.1 Loading characteristic and test frame

All prism specimens are tested for the determination of flexural toughness. Appropriate loading arrangement are made using 100 kN capacity servo-hydraulic actuator (make: MTS Inc., USA) having stroke length of 125 mm as shown in Figure 3.6. Tests are performed in displacement control mode in order to capture post peak behaviour. This test is carried out (Figure 3.6) by third point loading with middle third (200mm) under vertical load and the test is carried out to track the post crack behaviour until complete loss of load carrying capacity of the prism specimens. The area under the load deflection curve is used to evaluate the total strain energy stored or equivalent toughness of the specimen. One Linear Variable Displacement Transducer (LVDTs) is used to record the deflection continuously.

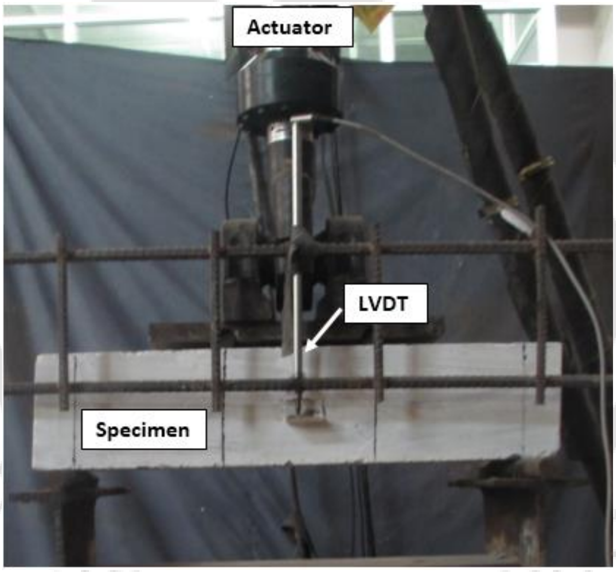

Figure 3.6. Arrangement for testing of prism specimen

3.2.3.2 Testing procedure

Fibre reinforced concrete, because of its high energy-absorption capability, is a noble material for numerous applications. This energy absorption capability is termed as “toughness”. The best fibre proportion is judged on the basis of toughness. There are many available procedures to evaluate toughness of FRC. The most common method to measure toughness is to use the load deflection curve obtained using a simply supported beam loaded at the third points (four point bending). The two widely used test methods are the ASTM C 1609 (1989) standard test method and the Japan Society of Civil Engineers (JSCE) standard SF 4 (1983) method. However, the basic limitation of both the methods is primarily due to the fact that the evaluation involves identification of first crack in the load-deformation curve, which is not always easy. In the present study, though flexural tests are performed in accordance with ASTM C 1018 (1989), the evaluation of toughness is done by using the post crack strength (PCS) method proposed by Banthia and Trottier (1995), where the identification of first crack is not required (Figure 3.7).

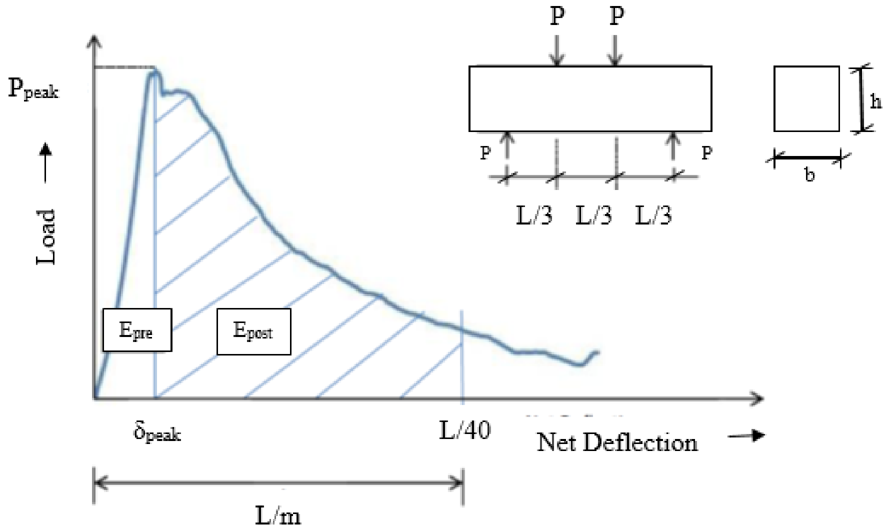

Figure 3.7. PCS Technique (Banthia and Trottier, 1995)

PCS is calculated in the post peak region at deflection of *L/m*. The value of *m* can be chosen depending on the concrete strength and for the present study the value of *m* is taken as 40 i.e. for a maximum deflection of 15mm. PCS is defined by the equation:

$$PCS = \frac{E_{post} \times L}{\left(\frac{L}{m} - \delta_{peak}\right) bh^2} \tag{3.1}$$

3.2.3.3 Results

Figure 3.8. Final damaged state after testing of conventional concrete specimen

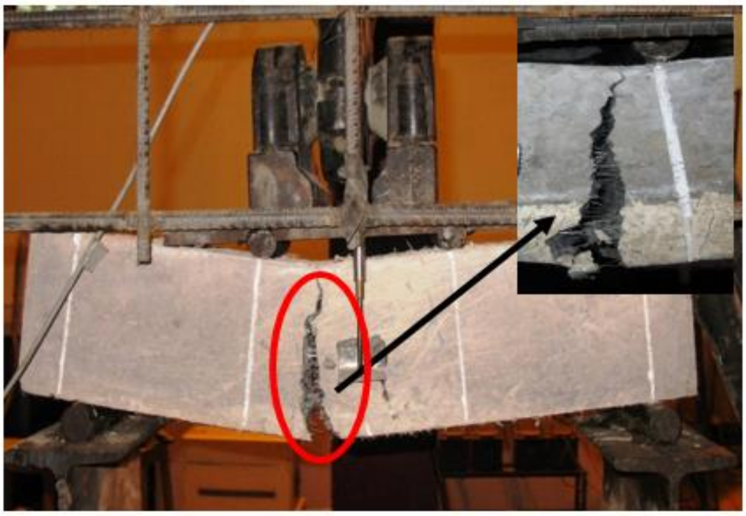

Figure 3.9. Final damaged state after testing of HyFRC specimen

Figure 3.8 and Figure 3.9 shows the failure states of tested prisms and Table 7 shows the detailed experimental results. The conventional concrete specimen shows a highly brittle failure mode while HyFRC specimens shows substantial improvement in the ductility. Bridging of cracks by the fibres helps in improving the ductility in HyFRC specimens. The load carrying capacity as well as modulus of rupture of HyFRC specimens are also observed to be higher than those of conventional concrete specimens (Table 3.7). The major improvement is seen however in the values of toughness of HyFRC specimens, which is observed to be 5.5-8.7 times than that for conventional concrete specimens. Thus, a great improvement is observed in the energy dissipating capacities of HyFRC specimens for the specimens tested with different combinations of fibres and their volume fractions.

Figure 3.10 shows typical individual load deflection curves of the tested prism specimens. It can be seen that after attaining the peak load, there is total loss of load carrying capacity for conventional concrete (PL) prism. However, all the HyFRC specimens attained higher peak load and also their first crack appears at displacement larger than that of conventional concrete specimen. Further, all the HyFRC specimens continue to carry some load till the deformation is significantly large. This property of HyFRC results in increasing their toughness in comparison to that of conventional concrete.

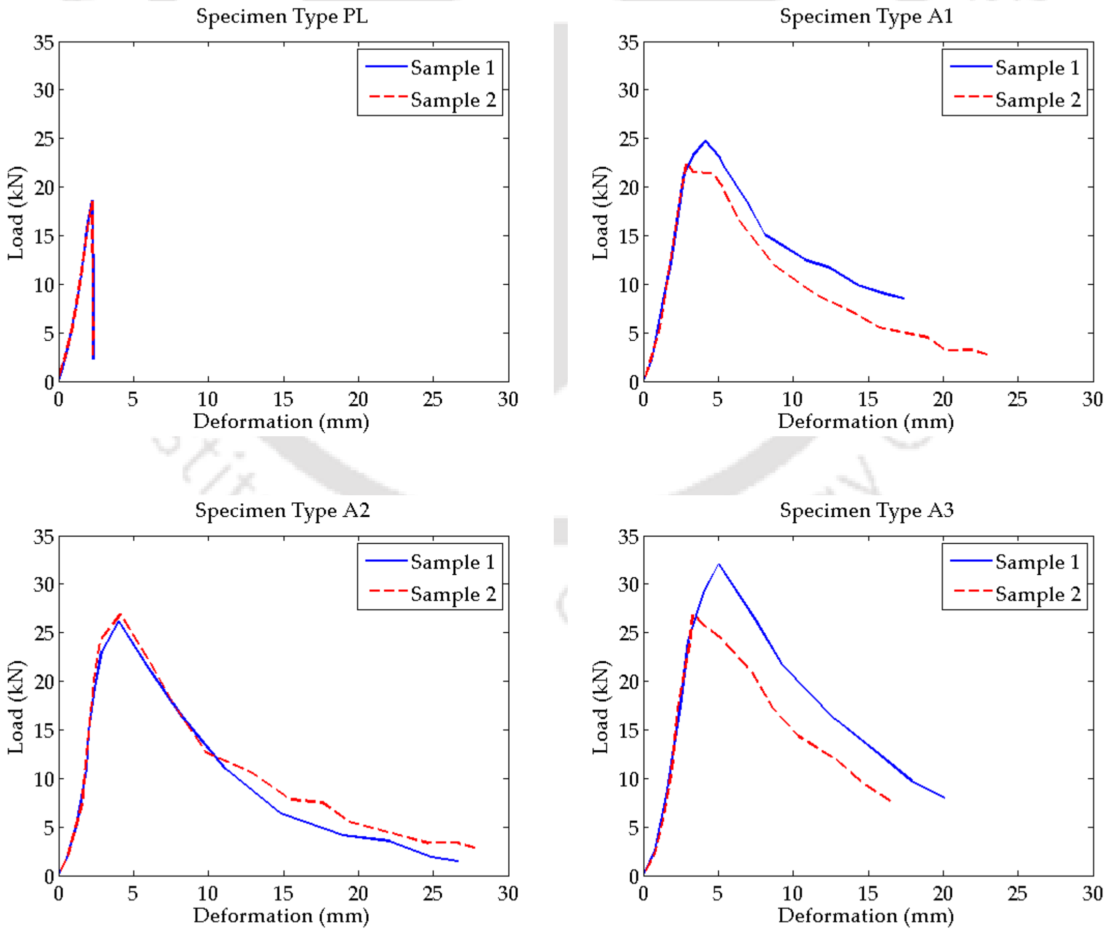

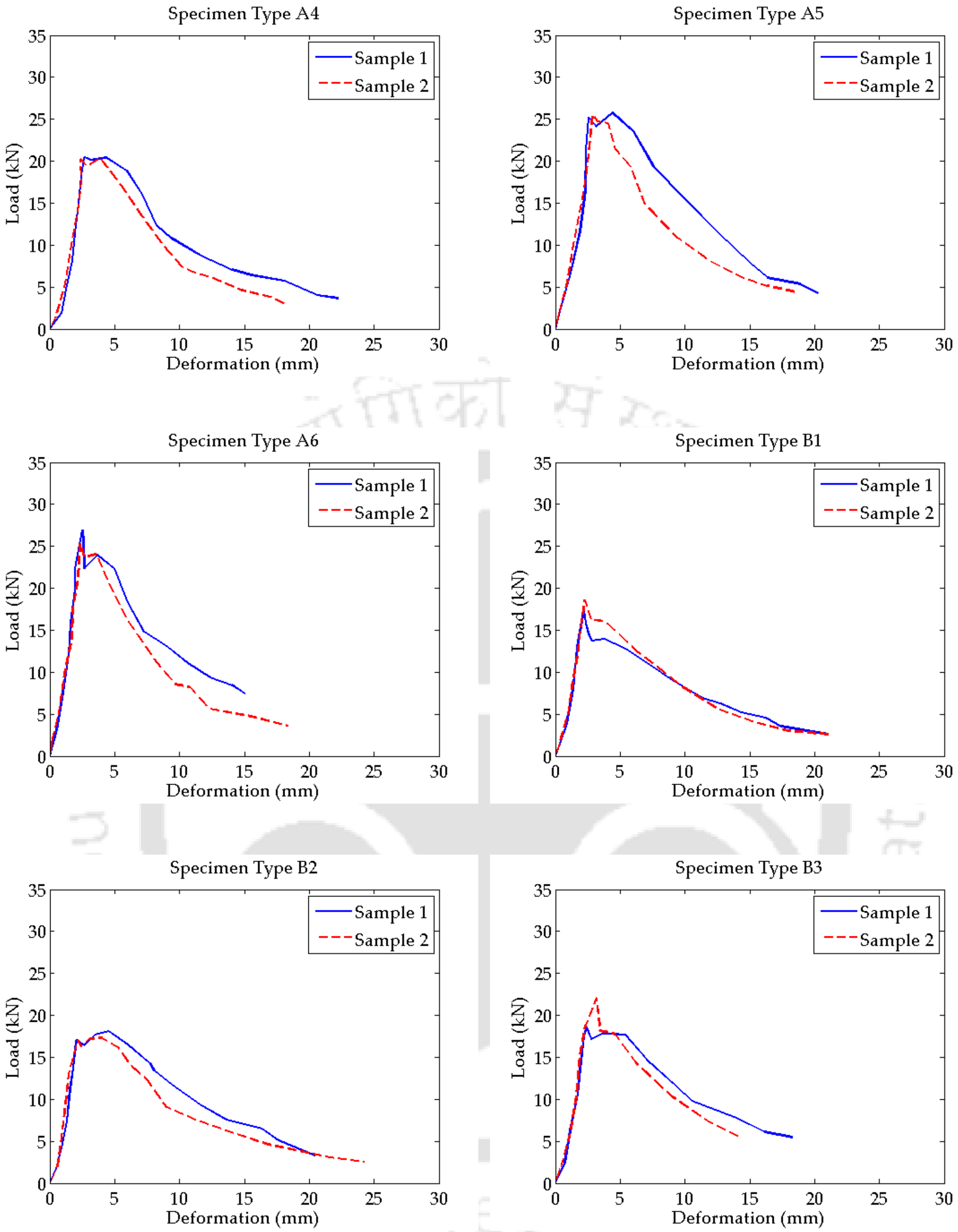
Specimen Type A4
Specimen Type A5
Specimen Type A6
Specimen Type B1
Specimen Type B2
Specimen Type B3
Sample 1
Sample 2
Load (kN)
Deformation (mm)
0
5
10
15
20
25
30
35

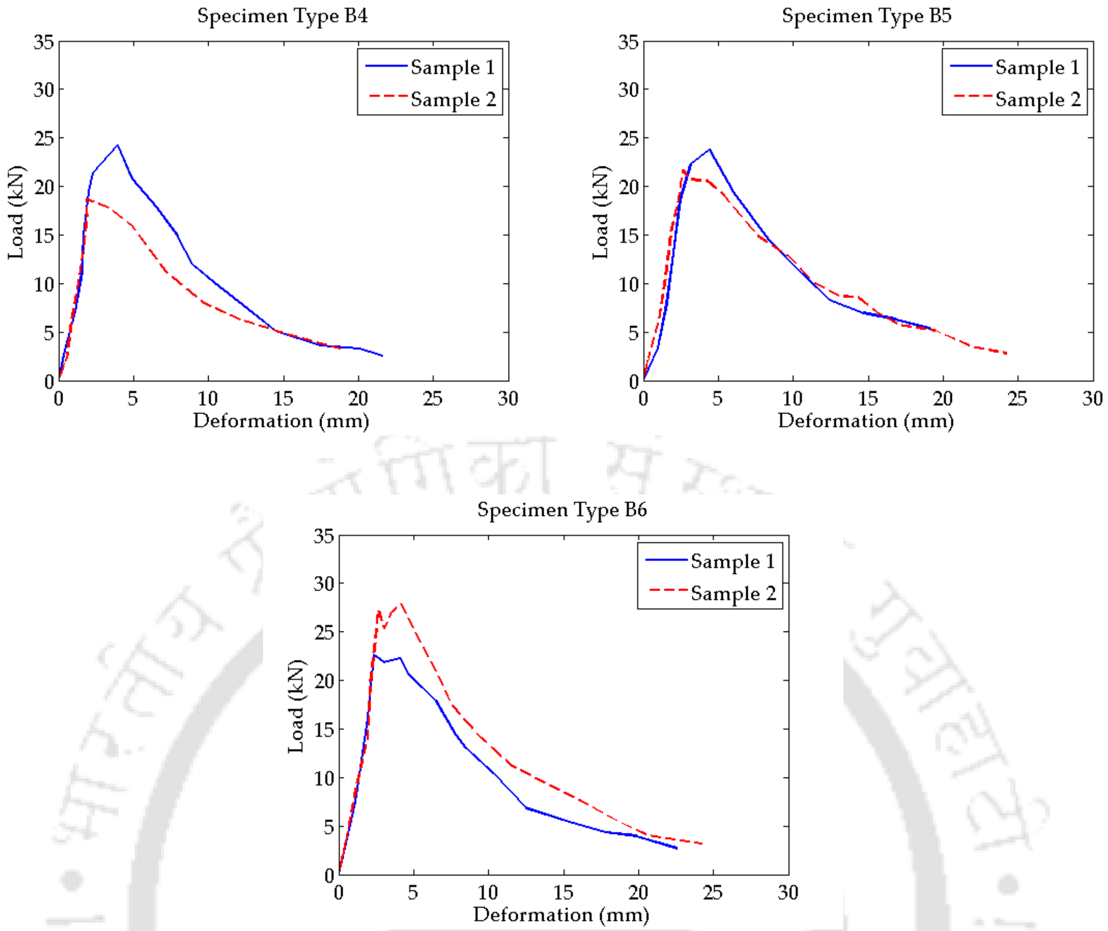

Figure 3.10. Load vs Deformation plots of different prism specimens from four point bending test

The magnitude of toughness is calculated from each of the load-displacement plot for conventional concrete specimen as well as for specimens with different combination of fibres. The evaluated toughness values are shown in Table 3.7. From the present experimental study, the best toughness is achieved with combination designated as A3 i.e. steel fibres (with two different aspect ratio as mentioned in Table 3.6) with 0.5% (SF1) and 0.5% (SF2) by volume fraction and 0.15% polypropylene (Recron 3s) by volume fraction. Kheni et al. (2015) and Ganesan et al. (2014) also used same proportions of fibres in their study. It may also be mentioned that all the HyFRC specimens have performed very well compared to the conventional concrete specimen. HyFRC specimens are observed to undergo much higher ultimate displacements, thus leading to a more ductile type of failure mode.

Table 3.7. Toughness evaluation of the prisms

Specimen Type	Average compressive strength (MPa)	Maximum load applied to the specimen (KN)	Toughness (J/m^3)	Modulus of rupture (MPa)
PL	34.23	18.27	0.34	3.9
A1	34.96	24.8	2.47	5.8
A2	33.65	27.44	2.67	5.7
A3	35.31	28.16	2.97	6.7
A4	34.22	20.18	2.11	4.9
A5	33.44	25.82	2.54	5.6
A6	34.6	25.07	2.57	5.7
B1	34.04	19.54	1.91	4.8
B2	34.65	17.98	1.87	5.1
B3	33.98	20.73	2.22	5.8
B4	34.17	22.32	2.45	4.3
B5	33.34	23.41	2.53	5.1
B6	34.16	25.1	2.61	5.2

3.3 TEST PROGRAM (PART II) –EVALUATION OF POSSIBLE REDUCTION IN SHEAR REINFORCEMENT IN HYFRC SPECIMENS

3.3.1 Details of test specimen

It is observed from literature review that the hybrid fibre reinforced concrete has superior shear resistance as compared to conventional concrete. Kumar et al. (2011) studied SC-HyFRC specimens with 50% lesser transverse reinforcement as compared to conventional RC bridge pier for improving ease of concreting and such HyFRC specimen also exhibited comparable seismic performance. It is noted that reduced transverse reinforcement in fibre reinforced specimen would also help in reducing honey comb formation in concrete at the time of casting as HyFRC has relatively lower workability. This is particularly important in the areas like beam-column joints and bridge pier-foundation interface, where congestions due to reinforcements are quite likely. In the provision included in the ACI 318 (2008)), it is allowed to use deformed steel fibres in volume fractions greater than or equal to 0.75% as minimum shear reinforcement in normal-strength concrete beams. In the present test program, the possibility of reduction in shear reinforcement is explored by conducting four point bending test on the prism specimen. Standard prism specimens of 150×150×700 mm with four numbers of 10 mm diameter longitudinal reinforcement are cast with the best fibre proportion evaluated from the section 3.2. Stirrup for conventional concrete specimen is 8 mm diameter @ 90 mm c/c, while that of HyFRC specimen is 8 mm diameter @ 180 mm c/c i.e. spacing for stirrups for HyFRC specimen is twice that of conventional concrete specimen as shown in Figure 3.11. Details of the design for stirrups as per IS 456 (2000) is given in Appendix B. Fe 500 grade TMT bars are used for both longitudinal and transverse reinforcements. The difference in detailing between specimen with conventional concrete and HyFRC can be seen from reinforcement cage in Figure 3.12. While casting the test specimen, vibrating table is used to for achieving proper compaction. Details of preparation of prism specimens is shown in Figure 3.13. Two specimens cast with conventional concrete and two with HyFRC are tested for comparison.

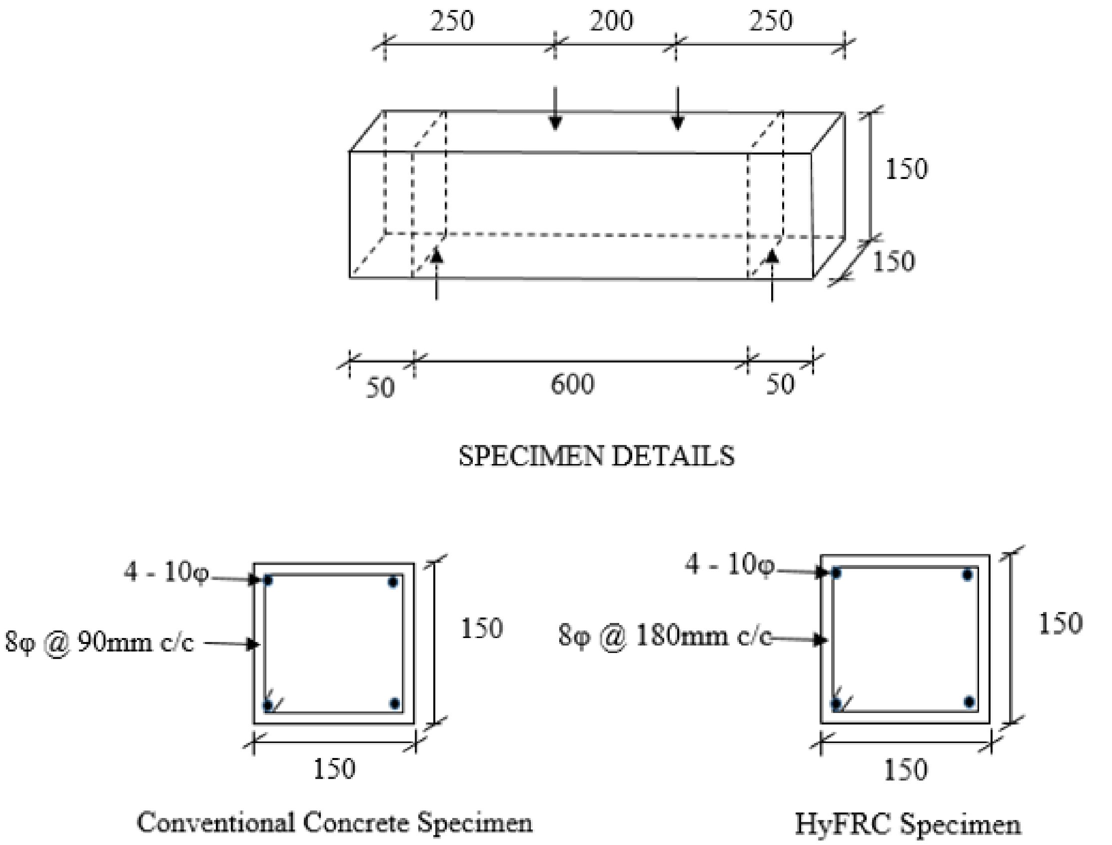

Figure 3.11. Reinforcement detailing of the prism specimen

(a) (b)

Figure 3.12. Reinforcement cage for (a) conventional concrete specimen (b) HyFRC specimen

Figure 3.13. Casting of prism specimen

3.3.2 Loading characteristic and test frame

Four prism specimens are tested for the evaluation of flexural toughness through four point bending test. The loading arrangement is done using 1000 kN capacity servo-hydraulic actuator (make: MTS Inc., USA) having stroke length of ±250 mm. The other details related to the test procedure are similar to section 3.3.1.

3.3.3 Results

The failure pattern of both the specimens after test is shown in Figure 3.14.

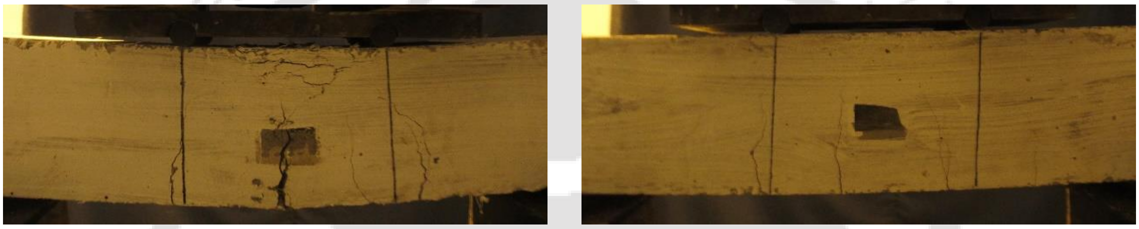

(a) (b)

Figure 3.14. Failure pattern of specimen after test (a) conventional concrete (b) HyFRC

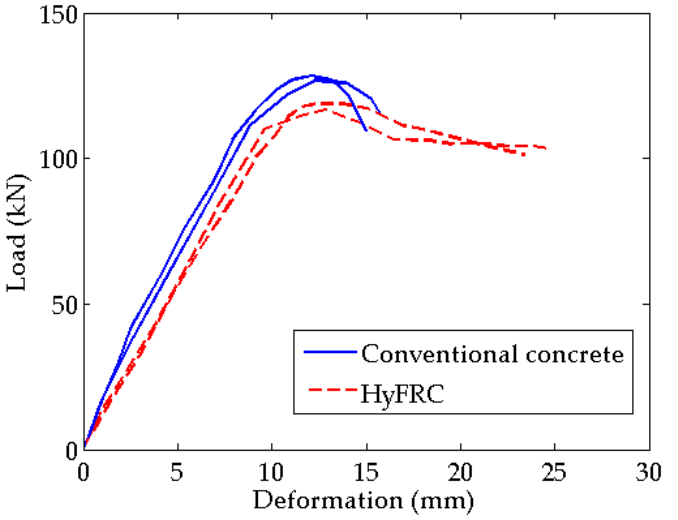

Figure 3.15. Load vs deformation curve of reinforced prism specimens

Reinforced HyFRC specimen showed marginally lesser (3%) load carrying capacity as compared to reinforced concrete specimen with designed shear reinforcement. Table 3.8

shows the details of experimental results with conventional concrete and HyFRC specimens. The test results of specimens without reinforcements are also included for comparison. Further, from the load deformation curve in Figure 3.15, it is seen that HyFRC specimens maintain a stable behaviour after the initiation of first crack, which indicates higher energy dissipation capacity of these specimens than that of the conventional concrete specimen. The test results are quite encouraging since with 50% reduction in shear reinforcement, HyFRC specimen still exhibits load carrying capacity similar to specimen with conventional concrete and design shear reinforcement as per IS code requirement. The failure mode is far more ductile, which is always desired for structures in seismic zones.

Table 3.8. Summary of experimental results

Specimen Type	**Average f_c (MPa)**	**Average P_u for unreinforced (kN)**	**Average P_u for reinforced (kN)**
Conventional Concrete	34.23	18.27	127.23
HyFRC	35.31	28.16	117.46

* *Pu = Peak load and fc = Cube compressive strength*

3.4 Concluding Remarks

In this chapter, detailed testing is carried out for arriving at the best fibre proportions (1% steel and 0.15% polypropylene fibres) for HyFRC specimens from the viewpoint of enhancements in toughness. Further, four point bending tests are carried out on prisms to explore the possibility of reduction in shear reinforcement in HyFRC specimens. Reduction of shear reinforcement by 50% in HyFRC specimens is observed to provide almost similar load carrying capacity as that of specimens made of conventional concrete and with reinforcement as per IS code. Best performing proportions of fibres and 50% reduction in shear reinforcements are considered in the experimental investigations of HyFRC bridge piers in subsequent chapters.

Chapter 4

NUMERICAL MODELLING OF BRIDGE

4.1 GENERAL

The present study is broadly focused on the hybrid simulation of a bridge with its pier made of conventional concrete in one case and HyFRC in another case. The hybrid simulation has both experimental module as well as numerical module. The experimental module would be discussed in details in the next chapter, where other details of hybrid simulation of the sample bridge is introduced. The laboratory testing of structural elements are very much involved and hence any repetition of tests with slight modification in structural, material or loading properties is not easily achievable. Thus, in order to design the laboratory requirements in hybrid simulation for the present study, a prior analysis of the entire bridge system using a numerical model is undertaken. Numerical modelling of the sample bridge is carried out for ascertaining the range of maximum displacement, strain etc., which are useful in deciding selection of actuator of specified stroke length, range of LVDT, strain gauge type etc.

Further, numerical model is an integral part of the hybrid simulation, where the elements of the sample prototype structural system without any probable uncertainty are modelled using finite elements and become part of the numerical module. The elements with likely uncertainty in load-displacement characteristics constitute the experimental element in hybrid simulation. In this research work, circular reinforced concrete piers, made of both conventional concrete and HyFRC, are considered as experimental elements. Scaled models of bridge piers are cast in the laboratory, while the remaining parts, i.e. the entire bridge deck is modelled numerically.

Large library of material models, elements and analysis commands make OpenSees program a powerful tool for numerical simulation of any structure. This chapter presents the steps to develop 3D finite element model of a bridge in OpenSees. Detailed responses are evaluated using nonlinear static and nonlinear time history analysis of the bridge models with piers made of conventional concrete and HyFRC. It may however be mentioned that the numerical model considered at this stage are likely to have errors. Numerical model is subsequently improved by model calibration, which is presented in detail in Chapter 6. The experimental observation from hybrid simulation as reported in Chapter 5 is used for the numerical model calibration. The updated numerical model would simulate responses of bridge structural system close to realistic level.

4.2 Numerical Model of Bridge Structure

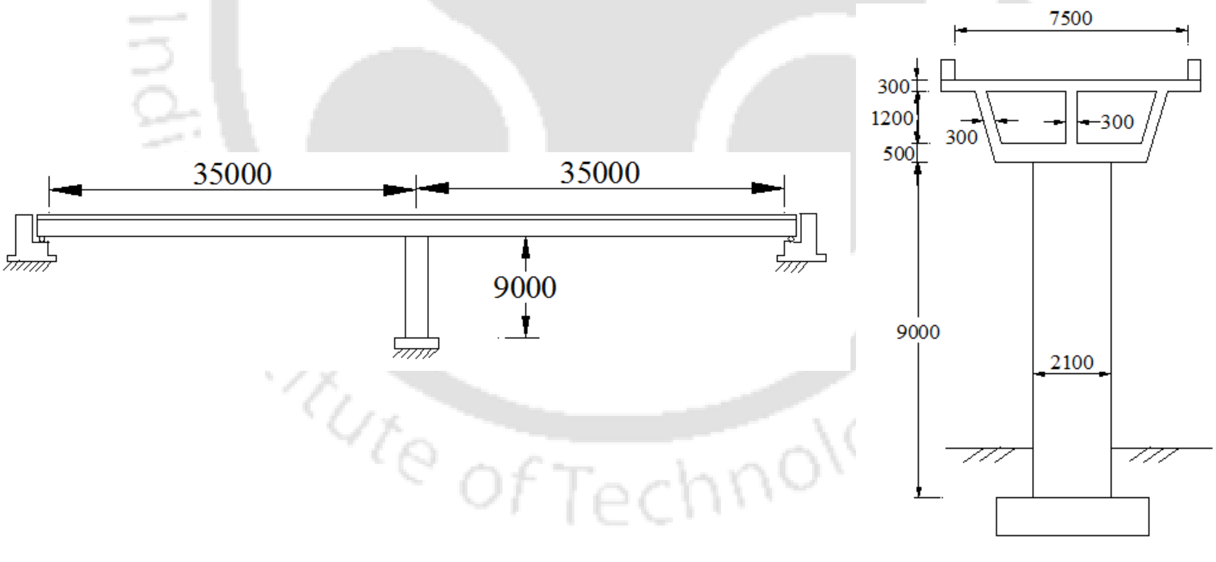

Figure 4.1. Elevation of Prototype Bridge (All dimensions are in mm)

A prototype bridge in Tripura, India is considered in the present research work (Figure 4.1). The bridge is semi-integral type, where the superstructure is integrally connected to pier. Appropriate boundary conditions are maintained at both ends for facilitating any horizontal movement due to thermal, vehicular or seismically induced events. 3D finite element model of the full scale bridge is created using the numerical platform OpenSees developed by McKenna (1997). A schematic representation of the considered bridge along with the FE model are shown in Figure 4.2. Details of modelling of various components of bridge along with material and mass are presented in the following subsections.

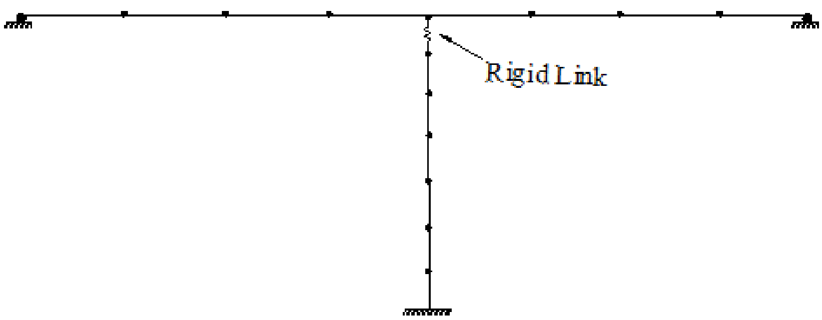

Figure 4.2. Three dimensional finite element model of the bridge

4.2.1 Modelling of Superstructure

The superstructure of a bridge refers to the portion of the bridge above the pier top. The deck of the bridge represents the superstructure and is assumed to remain elastic during earthquakes. The deck is thus modelled using the *elasticBeamColumn* element available in OpenSees platform. The 3D elastic element requires cross-sectional area *A*, Young's modulus of elasticity *E*, torsional moment of inertia of cross-section *J*, and second moment of area about the local axes (I_z, I_x) as input. The element has 6 degree of freedom per node (3 translational, 3 rotational). The element orientation with its local and global coordinate system and degrees of freedom are shown in Figure 4.3. The superstructure is discretized using *elasticBeamColumn* element and 8 numbers of elements of equal length are considered as shown in Figure 4.2 . Based on tributary length, lumped masses are assigned to each nodes. The imposed boundary conditions at the deck ends are as follows:

- Restrained degrees of freedom: vertical (U_Y) and transverse displacement (U_Z)

- Restrained torsional rotation (R_X)
- Remaining degrees of freedoms are unrestrained

For RC bridge, the deck parts are much stiffer under in-plane loading and thus behave like rigid diaphragm. Although the response of the bridge system is not that sensitive to any small variation in stiffness of the deck, it is sensitive to the mass of the deck. Therefore, care is taken to accurately model the mass of deck by considering appropriate discretization of the superstructure. The sectional properties of the deck of the bridge under study are given in Table 4.1

Table 4.1 Sectional properties of the deck

E (kN/m^2)	I_z (m^4)	I_y (m^4)	Area (m^2)	Weight (kN/m)
2.96 x 10^7	1.25	1.57	3.91	125.43

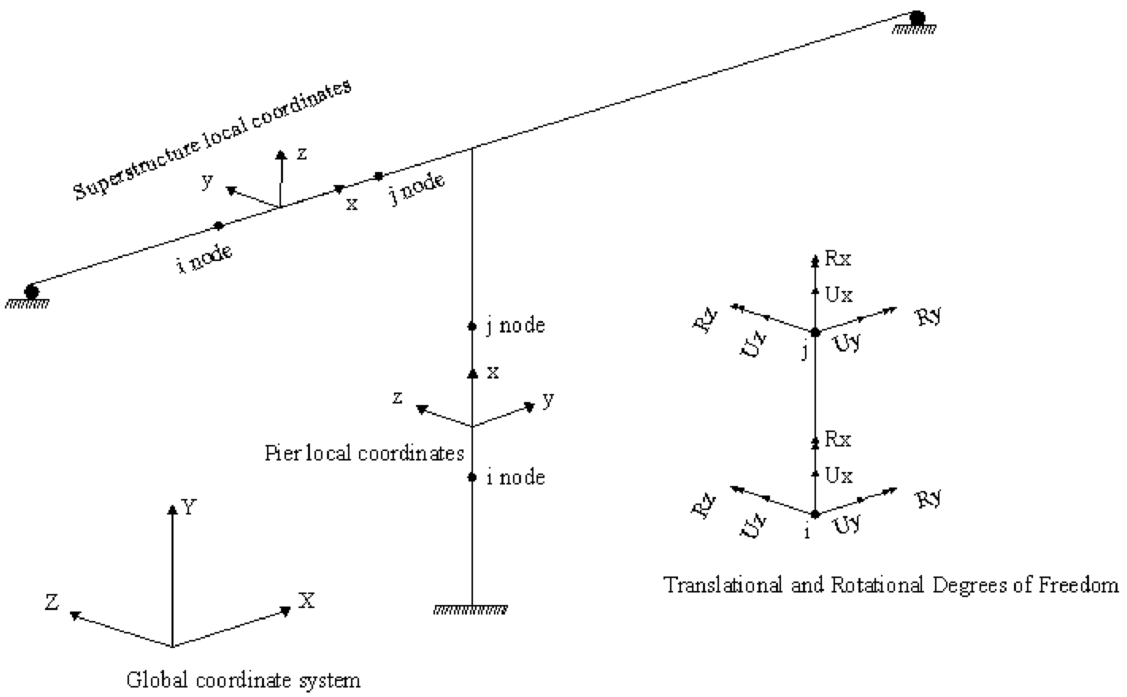

Figure 4.3. Representation of local and global coordinate system and degrees of freedom of the bridge

4.2.2 Pier modelling

The pier, which is expected to exhibit inelastic response under earthquake is modelled with *dispBeamColumn* element of OpenSees using the *FiberSection* approach, which considers spread of plasticity along the length of the element. The *dispBeamColumn* element is formulated using displacement-based approach and follows standard finite element procedures, where section deformations are interpolated from an approximate displacement field, then the principle of virtual displacement is used to form element equilibrium relationship. Constant axial deformation and linear curvature distribution are enforced along the element length to approximate nonlinear element response. Further, sufficient refinement of the pier model is needed to represent higher order distributions of deformations and accordingly, the pier is discretized into 6 elements. The element orientation and degrees of freedom are shown in Figure 4.3. The cross-section is defined using *FiberSection* approach with circular concrete patches and circular layers of reinforcement. *Fibersection* allow the creation of a composite section such that the constituent materials are appropriately placed at desired spatial locations. For illustration purposes, the fiber discretization of the circular columns is given in Figure 4.4. The boundary condition of pier is considered as fixed at the pier-foundation interface.

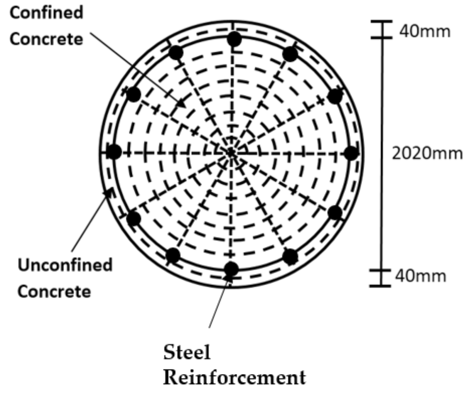

Figure 4.4. Fiber discretization of pier section

4.2.2.1 Material modelling

The major benefit of using *FiberSection* to model the RC sections is that it allows for the specification of different material properties at different location through the cross-section. The concrete is modelled using the *Concrete04* model available in OpenSees program. *Concrete04* material model is used to model a uniaxial concrete material as proposed by Popovics (1973). This material use degraded linear reloading stiffness as proposed by Karsan et al. (1969) and tensile strength with exponential decay. The parameters of *Concrete04*, namely, the peak compressive strength (f_c), strain at peak compressive stress (e_c), strain at crushing strength (e_{cu}), maximum tensile strength (f_{ct}) and ultimate tensile strain (e_t) are obtained from the results of compressive test of concrete cube and split cylinder test of concrete. The stress-strain curves for conventional concrete and HyFRC are shown in Figure 4.5 and Figure 4.6 respectively. These are developed utilizing the laboratory based material test data. The reinforcing steel is modelled as a bilinear material with kinematic hardening using OpenSees *Steel01* material. Based on laboratory test, yield strength of steel is taken as 500 MPa and elastic modulus of steel is considered as 200 GPa. A strain hardening value of 0.018 is used for this material.

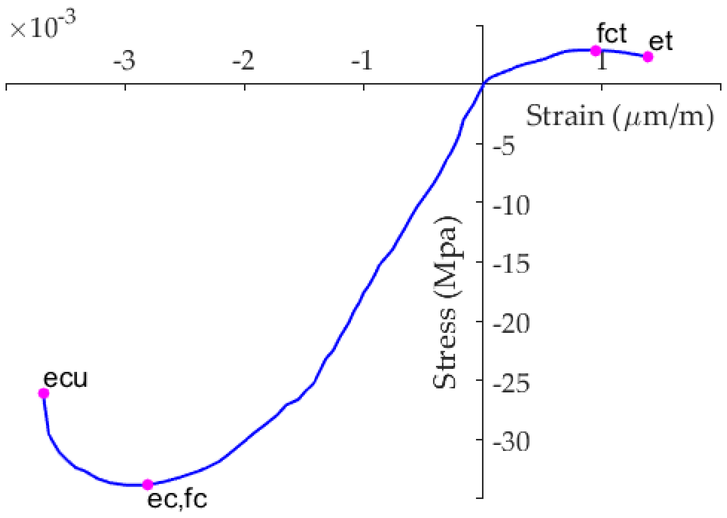

Figure 4.5. Stress-Strain curve for conventional concrete

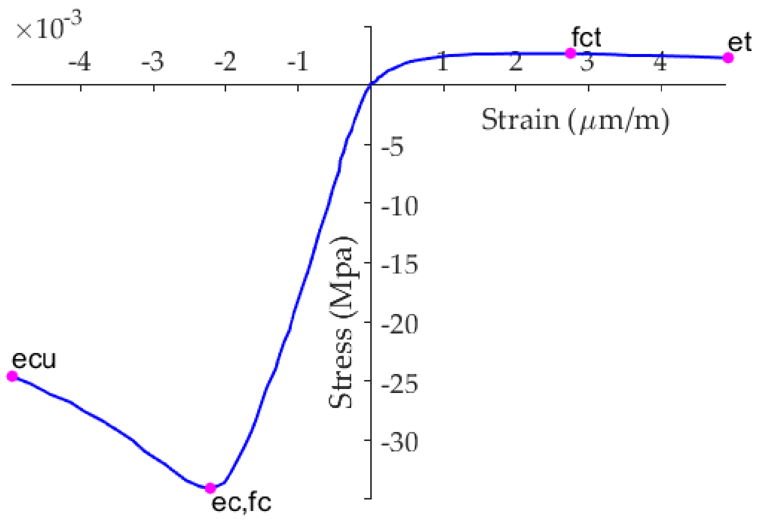

Figure 4.6. Stress-Strain curve for HyFRC

4.2.2.2 Modelling of mass

It is important that the mass of the bridge components are quantified accurately as the seismic response of a bridge is sensitive to mass (Nielson 2005). Preferably, all bridge elements should be approximated with a distributed mass along their length. However, OpenSees along with other finite element software use the concept of lumped mass at each node, where masses of elements are lumped based on tributary lengths. As suggested by Aviram et al. (2008), deck should be sufficiently discretized and translational masses are lumped at each node based on tributary length. The translational mass of the deck is calculated as the volume of the element multiplied by the density of the concrete. The translational mass of the pier is also lumped at the respective nodes based on the tributary length. The rotational masses are not considered as the bridge is straight and torsional behavior is not significant.

4.2.2.3 Modelling of damping

Damping is an energy-dissipation mechanism that results in the decay of motion in a vibrating linear or nonlinear system under the action of external exciting forces or imposed deformations. Damping of the bridge depends on the condition of the bridge. For instance, the recommended damping values (Newmark 1982) for reinforced concrete bridges with considerable cracking undergoing small deformation or subjected to low intensity ground motion is estimated at 3–5% of critical damping. However, for a yielding bridge structure, the hysteretic behavior and structural damage occurring in ductile components due to severe seismic conditions is estimated at 7–10% of critical damping for bridges (Aviram et al. 2008). Since the damping depends on the condition of the bridge i.e. whether it’s cracking or yielding, for initial numerical model, damping is taken as 5 % of critical as prescribed in various design codes for reinforced concrete structures. It is noted here that this damping will be updated in the later stage when calibration of the model will be done using response from hybrid simulation.

The Rayleigh damping approach is used to construct damping matrix for dynamic analysis by considering a constant value of damping ratio. In this approach, the damping matrix is assumed proportional to mass and stiffness matrix of the structure and first two modal period of the structure is used to calculate Rayleigh damping coefficients.

4.3 Results from Numerical Analysis

The simulated numerical models of the entire bridge in OpenSees are utilized for the evaluation of responses using both nonlinear static (pushover analysis) as well as nonlinear time history analysis. The modal characteristics of the bridge structure are also evaluated. The evaluated response parameters from numerical analysis are examined carefully for designing the requirements in experimental module of the hybrid simulations.

4.3.1 Modal analysis

Modal or eigenvalue analysis is carried out first to determine the natural periods and mode shapes of the structure. Eigenvalue analysis is performed using OpenSees and the modal characteristics of first two modes are presented in Table 4.2. The fundamental time period is 0.40 sec with the predominant motion being in the longitudinal direction. About 99% of bridge mass is represented by first mode in the longitudinal direction. The second mode is along transverse direction with a time period of 0.32 sec and representing about 92% of mass of the bridge.

Table 4.2. Modal properties of the bridge

Mode No.	Time Period (sec)	Modal Mass Participation factor		
		Longitudinal	Transverse	Vertical
1st	0.40	0.99	0	0
2nd	0.32	0	0.92	0

4.3.2 Nonlinear static analysis

Non-linear static analysis (or Pushover analysis) is one of the methods to predict the lateral response of any structure by considering both material and geometry nonlinearity. The nonlinear static analysis is widely used for seismic performance evaluation of existing or new structures. The analysis provides adequate information on built-in seismic capacity of a structural system to resist earthquake induced shaking. The approach involves applying a lateral load pattern to the gravity load deformed structure. The lateral forces are then monotonically increased in constant proportion with a displacement control at the control node of the structure, until a certain level of deformation is reached. The obtained base shear and the associated lateral movement at the control node at each load increment are plotted. Based on the load-displacement curve, ultimate displacement can be determined which is an estimate of the displacement capacity of the structure. Thus, before finalising the requirements in experimental module of the hybrid simulation, it is important to have an idea from this analysis of the maximum displacement the specimen can undergo before collapse. The available resources can thus be effectively used to carry out the experiment.

Nonlinear static analyses are done on the sample bridge pier models made of conventional concrete and HyFRC. Masses are lumped at the top by considering the tributary mass of superstructure of the bridge. The analyses provide a comparison of capacity of the bridge pier made up of two different materials - conventional concrete and HyFRC. Differences are observed in load-deformation curves of the bridge pier modelled with conventional concrete and HyFRC as shown in Figure 4.7. The load carrying capacity as well as displacement at failure are observed to be higher in HyFRC specimen compared to those from pier with conventional concrete.

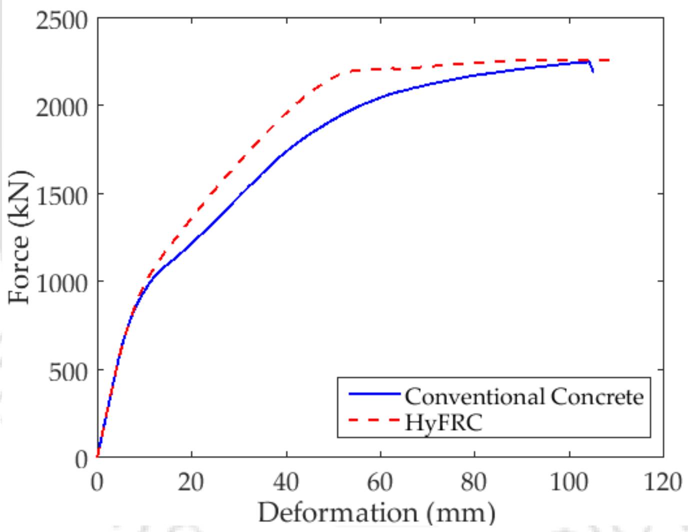

Figure 4.7. Force-deformation curve of bridge pier

4.3.3 Nonlinear time history analysis

Prior to actual hybrid simulation involving both numerical model and experimental elements, a sample nonlinear time history analysis (NLTHA) is carried out for the entire bridge simulated using OpenSees. Separate analyses are carried out for bridge pier made of conventional concrete and HyFRC to observe the influence of HyFRC on the seismic response of the bridge.

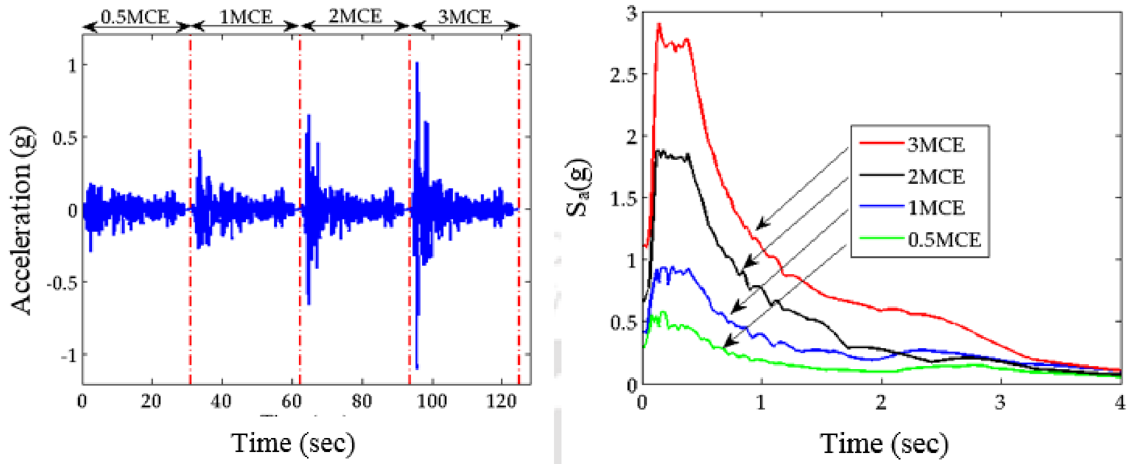

(a) (b)

Figure 4.8. (a) Simulation of scaled El Centro (1940) acceleration time histories for four different intensity levels (b) Simulated response spectra of the four intensity levels

The Elcentro N-S component (1940) ground motion, which is commonly used for seismic performance assessment is used in this study. This ground motion is made compatible with design response spectrum of the case-study bridge location (Zone V of IS 1893 Part I-2002) using WAVEGEN software (Mukherjee and Gupta 2002). The record has a peak ground acceleration (PGA) and duration of 0.319g and 32 sec respectively. This record is scaled to four different MCE levels and the bridge is analysed for all the four ground motions of different intensity levels. These four levels are selected to study structural behaviour in the entire spectrum of damage levels commencing from minor cracking to major damage. The earthquake records comprising of four scaled 32 sec segments applied in sequence is shown in Figure 4.8 (a). The response spectra of the scaled records matched the respective target spectrum for Zone V as per IS 1893 Part I (2002), which are plotted in Figure 4.8 (b). Similar input excitation is used in hybrid simulation presented in Chapter 5.

Gravity loads (self-weight and super imposed dead load) are applied to the specimen as vertical concentrated forces at deck nodes. Gravity forces are calculated as per their respective tributary areas. P–Delta effect is also incorporated in the simulation. The considered acceleration time histories are used for the analysis with time step of 0.02 sec. Rayleigh damping is considered for formation of damping matrix considering 5% damping ratios and time period of 0.40 sec and 0.32 sec for modes 1 and 2 respectively. The *Generalized-Alpha-OS* direct integration scheme available in OpenSees with α = 0.5 is chosen for the integration of the equations of motion. This method is similar to the Alpha-OS scheme originally developed by Nakashima (1988). The algorithm is a combination of the Operator-Splitting technique proposed by Hughes et al. (1979) and the Generalized-Alpha method developed by Chung and Hulbert (1993). The resulting integration scheme is a predictor-one-corrector method that does not require iterative solution algorithms and that inherits the optimized algorithmic dissipation characteristics of the family of Generalized-Alpha methods. The Operator-Splitting technique is utilized to approximate the deviation of the structural response from linearity, which means that the nonlinear resisting forces are expressed as the difference between the corresponding linear-elastic resisting forces and an approximate corrective part. The advantage of the class of Alpha-OS integration methods is that unconditional stability can be achieved without the need to employ computationally expensive, iterative equilibrium solution algorithm (Combescure and Pegon 1997).

As mentioned earlier, two bridges are analysed for a series of earthquake ground motion as shown in Figure 4.8. (a). This is done to illustrate the influence of two different materials to the response of the bridge under seismic loading. Modal analysis shows that the first mode with high modal mass representations is in longitudinal direction. In view of this, the bridge is analysed for seismic loading applied in the longitudinal direction of the bridge.

Figure 4.9 shows the comparison of displacement response from the top of the pier made of two different material types. It is observed here that there is about 13%, 16%, 19 % and 22% reduction in peak displacement of the pier when HyFRC is used instead of conventional concrete for input excitations of 0.5 MCE, 1 MCE, 2 MCE and 3 MCE intensity levels respectively. Further, major advantages of using HyFRC in form of enhanced energy dissipation capability and ductility are discussed later.

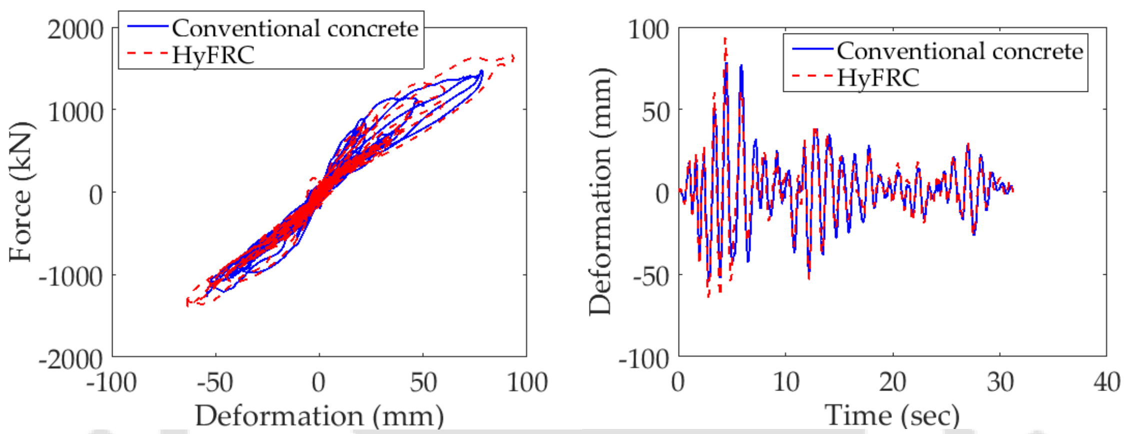

0.5MCE intensity level

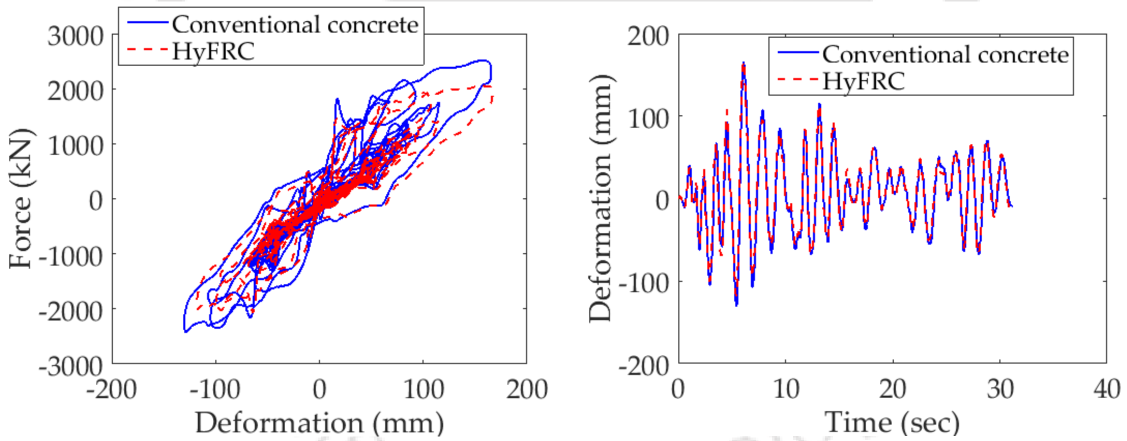

1MCE intensity level

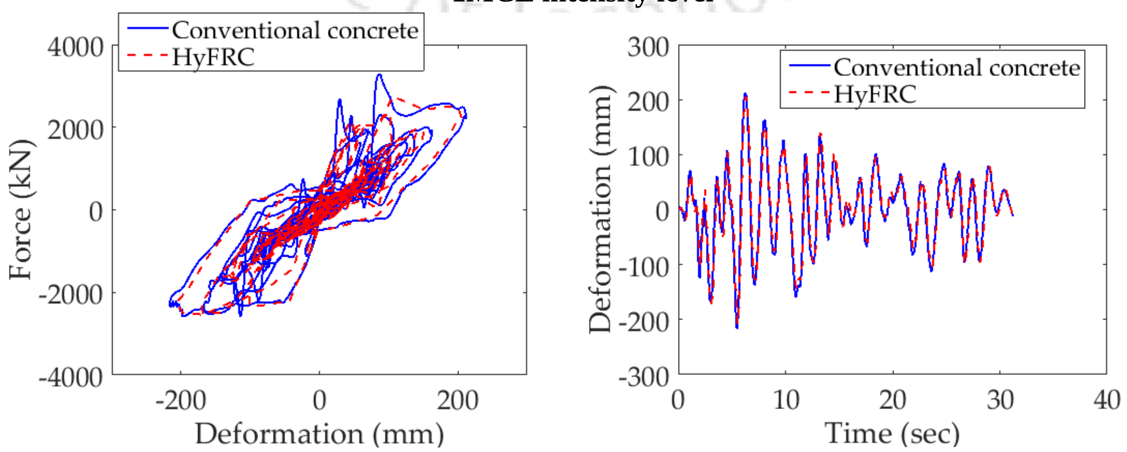

2MCE intensity level

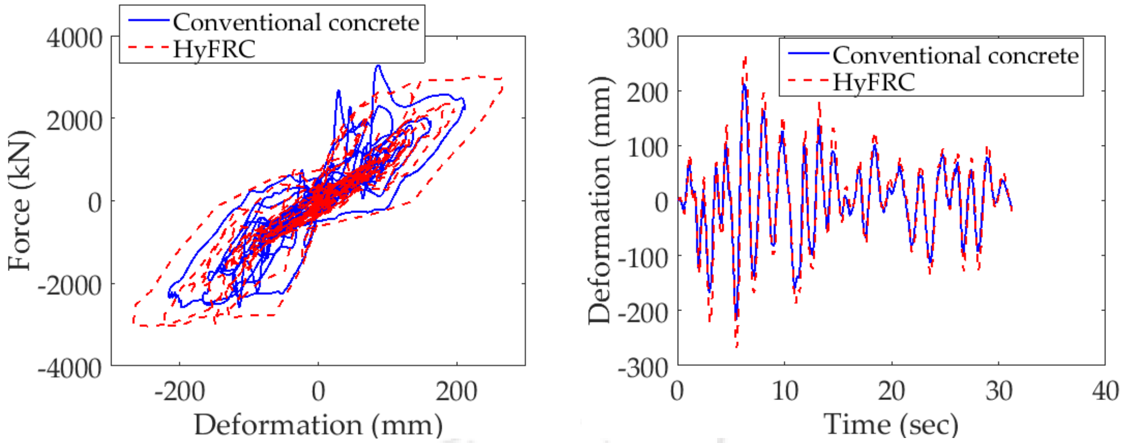

3MCE intensity level

Figure 4.9. Force-displacement response from NLTHA

Table 4.3. Evaluation of peak responses for all intensity levels

Intensity level	For Prototype		For Scaled Specimen	
	Force (kN)	Displacement (mm)	Force (kN)	Displacement (mm)
0.5 MCE	1840.5	65.38	73.62	13.076
1 MCE	2516.4	165.37	100.656	33.074
2 MCE	2677.8	216.14	107.112	43.228
3 MCE	2951.4	310.23	118.056	62.046

4.4 Concluding Remarks

This chapter presents a detailed description of the numerical model of the sample bridge. A 3D finite element model is developed in OpenSees platform and preliminary seismic responses of bridge pier made of conventional concrete and HyFRC are compared using nonlinear static and nonlinear time history analysis. The primary purpose of numerical analysis is to ascertain effectiveness of HyFRC in enhancing seismic performance of the semi-integral bridge. The numerical exercise has also provided some important data for finalization of specification of actuators, sensors etc. required for the experimental component in hybrid simulation. However, it may be noted that the preliminary numerical models are based on a few assumptions. These include assumption of deck to remain elastic, adoption of constant damping ratio of 5% and rigid connection between pier and foundation. Some of these assumptions may actually change when the bridge is subjected to high level of seismic excitations. The numerical model is calibrated subsequently based on observed response from hybrid simulation and revisiting some of the assumptions made in the simulation of initial numerical model.

This page is intentionally left blank

Chapter 5
TESTING OF BRIDGE BY HYBRID SIMULATION

5.1 GENERAL

The prime emphasis of the current research program is on hybrid simulation of an existing bridge, where HyFRC is used in the scaled model of the bridge pier. In the beginning of this chapter, hybrid simulation framework is explained in details. The numerical module of hybrid simulation is already explained in chapter 4. This chapter presents the details of the experimental module of hybrid simulation. Investigation of the influence of additional detailing features at the pier-foundation interface is also carried out. This is undertaken to observe any possible relocation of crack away from the pier-foundation interface zone, where most of the damages are observed to be generally concentrated. To fulfil the objective of the research program, scaled model of bridge piers made of conventional concrete and HyFRC are considered as experimental elements in the hybrid simulation. Tests are done under scaled earthquake acceleration time history of different intensity levels. The criteria for selection of the ground motions is also outlined. After completion of hybrid simulation, cyclic tests are carried out to find the ultimate capacity of these test specimens. The comparison of response of HyFRC specimen with that of conventional concrete specimen are explained in details. Elaboration of the results of growth of strain in concrete as well as reinforcement, correlation of damage pattern at different stages of loading, gain in ductility and energy dissipation in different specimens are presented.

5.2 TESTING PROCEDURE BY HYBRID SIMULATION

This section discusses the development details of the hybrid simulation framework and the procedure involved in the testing of a structural system by hybrid simulation.

5.2.1 Hybrid simulation framework

In hybrid simulation, finite element method is used to discretize the structural system and an integration algorithm is used for the solution of governing differential equation (Schellenberg et al. 2006). The resulting dynamic equations of motion for the discrete system is

$$\mathrm{M}\,a(t) + \mathrm{C}\,v(t) + r(t) = f(t) \tag{5.1}$$

In the above equation, M is the assembled mass matrix, C is the assembled viscous damping matrix, $a(t)$ and $v(t)$ the acceleration and velocity vector, $r(t)$ the structural restoring force vector and $f(t)$ the external force vector applied to the system. The incremental response i.e. the displacements determined by the integration algorithm is applied to the physical pier model of the bridge system by transfer system consisting of controller and actuator. An OpenSees-OpenFresco-MTS controller based hybrid testing framework for the pseudo static hybrid simulation was used in this study. In the adopted hybrid simulation framework, OpenSees was selected as the computational driver. OpenFresco is a middleware software package for performing hybrid simulations involving numerical models, test specimens, experimental setups and loading conditions (Schellenberg et al. 2009). The generalized α -operator splitting (α-OS) scheme (Chung and Hulbert 1993), a non-iterative implicit time integration method, was used for hybrid simulation. Value of α was taken as 0.5. The integration is elaborated in the subsequent section. On the physical testing side, OpenFresco was connected to MTS Flex-Test GT controller (4 channels) through MTS Computer Simulation Interface. Application of command signal to the MTS 244 series dynamic actuator (Capacity: 250 kN, Stroke: 125 mm) and acquisition of feedback signal was carried out using in-built DAQ of the controller. The numerical module consisted of 3D numerical model of full scale bridge structure with all the components along with the experimental element (pier). The experimental module consists of physical testing of scaled model of the critical element(s) i.e. bridge pier in this study. Experimental control took care of required scaling process for applied loading, i.e.1/5 of displacement response from numerical model was applied at the pier top of experimental module and 5^2 of spring force acquired from the experimental element was applied to the numerical module. Vertical loading on the scaled pier model was kept constant throughout the test, which was 1/25 of the total superstructure load of the prototype. The response of pier of the bridge, defined as 'experimental element' in the numerical module of Opensees model was monitored throughout the hybrid simulation. Each load step in hybrid simulation consist of ramp time due to which the actual time of the excitation was extended during hybrid simulation. The method adopted for the current research is pseudo-static hybrid test and hence the actuators had enough time to achieve the desired motion and did not require any time delay compensation.

5.2.2 Integration scheme

All the time stepping integration methods are classified into two types - the explicit methods and the implicit methods. The state of a system at a next time step is calculated from the state of the system at current time step by explicit methods. Implicit methods on the other hand find a solution by solving an equilibrium equation involving both the current state of the system and the later one. Mathematically if $u(t)$ is the current system state and $u(t+\Delta t)$ is the state at a later time $t+\Delta t$, where Δt is a small time increment then :

Explicit method: $u(t+\Delta t) = f(u(t))$

Implicit method: $u(t+\Delta t) = f(u(t), u(t+\Delta t))$

In general, the implicit methods require iterations for nonlinear problem and are difficult to implement in hybrid simulation. The three major requirements for any numerical time stepping method are (Chopra 2001) –

- **Convergence:** As the time step decreases numerical solution should converge to exact solution
- **Stability:** Should be stable in presence of numerical round off errors
- **Accuracy:** Numerical solutions should give result close enough to exact solution

For the present study, the Generalized-Alpha-OS direct integration method is implemented. The accuracy and stability of the α-OS was thoroughly studied by Combescure and Pegon (1997) and their main observations are summarized below.

- The initial stiffness matrix in hybrid simulation is generally close to the elastic range. In any case, it is higher or equal to the current tangent stiffness of the structure, the approximation condition ensures that the integration scheme is unconditionally stable. The time step for integration may be arbitrarily chosen, without considering any stability consideration. Hence, during the hybrid simulation, this integration scheme would be a good alternative to more complex iterative schemes.
- However, when the structure undergoes severe stiffness degradation the scheme is still accurate and stable for the low frequency modes of the structure, which are usually dominant.
- The calculated response using the integration scheme could be improved by choosing appropriate time step for any frequency band of interest.

The state of a structure, i.e. displacement, velocity, and acceleration, at the $(n+1)^{th}$ step consists of known terms from the n^{th} step and unknown terms, which need to be determined. In hybrid simulation, using α-OS method, the known term displacement is applied to the structure and the measured restoring forces from the structure is used to evaluate the unknown terms.

The hybrid simulation procedure using α-OS scheme (Combescure and Pegon 1997) is summarized as flowchart in Figure 5.1. The solution at new time step is obtained as function of values at previous steps. Δt is the small equal time interval, u_n, v_n and a_n are the known displacement vector, velocity vector and acceleration vector at time t_n which is used to obtained response at time $t_{n+1} = t_n + \Delta t$. The initial stiffness matrix, K^1, is used to correct the restoring force and to establish the equivalent mass matrix, which is used to calculate the acceleration of the next step, a_{n+1}. Thus, for use the generalised α-OS method for hybrid simulation, the initial stiffness matrix should be established prior to the dynamic analysis.

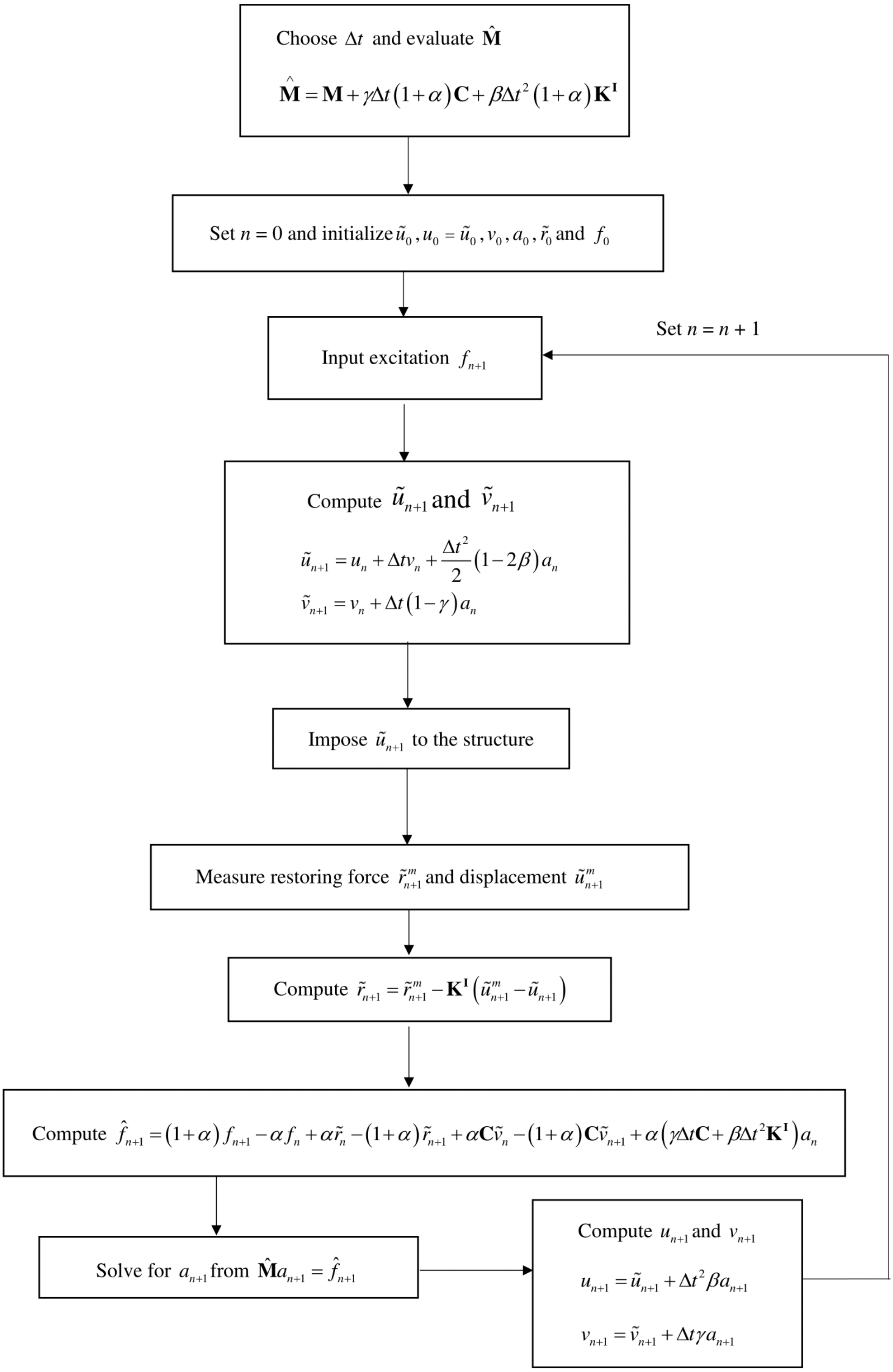

Figure 5.1. Flow chart for hybrid simulation procedure

5.3 DETAILS OF TEST SPECIMEN

Six 1:5 scaled models of pier of a prototype bridge in Tripura, India as shown in Figure 4.1 are cast in the Structural Laboratory of Civil Engineering Department of IIT Guwahati for a research program. Details of scaled down test model is shown in Table 5.1 and details of reinforcement of the test model are shown in Figure 5.2. Three specimens are cast with conventional concrete, while another three are cast with HyFRC as a part of current research project. The specimens are cast with designed mix having target cube compressive strength of 30 MPa. The specimens are cast in stages which will be discussed in subsequent section. HyFRC specimens are cast as per the best volume fraction found from the test carried out in section 3.2. Conventional concrete and HyFRC test specimens are identical in terms of their geometry and longitudinal reinforcement details. However, there is difference in the transverse reinforcement. HyFRC specimens for the present study is cast with only half the transverse reinforcement as compared to those of conventional concrete specimens.

Table 5.1. Details of scaled bridge pier model

Item	Prototype	Model	Remarks
Longitudinal steel ratio	1.12%	1.12%	Conserved during scaling
Longitudinal steel reinforcement	36 mm Ø – 38nos	16mmØ -8nos	
Transverse reinforcement dia.	20 mm	8mm	Volumetric ratio conserved during scaling
Spacing of transverse reinforcement	75 mm	60 mm	
Pier dia.	2100 mm	420 mm	1/5 scale
Pier height	9000 mm	1800 mm	1/5 scale
Cover	40 mm	20 mm	Conserved during scaling

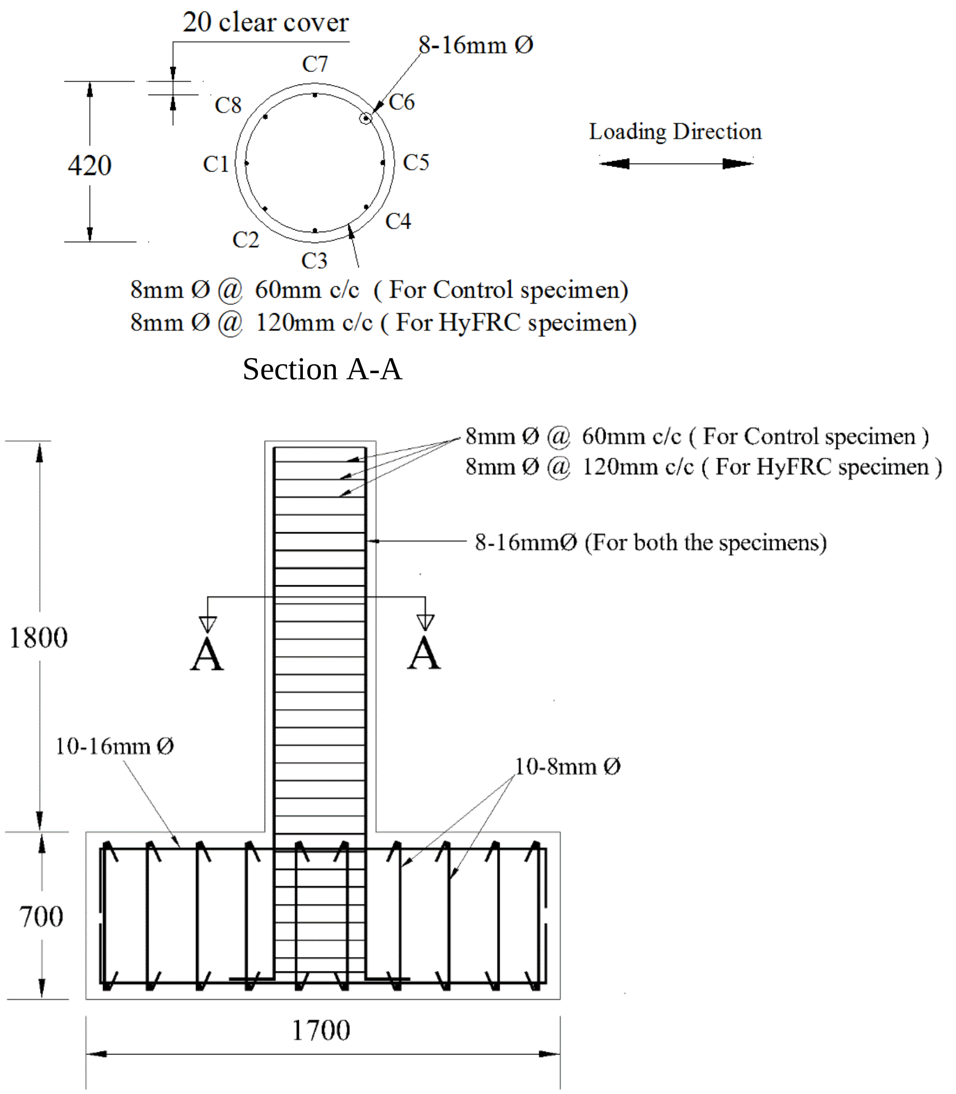

Figure 5.2. Reinforcement details of scaled pier model (All dimensions are in mm)

The three specimens cast with conventional concrete are designated as Type A, while remaining three cast with HyFRC are identified as Type B throughout the thesis. In each of the two material types, three possible detailing is used at the pier-foundation interface portion. Different detailing is done with an objective of shifting the major damage location away from the interface. Type 1 have conventional reinforcement detailing, Type 2 have dowel bars of 390 mm which is 10% more than the plastic hinge length and Type 3 have corrugated sheet duct embedded into the foundation with diameter about 10% more than that of the bridge pier. The numbers of dowel bars are equal to the main longitudinal reinforcement and half the length of these bars are above while the other half is below the pier foundation interface. The necessary information about the different features in the specimens are furnished in Table 5.2. The footing is designed as a block foundation. The design for footing is same for all the specimens. The specimen is anchored to the strong floor of the test bed using high strength friction grip bolts.

Table 5.2. Details of special features of the test specimens

<table>
<tr><th>Specimen</th><th>Type of concrete</th><th>Additional features</th></tr>
<tr><td>A-1</td><td>Conventional concrete</td><td rowspan="2">Conventional reinforcement details as shown in Figure 5.2.</td></tr>
<tr><td>B-1</td><td>HyFRC</td></tr>
<tr><td>A-2</td><td>Conventional concrete</td><td rowspan="2">16mm Ø additional longitudinal bars are used over 175mm above and below the pier-foundation interface
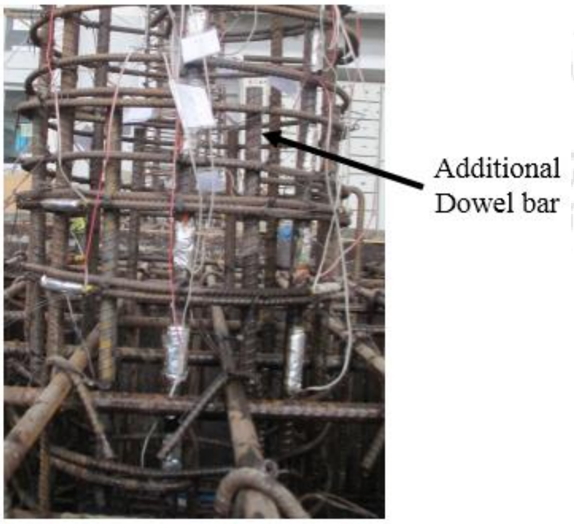
</td></tr>
<tr><td>B-2</td><td>HyFRC</td></tr>
<tr><td>A-3</td><td>Conventional concrete</td><td rowspan="2">A corrugated sheet pipe over the depth of foundation
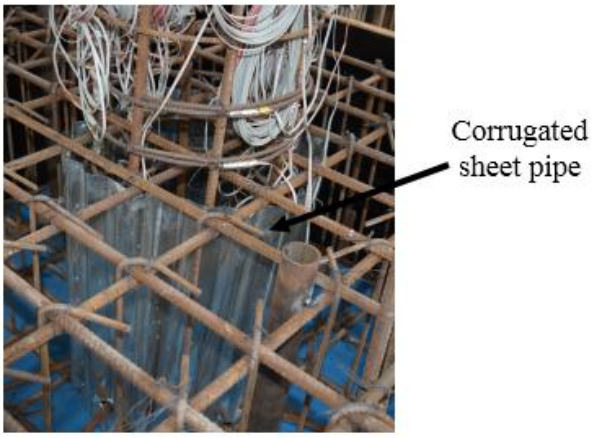
</td></tr>
<tr><td>B-3</td><td>HyFRC</td></tr>
</table>

5.3.1 Description of material used in construction

Conventional concrete and HyFRC are designed for a target strength of 35MPa. The details of concrete mix are presented earlier in chapter 3. Tensile test results steel reinforcement of different diameters are presented in Appendix C.

5.3.2 Fabrication of specimen

Each of the test specimen is cast in two phases. The foundations of piers are cast prior to the casting of the main piers. Three 150×150×150 mm cubes are cast in standard steel moulds from each mix in order to evaluate compressive strength of hardened concrete cubes after 28 days. Three 150×300mm cylinder are also cast for tensile test. Stress-strain curves of the mix is shown in the result chapter. A well graded aggregate with a maximum size of 10 mm is considered in the mixes as per ACI 544.3R-08. The concrete is mixed in a mechanical drum type mixer (Figure 5.3). Galvanized steel tube is used to separate HyFRC and conventional concrete in the footing as shown in Figure 5.4. While casting the test specimen, a 3mm-diameter stick vibrator is used to lightly vibrate the concrete placed inside the formwork. The whole set up of casting is shown in Figure 5.5. Figure 5.6 shows the photos of construction procedure of a single specimen at different stages.

Figure 5.3. Mixing of concrete in a mechanical drum type mixer

Figure 5.4. Galvanized steel tube used to separate HyFRC from conventional concrete in the footing

Figure 5.5. Photograph showing cast of test specimen

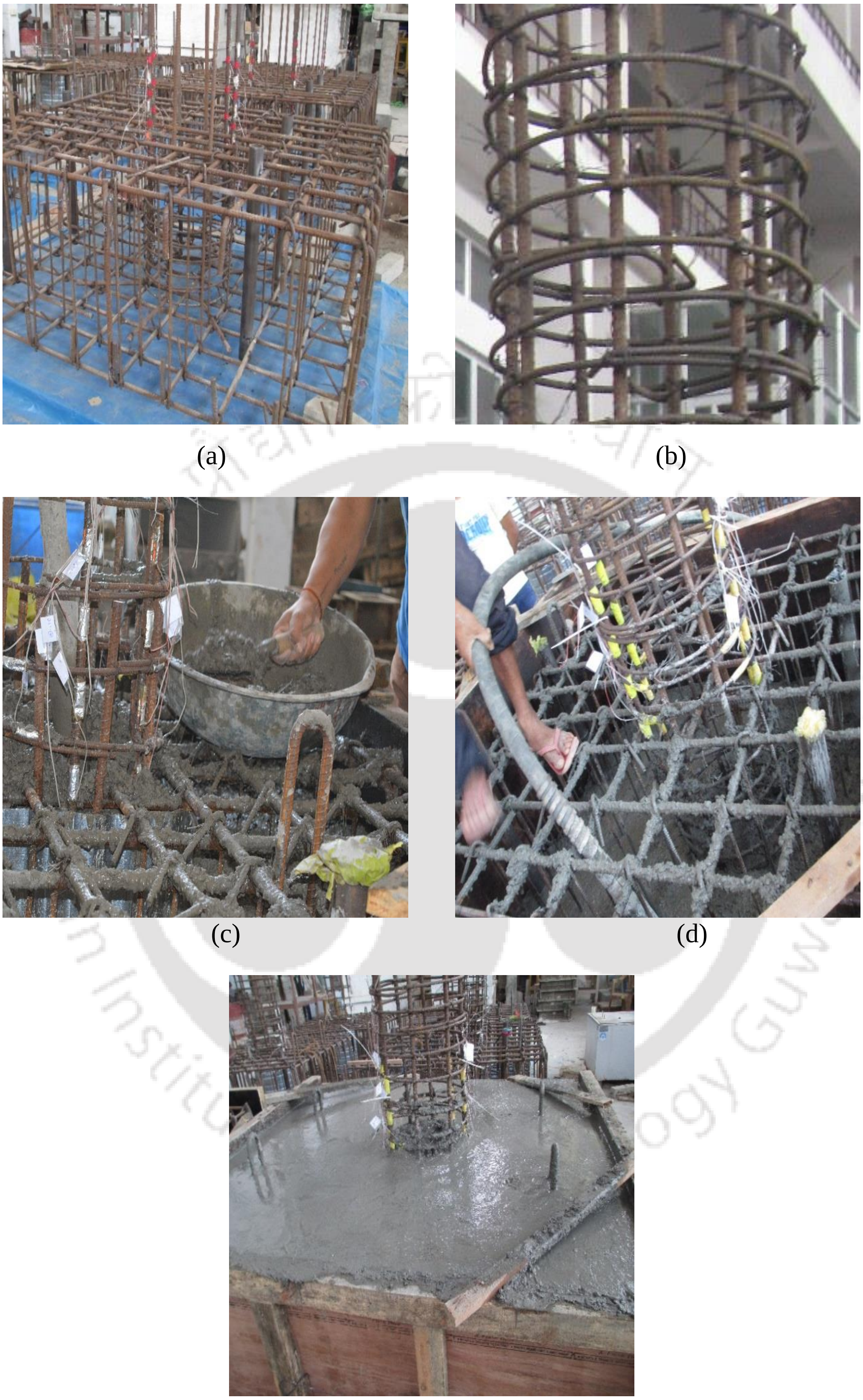

Figure 5.6. Construction phases (a) foundation and column reinforcement cage (b) close up of top of circular reinforcement cage (c) pouring of foundation concrete (d) vibration with stick vibrator (e) foundation after cast

5.3.3 Loading characteristic and test frame

The self-weight of the bridge deck is calculated from the detailed drawing of the prototype bridge deck and its 1/25th (1/ S^2, S is the scale factor) value is applied through a loading arrangement using 1000 kN capacity servo-hydraulic actuator (make: MTS Inc., USA) having stroke length of 250 mm. The actuator is supported by the test frame as shown in Figure 5.7. The lateral displacement is imposed to the specimen by 250 kN dynamic actuator with stroke length of 250 mm and this actuator is supported against the strong wall of the laboratory. The arrangement at the pier head ensured free lateral movement of the specimen, while verticality of the applied dead load is maintained throughout the tests. The specimen is fixed to the strong floor by means of four numbers of high tension bolt as can be seen from the global view in Figure 5.8.

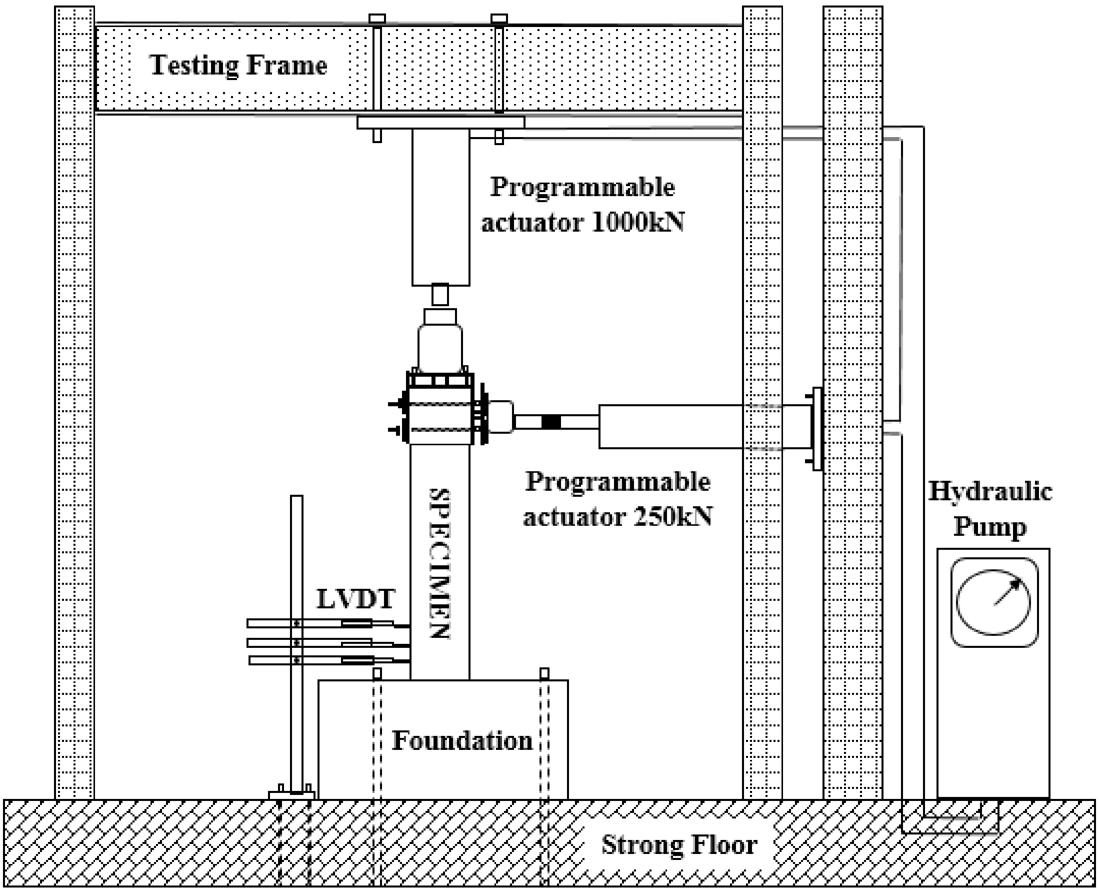

Figure 5.7. Schematic representation of test set up

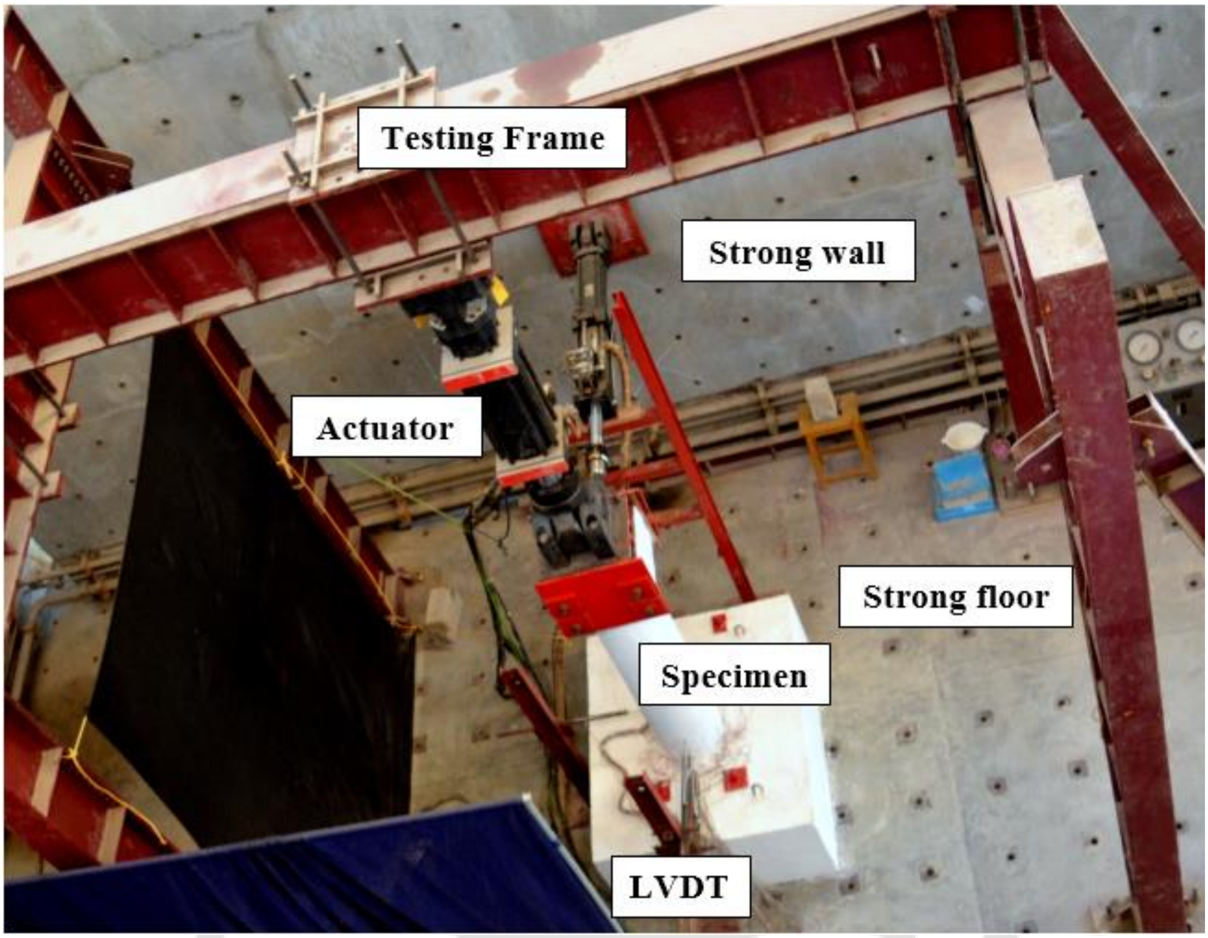

Figure 5.8. Photograph showing the overall view of the test set up

5.3.4 Instrumentation

The major objectives of testing scaled models of bridge piers are to develop an in-depth understanding of the behaviour of the bridge under seismic excitation with piers made of conventional concrete and HyFRC. Longitudinal and transverse reinforcements are instrumented with strain gauges for recording strain values during the experimental program. Strain in concrete is measured by embedded strain gauges while deflection along the height of the pier is measured by linear variable differential transformers (LVDT).

Alemdar (2010) have done a detailed review of formulae that are available to calculate the plastic hinge length for reinforced concrete columns for both static and dynamic test. The studies conducted by Dodd et al. (2000) and Hachem et al. (2003) utilized the equation proposed by Paulay and Priestley (1992) to estimate the plastic hinge length before testing the circular columns under earthquake loading . This equation was developed using the static test results of 20 bridge columns having a shear-span-to-depth ratio between 2 and 5.5.

The following formula is proposed by Paulay and Priestley (1992) to consider the effect of flexural reinforcement with different strengths on the length of a plastic hinge formed at the bottom of a cantilever column:

$$l_p = 0.08l + 0.022d_{bl}f_{ye} \geq 0.044f_{ye} \tag{5.2}$$

where l is the height of the cantilever column, f_{ye} is the yield stress of longitudinal reinforcement, and d_{bl} is the diameter of the longitudinal reinforcement. The second term in the equation makes allowance for additional rotation at the critical section resulting from strain penetration of the longitudinal reinforcement into the footing. Length of plastic hinge for sample piers considered in the study is 352 mm.

By the strain plots of Kumar et al. (2011), a general conclusion can be drawn for bridge column that there is increase in strain in plastic hinge length in comparison to other portion throughout the length. In order to capture the expected strain profile shown in Figure 5.9, the placement of strain gauges is concentrated only in the plastic hinge region spreading over a length of 400 mm (200 mm above and 200 mm below the pier-foundation interface) as the calculated plastic hinge length is 352 mm. To capture the strain penetration effect of the longitudinal reinforcement into the footing strain gauges are places at 50 mm and 150 mm levels below the column base.

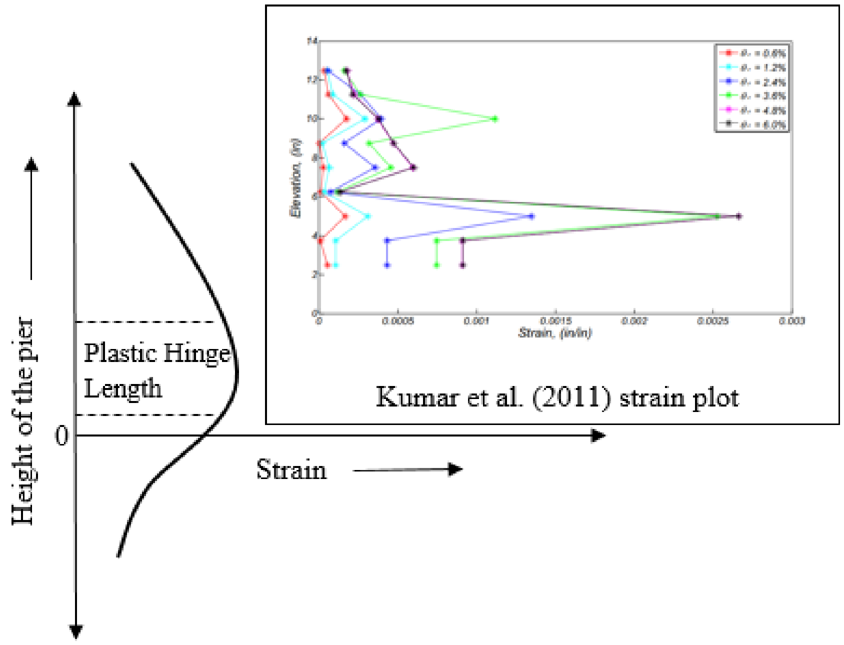

Figure 5.9. Expected strain profile along the height of the column

A total of twenty six electrical strain gauges are fixed on longitudinal and transverse reinforcement in each of the test specimens at predefined location. It is known that damage in a pier is most likely to be localized around the pier-foundation interface zone when the bridge is subjected to transverse excitation. Variation of strain in longitudinal bars within the plastic hinge length of the piers are monitored using eighteen electrical resistance strain gauges of 350-ohm resistance (Make: HBM GmbH, Germany; model: Type K-LY41-6/350), by pasting these sensors at an interval of 100 mm. The cross section of scaled bridge pier with reference numbers of eight 16 mm diameter longitudinal rebar is shown in Figure 5.2. Five strain gauges are fixed on each of the longitudinal bars C1 and C5, while four strain gauges are fixed on each of C2 and C6 as shown in Figure 5.10 (a). In order to capture the hoop strain development in the most vulnerable region, the strains of the transverse reinforcement are measured by eight strain gauges. Four strain gauges are placed on outer surface of two transverse reinforcements at two identified locations in the plastic hinge region as shown in Figure 5.10 (b). To measure strain in concrete, two concrete embedded strain gauges (make: TML, Japan) are used in each of the test specimen. These strain gauges are placed in the core concrete region of the pier just above the pier foundation interface and 10 mm away from the longitudinal rebar. All these strain gauges helped to visualize the difference in growth of strain in two types of specimens and compare their performances. Figure 5.11 and Figure 5.12 show the strain gauges location in the reinforcement and concrete of test specimens. Three LVDT are used at locations 80 mm, 160 mm and 320 mm respectively from the pier foundation interface to record the lateral displacement at these points as shown in Figure 5.7.

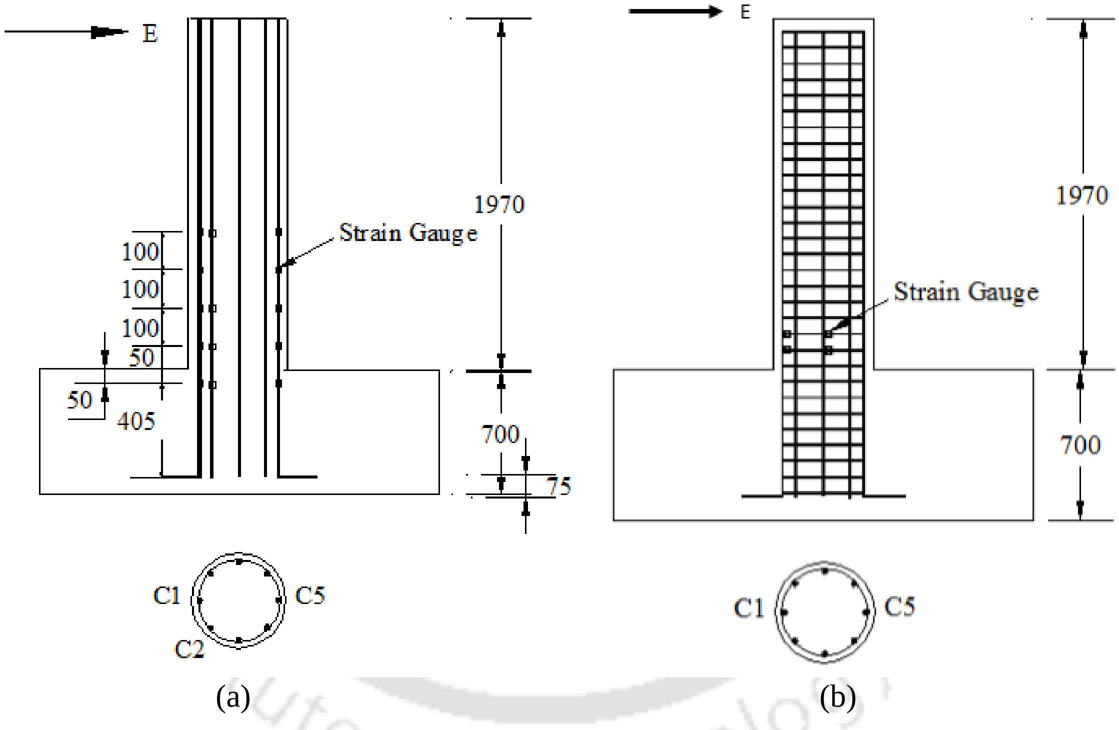

Figure 5.10. Location of strain gauges on the (a) longitudinal reinforcement (b) transverse reinforcement.

Figure 5.11. Photograph showing strain gauges fixed on rebars

(a) (b)

Figure 5.12. (a) Location of concrete embedded strain gauge in the specimen (b) photograph showing a sample embedded strain gauge

5.3.4.1 Procedure for fixing strain gauge

Different bonding materials used for fixing strain gauges in the reinforcement and for protecting them during casting. Figure 5.13 shows the step by step procedure used for fixing the strain gauge over the reinforcement. First, the ribs of reinforcement bars are gradually removed at identified locations and the surface is smoothened. Before fixing the strain gauge on the reinforcement, the smoothed reinforcement bar is cleaned with RMS1 (mixture of Isopropanol and Acetone). Z70 (Cyanacrylate) is used for perfect bonding between the strain gauge and the reinforcement. After fixing the strain gauge, PU140 (single component solvent based polyurethane lacquer) and Anabond 673 (silicon rubber) are applied over the strain gauge and thereafter ABM75 (0.05 mm thick aluminium foil coated with 3 mm thick kneading compound) is used as a protective cover. All these materials are used following their respective curing time. Concrete embedded strain gauges are placed in plastic hinge region near the reinforcement bar.

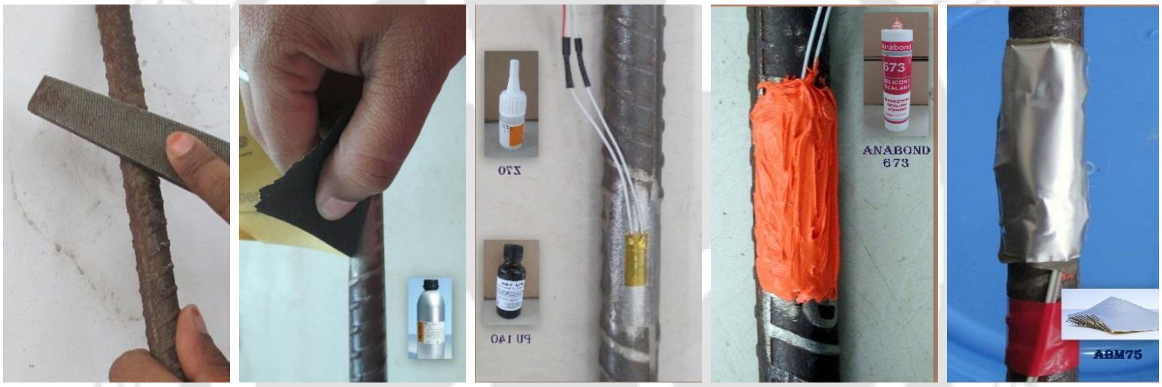

(a) (b) (c) (d) (e)

Figure 5.13. Procedure of fixing strain gauge in the reinforcement bar (a) removing ribs of the bar by filing (b) smoothing of the surface by sand paper and cleaning by RMS1 (c) fixing of the strain gauge by Z70 and application of P140 protective coat (d) application of protective coating of Anabond 673 (e) fixing of ABM75

5.3.5 Selection of earthquake time history

The extent of damage in a structure during earthquake depends on the type of loading. Similar sample earthquake records used in section 4.3.3 are applied in sequence to dynamically excite the model (Figure 4.8 (a)).

5.3.6 Details for cyclic test

In order to determine the ultimate capacity of the conventional concrete specimen and HyFRC pier specimen, cyclic loading tests are carried out after the completion of hybrid testing. The specimens are subjected to cyclic displacements corresponding to different values of drift ratio with gradually increasing amplitudes. Drift ratio is defined as the ratio of pier lateral displacement at the loading point and the effective pier height. Thus 1% drift ratio for the present loading protocol correspond to 18 mm. This test programs is performed as quasi-static test with a cyclic loading frequency of 0.025 Hz. The first three cycles of applied displacement amplitudes are ±10 mm and thereafter displacement amplitude increment of 10 mm is implemented till the end of the test. The applied lateral displacement history is shown in Figure 5.14. The tests are stopped, when the reinforcement got snapped off and/or the degraded load carrying capacities of specimens are in the range of 70–80% of the peak load. Further, the damage pattern in the pier-foundation interface zone is monitored and the test is stopped when the damage in that zone is serious enough from the view point of overall safety of the set up.

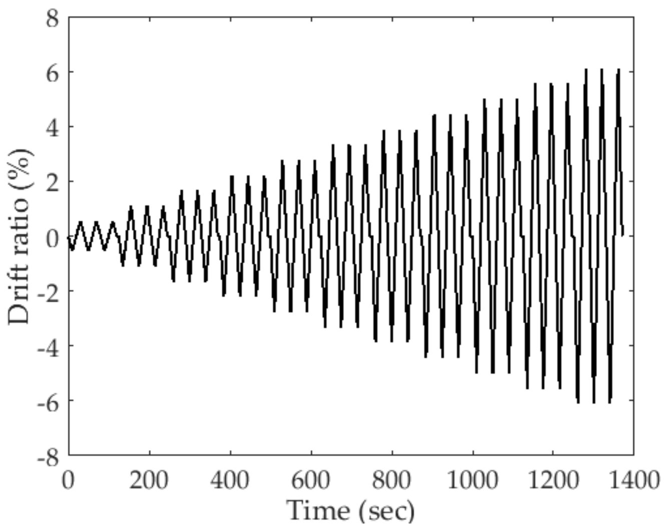

Figure 5.14. Cyclic load history

5.4 SIMULATION RESULTS

First, the observed behaviours of the test specimens are described in the following section in terms of visual damage at different stages of loading. Next, the measured responses based on the external and internal instrumentation are presented, and the performances of different types of specimens are compared.

5.4.1 Observed distribution of damage

The damage states of both conventional concrete and HyFRC specimens of Type 1-3 at various displacement levels are shown in Figure 5.15 (a–f). At the end of test under 0.5 MCE, hairline cracks are seen near the base of the pier of the Type 1 specimen. However, a clear shift in the initial crack location from pier-foundation interface could be seen for Type 2 and 3 specimens. The hairline crack subsequently coalesced at the end of 1MCE test and became more visible for all the specimens. Multiple cracks are also observed distributed over the pier-foundation interface region mostly in Type 1 specimens. The position of first crack for specimen Type 2 is at the location 150 mm from pier-foundation interface, which is in the vicinity of the terminating point of the dowels. Interestingly, specimen Type 3 also had first crack almost at similar location, i.e. 150 mm from pier-foundation interface. However, on further increase in the intensity of excitation, the crack location in specimen Type 3 got shifted towards pier-foundation interface region. The maximum strain corresponding to the moment for 0.5 MCE intensity level and available stiffness at 150 mm from the pier-foundation interface is likely to be higher than the cracking strain of concrete due to which the first crack appeared in that location. At the same loading stage, due to the increase in stiffness provided by the corrugated sheet near the pier-foundation interface, the imposed strain is perhaps lower than the concrete cracking strain, though the moment is maximum at that location. However, with the increase in loading, the strain in the interface zone possibly became higher than the cracking strain and cracks started appearing at that location. This is a typical case of relative increase in moment vs increase in stiffness due to the corrugated sheet. However, when the gauge size of corrugated sheets are further increased, it may be possible that the cracks will occur only in the zone away from the pier-foundation interface. Concrete spalling occurred in the zone of initial crack in Type 1 and 2, while in Type 3 spalling occurred near the pier-foundation interface during the test under 2MCE intensity level. At the end of 3MCE intensity level test, the concrete spalling is more prominent. It may be seen that the specimen Type B consistently suffered lesser damage in comparison to specimen Type A at any stages of intensity levels. Further, amongst all the specimens, Type 2 performed relatively better with lesser damage than rest of the specimens. The damaged specimens are further subjected to cyclic displacement after 3MCE level tests of hybrid simulation for ascertaining the reserve strength.

During cyclic test, longitudinal reinforcement C1, C5 and C6 in specimen A-1 fractured at peak displacement of 90 mm, 100 mm and 100 mm respectively. In specimen B-1 longitudinal reinforcement C1 and C5 fractured at peak displacement of 100 mm. Crushing of the concrete near the interface zone of the pier A-1 occurred at displacement amplitude of 40 mm, however similar condition is observed at displacement amplitude of 60mm in specimen type B-1. Longitudinal reinforcement C1 and C5 of specimen A-2 and C1 of specimen B-2 fractured at peak displacement of 100 mm. Crushing of the concrete predominantly occurred at displacement amplitude of 50 mm located near the first crack of the specimen A-2, however similar condition is observed at displacement amplitude of 70 mm in specimen B-2. In specimen A-3, longitudinal reinforcement C1 and C5 fractured while in specimen B-3, C4 and C5 fractured at peak displacement of 100 mm. Crushing of the concrete near the pier-foundation interface occurred at displacement amplitude of 50 mm in specimen A-3, however similar condition is observed at displacement amplitude of 60 mm in specimen B-3. The damage in the pier-foundation interface zone became more prominent after the completion of cyclic test in specimen Type 3. The enhanced ductility of the HyFRC made piers is responsible for delay in concrete crushing as well as reduced number of reinforcement rupture in all the three specimen of Type B. Specimen B-2 performed best out of all six piers. Figure 5.15 (e-f) shows the damaged states of specimen A and B type respectively, when the experiments are stopped. Reinforcement got snapped and formation of flexural hinges are observed. However, from the Figure 5.15 (e-f) it is quite evident that damage level in HyFRC made piers is much lesser than that of conventional concrete specimens.

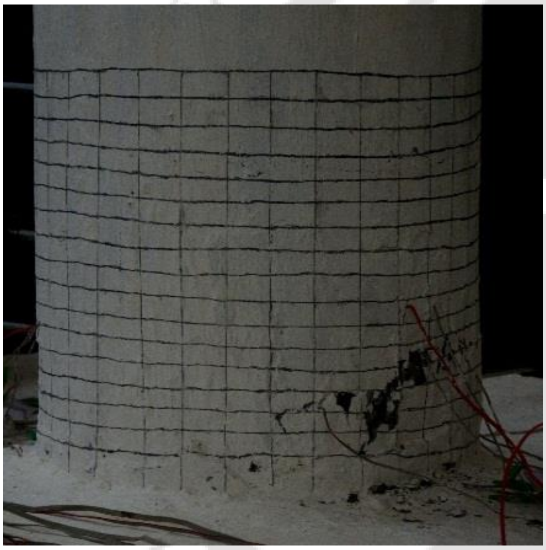

Type 1

Type 2

Type 3

(a) Conventional concrete specimens at the end of 1st level of of Hybrid test

Type 1

Type 2

Type 3

(b) HyFRC specimens at the end of 1st level of Hybrid test

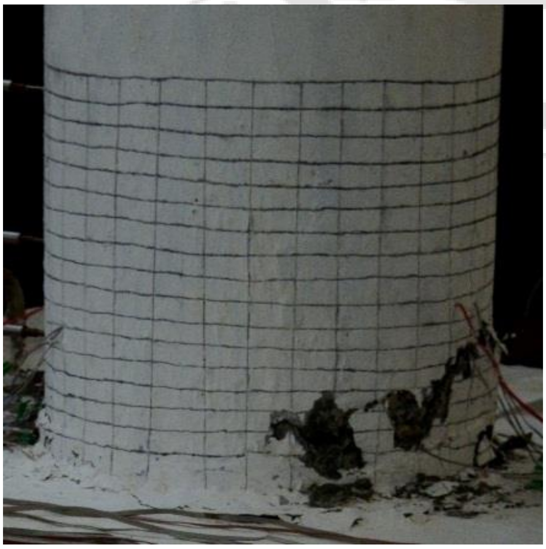

Type 1

Type 2

Type 3

(c) Conventional concrete specimens at the end of 4th level of of Hybrid test

Type 1 ***Type 2***

Type 3

(d) HyFRC specimens at the end of 4th level of Hybrid test

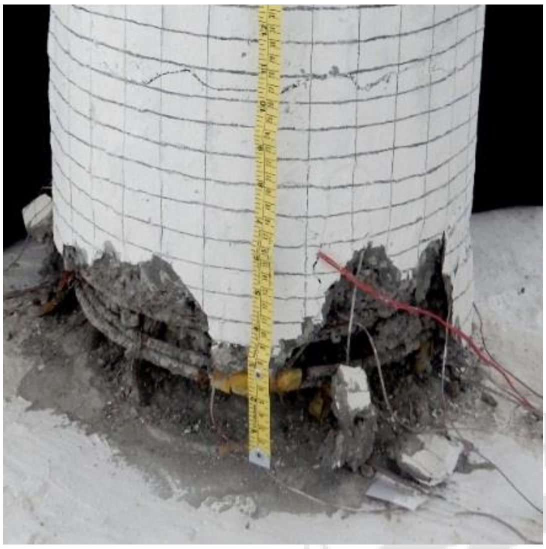

Type 1

Type 2

Type 3

(e) Conventional concrete specimens at the end of Cyclic test

Type 1

Type 2

Type 3

(f) HyFRC specimens at the end of Cyclic test

Figure 5.15. Damage states of the six test specimens

Fibres bridging cracks is the prime cause of this lesser observed in piers of Type B. Structural rehabilitation of HyFRC specimens will be much easier compared to specimens made of conventional concrete.

5.4.2 Force-displacement hysteresis

During 0.5 MCE intensity level, all the types of specimens performed almost in a similar manner. The measured lateral force versus lateral displacement responses of Type 1, 2 and 3 specimens are presented in Figure 5.16 (a-b) for excitation with intensity level of 3MCE. Responses of all the specimens after cyclic loading test, which are performed to check the ultimate load carrying capacity, are presented in Figure 5.16 (c-d). At about 3.8% drift ratio, all the specimens reached its peak load. The specimens reached a maximum drift ratio of 5.6% however withstanding its designed vertical load. The peak lateral load carrying capacity of specimen Type B is found to be higher than that of the corresponding specimen Type A. Further, specimen Type 2 showed higher load carrying capacity than other specimen types. This establishes that dowels provide additional resistance to imposed displacement. The peak lateral load of HyFRC specimens is around 1.2 times that of conventional concrete specimens for all the three detailing types, indicating its higher resistance to imposed displacement. It is evident that the presence of hybrid fibres contributed to the improved performance of test specimen Type- B.

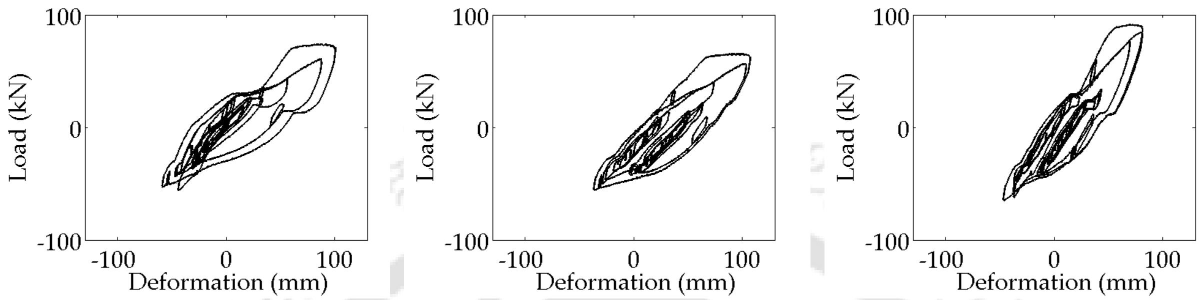

Type 1 ***Type 2*** ***Type 3***

(a) Conventional concrete specimens at the end of Hybrid test

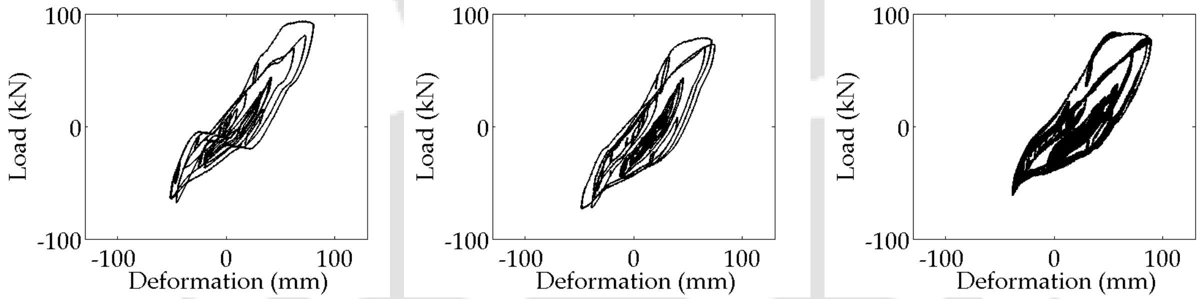

Type 1 ***Type 2*** ***Type 3***

(b) HyFRC specimens at the end of Hybrid test

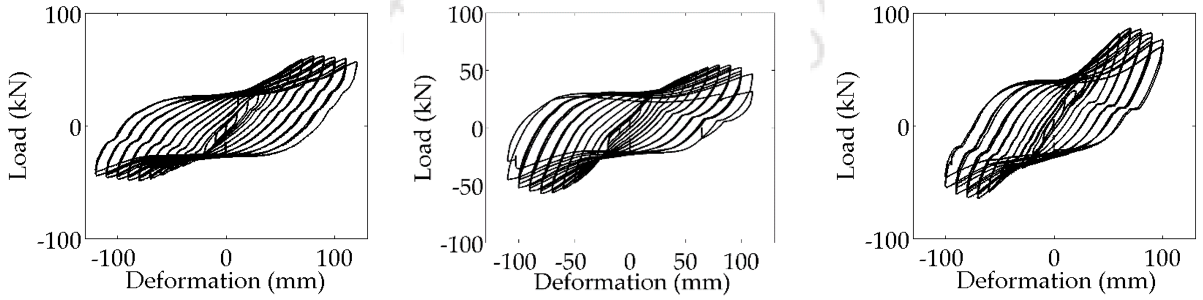

Type 1 ***Type 2*** ***Type 3***

(c) Conventional concrete specimens at the end of Cyclic test

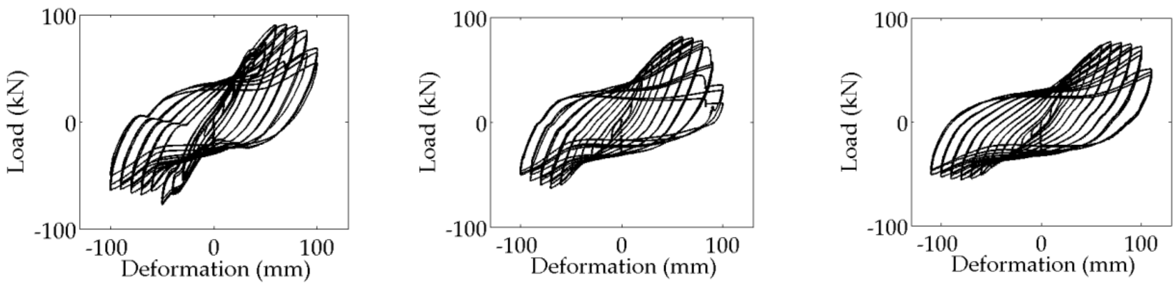

Type 1 ***Type 2*** ***Type 3***

(d) HyFRC specimens at the end of Cyclic test

Figure 5.16. Load vs deformation hysteretic response of the six test specimens

5.4.3 Cumulative energy dissipation

For the cyclic test, energy dissipation for each amplitude level is computed as the average area (3 loops for each amplitude level) enclosed under the hysteresis loops, and the cumulative energy dissipation at a particular displacement level is calculated by summing the individual areas of preceding displacement level with current displacement level. Figure 5.17 shows the additional energy dissipation capacities observed during cyclic test carried out after hybrid simulation. Energy dissipation is lower during the initial stages as damage is only confined to cover concrete. However, after significant damage in the specimen, energy dissipation became higher due to large rotation in the plastic hinge region of the specimen base. As expected, the rate of degradation of strength is relatively gradual in HyFRC specimens and so the energy dissipation in Type B for all the three detailing types during the cyclic test is about 20% higher than that of specimen Type A. Specimen Type 2 performed better in both the types of material.

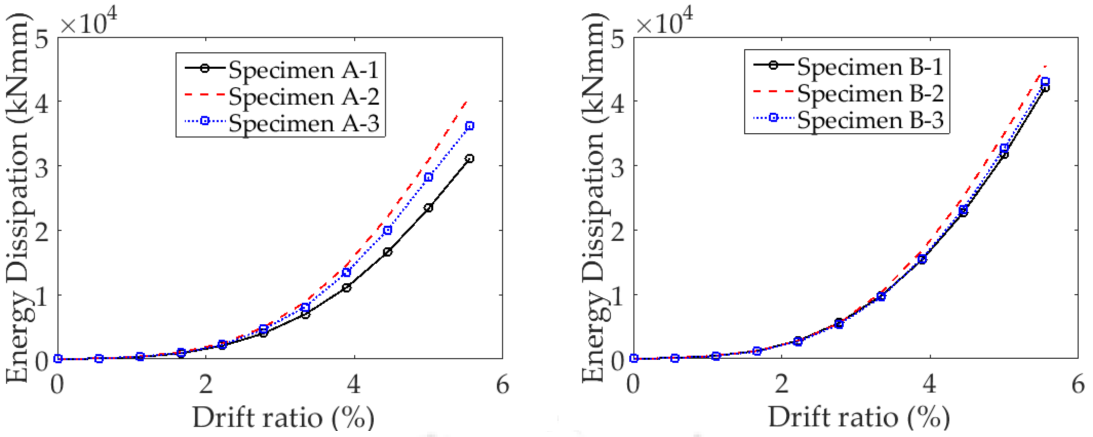

Figure 5.17. Energy dissipation at different drift ratio in cyclic test

5.4.4 Stiffness degradation during cyclic test

Stiffness is calculated as the slope of the line joining the peak of positive and negative load carrying capacity at a given cycle corresponding to that particular displacement amplitude. Figure 5.18 shows the change in stiffness with increased imposed displacement. It can be seen that the initial stiffness of specimen Type 2 is more than that of specimen Type 1 and 3. Further, available stiffness is also observed to be more in Type 2 as compared to others at any level of drifts. It is also observed that the rate of degradation of specimen B-2 is little lower in the beginning in comparison to specimen B-1 and B-3, when displacement are gradually increased. This behaviour may be attributed to the presence of hybrid fibres enhancing ductile behaviour. Further, presence of dowel bars in the plastic hinge region in turn led to lesser damage. The lower degradation is a desirable property in earthquake like situations.

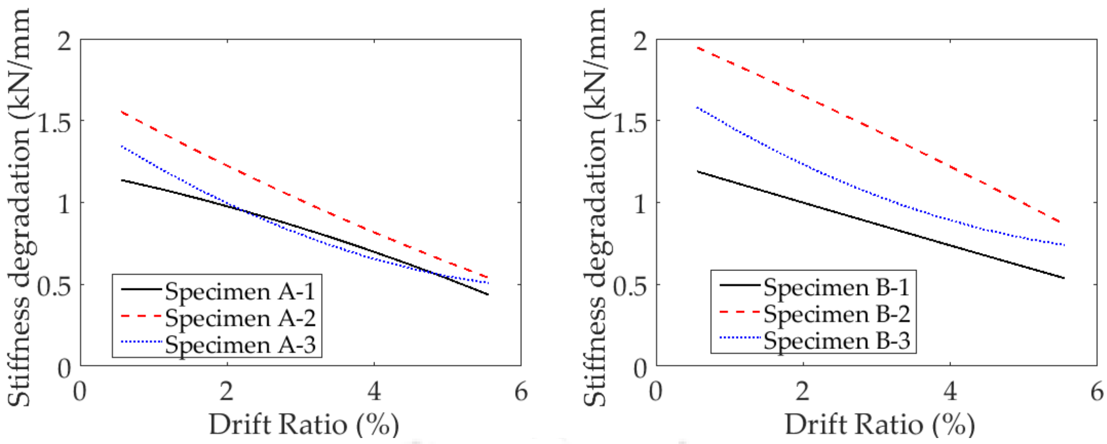

Figure 5.18. Stiffness degradation during cyclic test

5.4.5 Displacement ductility

Ductility is the ability of a structure to accommodate deformations well beyond the elastic limit. It also indicates the capacity of the specimen to dissipate energy and the capacity to sustain large deformations. The displacement ductility factor μ is defined by the ratio of the total imposed displacement Δ_u at any instant to that at the onset of yield Δ_y i.e. $\mu = \Delta_u/\Delta_y$. Yield deformation of the structure is however difficult to estimate since the load deformation curve may not present a well-defined yield point. Many alternative definitions are given by researchers to compute the yield displacement. For the present study, the yield displacement is calculated by the procedure proposed by Shannag et al. (2005) as the point of intersection between two idealized straight lines drawn in the envelop curve. The first line is obtained by extending the line joining the origin and 50% of ultimate load capacity point on positive and negative sides of the envelope curve, while the second line is obtained by drawing a horizontal line through the 80% of ultimate load capacity point on either side as shown in Figure 5.19.

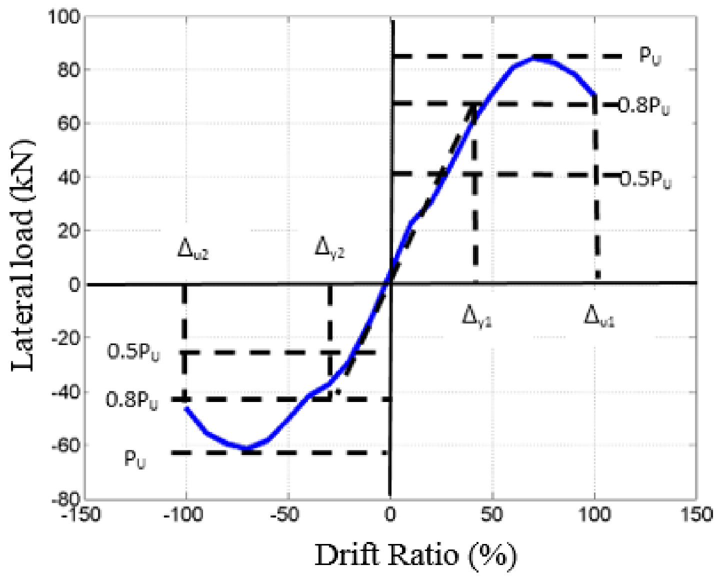

Figure 5.19. Procedure of ductility calculation

The average value of yield displacement obtained from both positive and negative directions is calculated. Table 5.3 presents the representative displacement ductility corresponding to only cyclic test results attained by specimen of two types. It is to be mentioned that both the specimens were damaged before the cyclic test as they were subjected to successive excitations from 0.5 MCE to 3MCE level. The rate of degradation of the load carrying capacity is however higher for conventional concrete specimens than those of HyFRC specimens as may be seen from Figure 5.16 (i-j). This has eventually led to the observation that conventional concrete specimen could not achieve the ductility values as good as the HyFRC specimen. However the difference in values of ductility between conventional concrete and HyFRC specimens is not much, although there is significant difference in degree of damage in specimens made of two different types of materials.

Table 5.3. Displacement ductility of the specimens

Specimen	**Δ_y , mm**	**Δ_u, mm**	**Δ_u/Δ_y**
Type A-1	40.47	100.235	2.47
Type B-1	37.1	100.242	2.7

**Note:* Δ_y= *Displacement at first yield,* Δ_u = *maximum induced displacement till reinforcement fractured*

5.4.6 Failure Surface of damaged specimen

Removal of cover concrete by chiselling is easy in the conventional concrete specimens, while the same is indeed very tough in the HyFRC specimens. It is found that crushing of even core concrete occurred quite extensively in the conventional concrete specimen, but crushing of cover concrete is more controlled in the HyFRC specimen. Evaluation of core concrete damage is difficult in the HyFRC due to the presence of fibers. Based on the damage observed in both the specimens, it is important to note that the damage of cover concrete, core concrete and buckling of reinforcement in HyFRC specimens after the cyclic test are much lesser than those in conventional concrete specimens. Figure 5.20 shows the cross-section for evaluation of surface failure and Table 5.4 shows all the measured data for comparison among all the specimens. All the three types of piers made of HyFRC are found to have lesser extent of damage compared to those in conventional concrete specimens. Further, specimens containing dowel bar are found to have least value of crack depth among specimens of each material type.

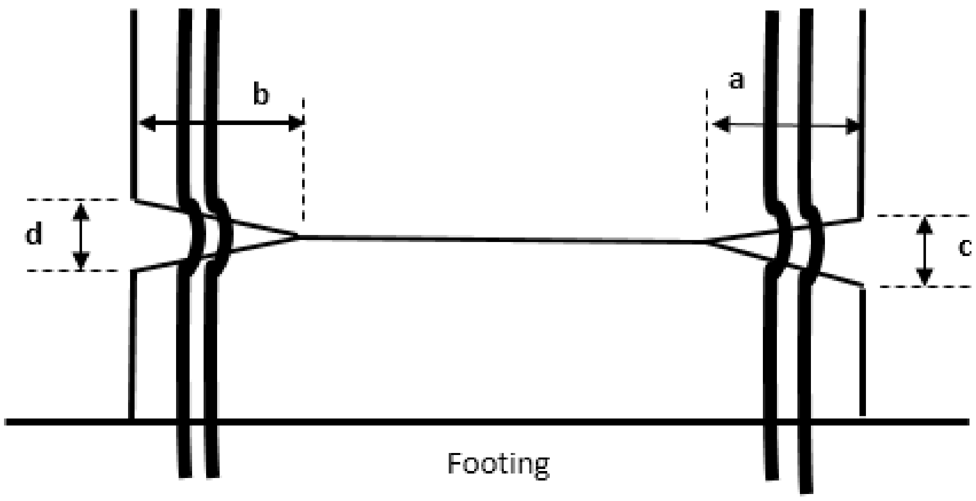

Figure 5.20. Schematic diagram of damage zone in the pier

Table 5.4. Surface failure evaluation

Specimen	a (mm)	b (mm)	c (mm)	d (mm)
A-1	70	80	15	10
B-1	40	55	8	5
A-2	60	55	9	11
B-2	35	40	5	4
A-3	65	70	12	10
B-3	45	55	6	8

5.4.7 Buckling length of ruptured reinforcement

Buckling length is observed to vary among various types of specimens. However, the maximum buckling length is observed to be about 120 mm in specimens made of conventional concrete as well as HyFRC. Figure 5.22 shows the image of a typical buckled reinforcement for Type A-1 and B-1 specimens. It may be seen from Figure 5.21 (a) that for specimen Type A-1, the transverse reinforcement in the middle of the buckled portion actually opened up and hence the buckling length is taken as twice the spacing between lateral ties in pier (i.e. 120 mm). The specimen type B-1 in Figure 5.21 (b) also showed a similar buckling pattern, while the spacing between successive lateral ties is 120 mm. Thus, the buckling phenomena for both Types A-1 and type B-1 are comparable, though specimen Type B-1 had double the transverse reinforcement spacing than that of Type A-1. The pattern of buckling in other conventional concrete specimens with different detailing at the interface are also observed to be comparable with those made of HyFRC. Thus, HyFRC is assumed to have provided sufficient lateral confinement and ensured similar bucking pattern of longitudinal reinforcements, while actual lateral reinforcements are only half of those provided in conventional concrete specimens satisfying the ductile detailing requirements.

Concrete specimen, A-1 ***HyFRC specimen, B-1***

Figure 5.21. Sample photograph of buckled reinforcement

5.4.8 Observation of strain distribution in reinforcement and concrete

Strain profiles along the longitudinal reinforcement, C1 of all the six piers are plotted in Figure 5.22. In both A-1 and B-1 specimens, the strain gauge at position 50 mm from the pier-foundation interface is observed to show highest strain in comparison with the other four strain gauges in the same longitudinal reinforcement. Thus, due to strain compatibility, concrete in that zone also must be having maximum strain developed leading to the formation of higher damage, which is also evident from Figure 5.15. It is observed that specimen Type 2 experienced lower growth of strain at all the stages of loading. In Type 2 and Type 3 specimens, the strain gauge at position 150 mm from the pier-foundation interface showed maximum strain during 0.5 MCE and 1 MCE intensity level of excitation.

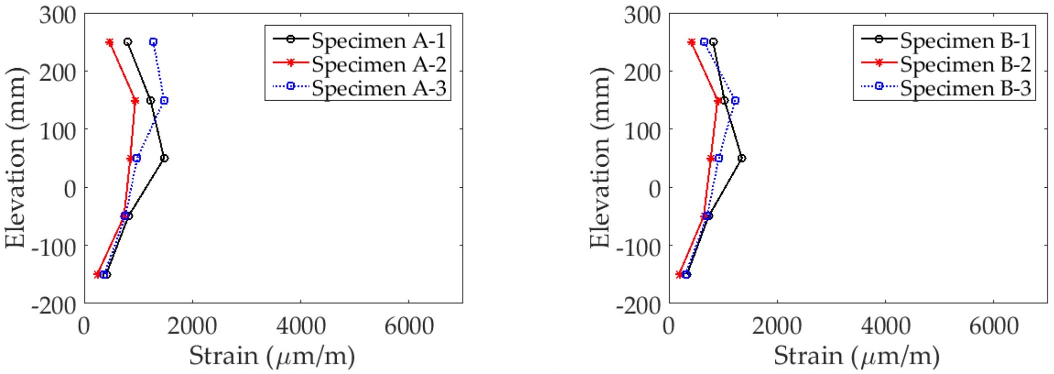

0.5 MCE levels of excitation

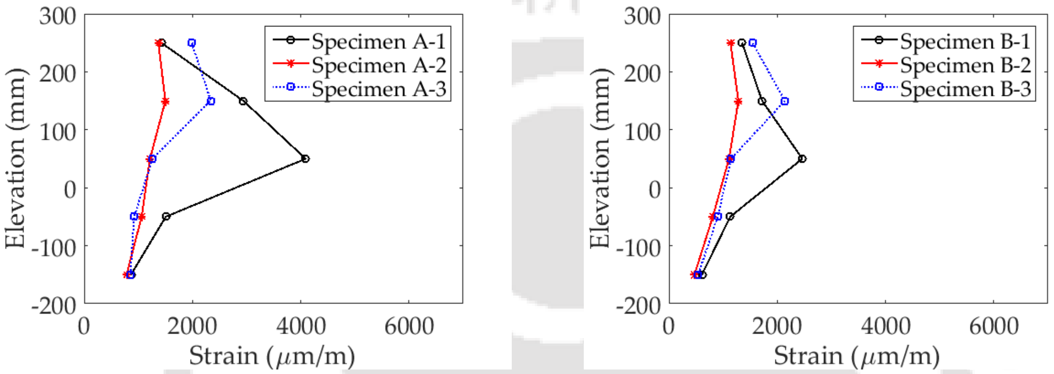

1 MCE levels of excitation

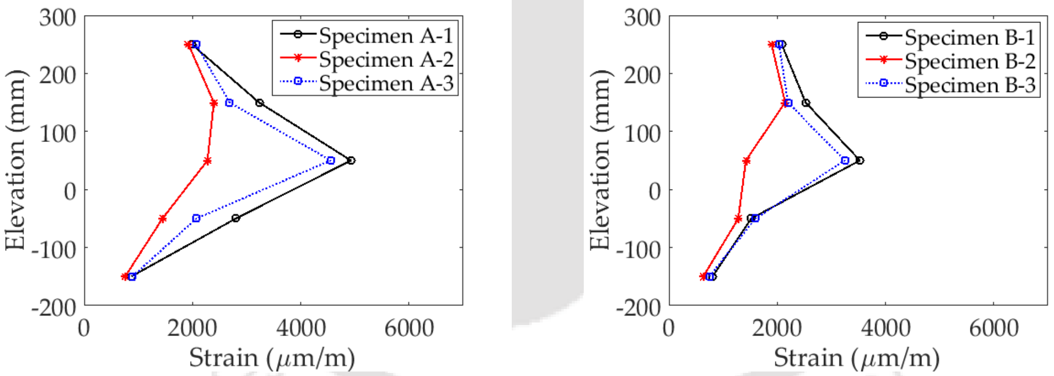

2 MCE levels of excitation

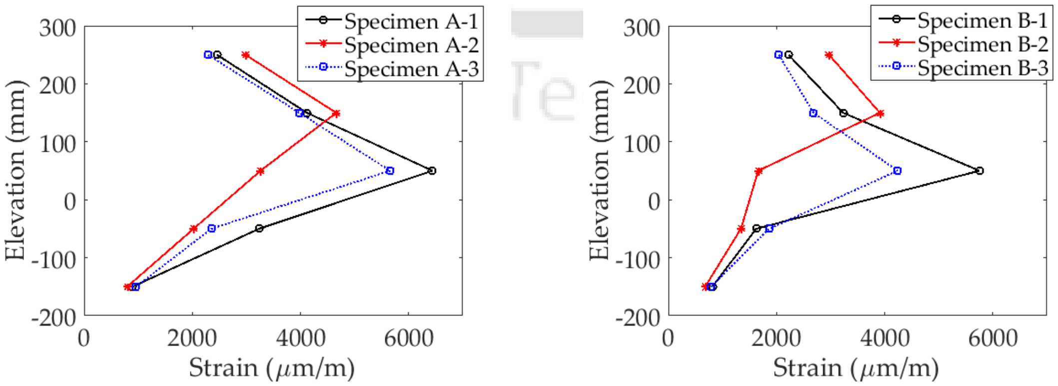

3 MCE levels of excitation

Figure 5.22. Strain profile of longitudinal reinforcement C1 at all levels of excitation

It is evident from the damage pattern shown in Figure 5.15 that the maximum crack location is at 150 mm from the pier-foundation interface during the corresponding intensity of loading. However, during 2 MCE and 3MCE intensity levels, the major crack location in Type 3 specimen got shifted back close to the pier-foundation interface. The strain pattern for Type 3 also showed maximum value at the interface zone during the same stage of loading. Further, Type 3 specimen showed lower strain for all intensity levels in comparison to Type 1 specimen. The yield strain of reinforcement found from the laboratory test is 2,890 μm/m. However, it may be noted that Type 2 reached yield strain value during 2MCE intensity level while the rest of the specimens reached the same yield strain value during 1MCE level. Further, at all intensity levels, HyFRC specimen consistently showed lower value of strain in comparison to their corresponding conventional concrete specimen.

The measured strain from gauges embedded in concrete revealed that specimen Type 2 experienced a little delayed growth of strain in the core concrete region as compared to the other types of specimen. Figure 5.23 shows typical concrete strain history for specimen Type 1, 2 and 3. In all the three detailing types, HyFRC specimens showed delayed growth of strain in the core concrete region as compared to their corresponding conventional concrete specimen. This delayed strain growth resulted better performance of HyFRC specimens under seismic excitation as compared to that of the conventional concrete specimens.

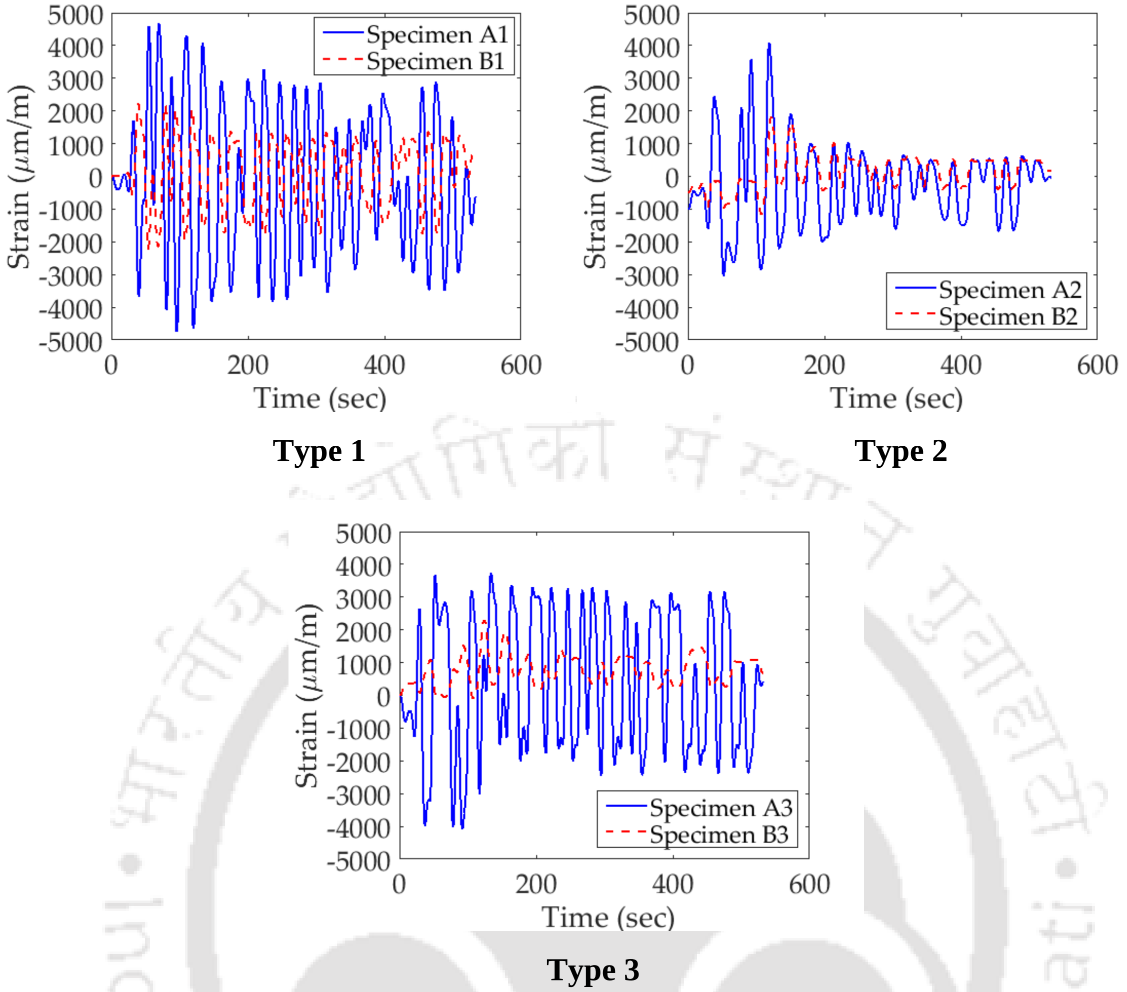

Figure 5.23. Strain history of concrete at 3MCE intensity level

Figure 5.24 shows a typical circumferential strain profile of transverse reinforcement for HyFRC and conventional concrete specimen based on the data obtained from strain gauges placed on transverse rebar located at 60 mm above the pier-interface foundation level of specimen type 1. These strain profiles correspond to tests carried out for 0.5MCE and 3MCE intensity level. In both the plots, it can be seen that measured strains in shear reinforcement are at comparable level in both conventional concrete and HyFRC specimen, even though HyFRC specimen had less transverse reinforcement. This showed that fibres improved shear strength of concrete and hence HyFRC specimen can have reduced shear reinforcement, thus enabling to have reduced congestion of reinforcement.

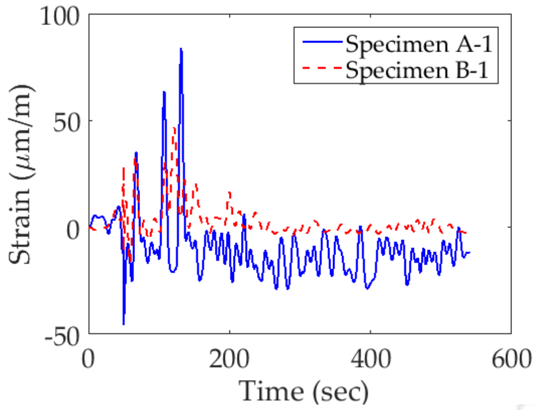

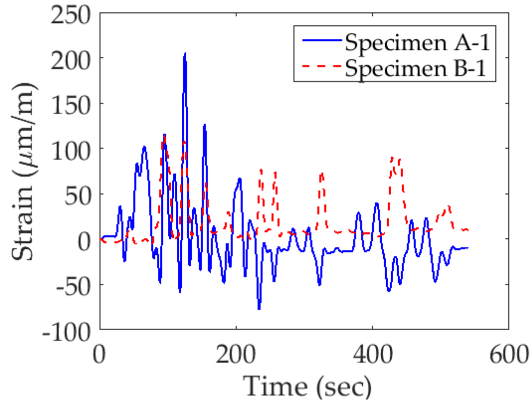

Figure 5.24. Strain profile of stirrup at (a) 0.5MCE intensity level and (b) 3MCE intensity level.

5.5 CONCLUDING REMARKS

The results obtained from hybrid testing of six different scaled pier specimens followed by their testing under cyclic loading are examined to explore the effectiveness of use of fibres as well as additional detailing features at pier-foundation interface region. Out of the six piers, two piers did not have any additional features at the pier-foundation interface, two piers had dowel reinforcement in the plastic hinge region and two others had corrugated sheet at the foundation in an attempt to shift the crack location. Strain gauges are used to measure strain in concrete as well as in reinforcement in all the specimens. Strains are monitored at the critical pier locations to correlate the growth of strain with damage in specimens. Extent of damage at the end of test is significantly lesser in all the three HyFRC specimens than the corresponding three conventional concrete specimens. HyFRC specimen with dowel bar showed least damage amongst all the specimens. HyFRC piers showed consistently higher energy dissipation capacity compared to conventional concrete piers. The strains in reinforcement of HyFRC piers are considerably reduced at all stages of loadings and displacement ductility of HyFRC specimens got improved compared to those of the conventional concrete piers.

Based on the observed results, the following important conclusions are drawn:

- Performance of HyFRC bridge piers is better compared to conventional concrete piers when subjected to seismic excitations.
- Dowel reinforcements in bridge pier are effective in shifting of damage away from pier-foundation interface zone.
- Piers with dowel reinforcement provides higher energy dissipation capacity as compared to that of the bridge piers with normal reinforcement detailing.
- Use of corrugated sheet also had the potential for crack relocation by appropriate selection of gauge size of the duct.
- On the basis of strain measurement, it is established that the crack initiation is delayed in HyFRC specimens and it is also observed that presence of special features shifted the damage zone away from the pier-foundation interface. This would enhance ease of rehabilitation after high intensity earthquake
- High confinement steel requirement in seismic resistant design procedure may be reduced by the use of HyFRC, without compromising displacement ductility. This would lead to better workability and reduce voids in concrete.

Chapter 6
CALIBRATION OF FINITE ELEMENT MODEL

6.1 GENERAL

This chapter first revisits the modelling assumptions made in Chapter 4 and evaluate them based on the detailed results and observations from hybrid simulation as presented in Chapter 5. The detailed scrutiny reveals some discrepancy in modelling assumptions which are modified in the calibration of the FE model in order to reduce discrepancies in load-displacement responses obtained from numerical model as compared to those obtained from hybrid simulation. The calibrated model could simulate the behaviour of the bridge very well. The detailed steps for calibration of the finite element model of the bridge are presented in subsequent section.

6.2 MODELLING ASSUMPTION

A reliable numerical model is critical to predict the response of bridge system subjected to earthquake-induced vibration. The numerical model described in Chapter 4 provides a preliminary idea for ascertaining the range of maximum displacement, strain etc. likely to occur in bridge components during the hybrid simulation. The initial numerical model is established using well-established finite element approach available in the literature. Detailed explanation of the initial numerical model is elaborately presented in Chapter 4. Some assumptions are made for development of the initial model as mentioned in Chapter 4. These assumptions are commonly used in modelling of bridge structure using finite element method (Frankie et al. 2013) and these are listed below.

1) **Deck remains elastic:** The assumption that deck remains within elastic range during an earthquake is well accepted and also numerical analysis carried by several researchers have shown that deck remains elastic during an earthquake. Additionally, seismic design codes across the globe including Indian codes advocate deck to be designed elastically. In past, researchers modelled deck using fiber section approach and found that demand placed on the deck due to earthquake loading remains in elastic region. Therefore, this is a valid assumption and no model calibration is performed in the superstructure components of the numerical model in the present study.

2) **Fixity at the base of the pier:** It is assumed that the base of the pier is perfectly fixed i.e. no translational and rotational movement occurs, which results in overestimation of stiffness and under estimation of displacement as compared to what is actually observed from hybrid simulation. The condition at the base no longer remains as fixed at high intensity of excitation. The development of crack at the pier-foundation interface reduces the stiffness of the joint region, which eventually leads to the formation of plastic hinges. Views of damage pattern (Figure 5.17) corresponding to all the four level excitations justifies the above-mentioned statement. Therefore, this is not a valid assumption and model calibration is required for improving the response of the numerical model.

3) **Rayleigh damping of 5% to account for non-hysteretic damping effects:** The damping is modelled in the initial model using Rayleigh damping in which a damping ratio of 0.05 is assumed and the Rayleigh damping coefficients are calculated using time period corresponding to first two modes. The assumed damping ratio is supposed to capture the response in line with the results of hybrid simulations.

The next section shows the comparison of the hybrid simulation result with the initial numerical model.

6.3 Comparison of Hybrid Simulation Results with Initial Numerical Model

The force displacement responses of bridge pier obtained from initial numerical model is compared with those responses obtained from hybrid simulation for both conventional concrete and HyFRC bridge piers. Figure 6.1 shows comparison of response of the experimental result with the initial numerical model for various intensity levels of input ground motion for conventional concrete bridge pier- Type 1.

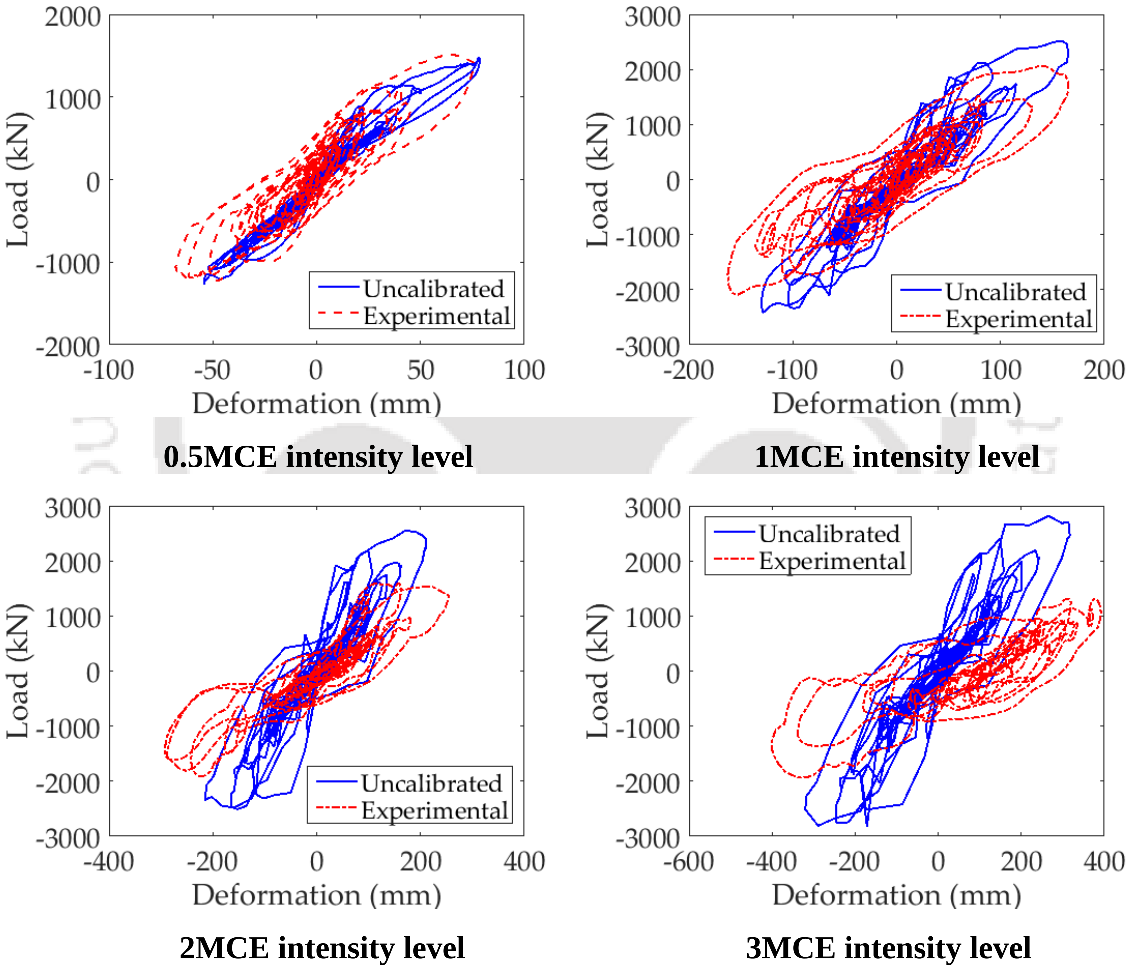

Figure 6.1. Comparison of the numerical results of conventional concrete bridge pier obtained from uncalibrated model with experimental results for different intensity levels

It is observed that at lower intensity level (0.5 MCE), the parameters like initial stiffness, peak force and displacement of initial numerical model broadly agree with experimental results. This is mainly due to the reason that pier remains in elastic range and no cracking of concrete and yielding of reinforcements are observed. However, due to the assumption of perfect fixity at the pier bottom in the initial numerical model, the stiffness corresponding to post elastic zone is not captured by the numerical model. At higher MCE intensity level, as cracking of concrete and yielding of reinforcement occurs, more amount of hysteretic energy is dissipated in the experimental model as compared to that in the numerical model. Therefore, the initial numerical model for the conventional concrete must be updated using experimental results.

Similar trend is observed with HyFRC bridge pier as well. At low intensity level, the initial stiffness, peak force and displacement of initial numerical model agree well with the corresponding experimental results. However, more energy dissipation is observed in the experimental model, which highlight the limitation of numerical model to capture actual response. Energy dissipation comparisons are shown in section 6.4.1.3. Further, at higher intensity level of excitations, degradation in initial stiffness is observed in the experimental model. This is mainly due to the cracking observed in the pier-footing interface. Initial numerical model is however unable to capture this decrease in stiffness due to the assumption of perfect fixity at the pier base. Figure 6.2 shows comparison of response of the experimental result with the initial numerical model for all the four intensity levels of input ground motion for HyFRC bridge pier-Type 1.

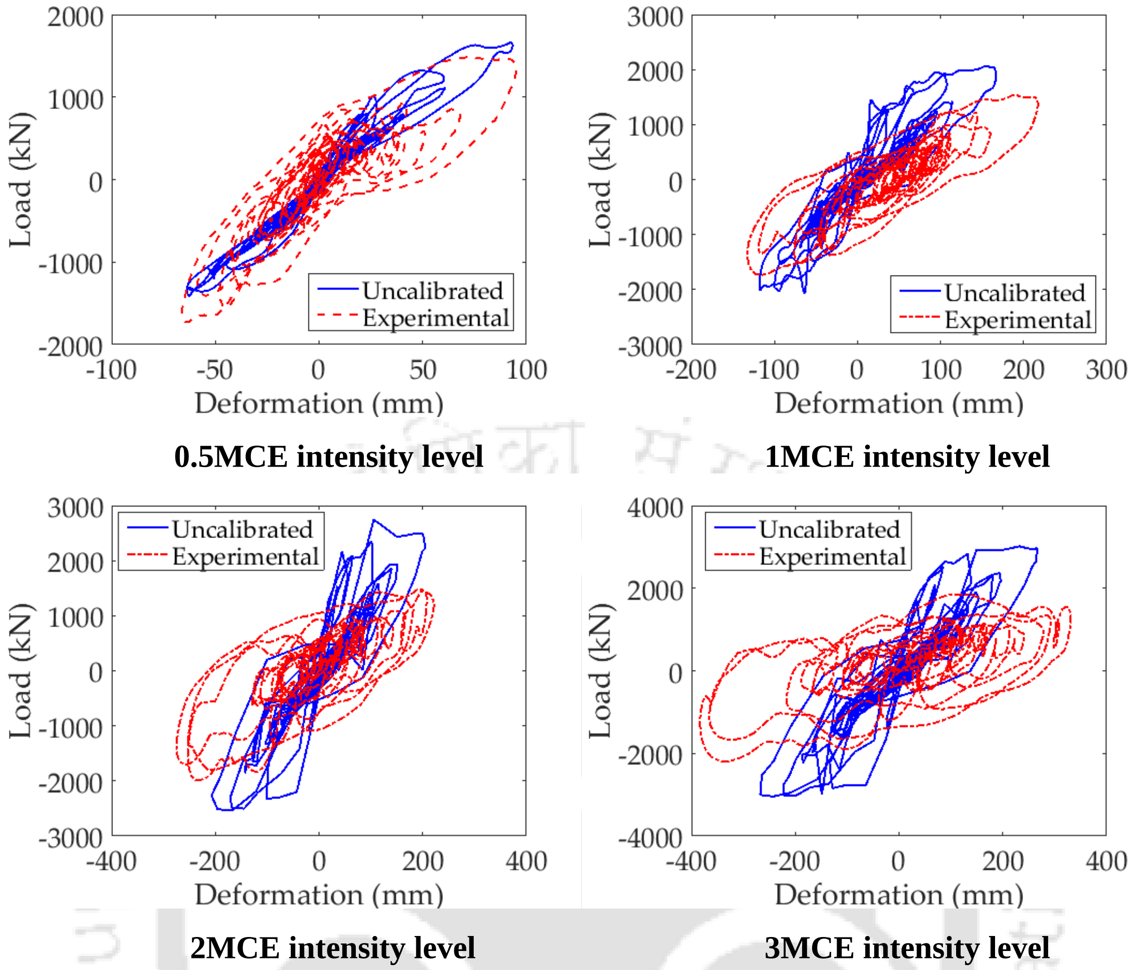

Figure 6.2. Comparison of the numerical results of HyFRC bridge pier obtained from uncalibrated model with experimental results for different intensity levels

The comparisons of results demonstrate the requirement for substantial improvement in the initial numerical model. The hysteretic behaviour of experimental specimens is used to calibrate the initial numerical model. Procedure for calibration of initial numerical model is presented in next section.

6.4 Model Calibration Procedures and its Results

In the previous section, it is shown that there is significant difference in response observed from initial numerical model as compared to the response observed from hybrid simulation. This is attributed to the assumption made in the numerical model as stated earlier. This section describes the modification made in the initial model in order to accurately predict the response in line with experimental results. Steps are taken to adjust the response of initial numerical model so that the results from numerical model are in line with the experimental results. These include addition of translational spring at the column base. In the experimental results, rotations are observed at the pier-foundation interface, which clearly contradicts the assumption of fixity at pier base in the initial numerical model. Major cracking at these locations are observed at higher MCE levels resulting in reduced stiffness and increase in displacement. Therefore, a nonlinear zero length translational spring model is introduced to account for stiffness and strength degradation. The sample *hysteretic* material model used to develop the nonlinear spring is as shown in Figure 6.3 (a).

The properties of nonlinear spring model is developed from the backbone curve of the force-deformation relationship obtained from hybrid simulation. The resulting model is able to capture the stiffness and strength degradation effects at each intensity levels of loading, which is shown in subsequent section. The uniaxial *hysteretic* material model available in *OpenSees* platform (McKenna et al. 1997) is used to define the constitutive relationship for the nonlinear spring. Hysteretic material has a predefined trilinear backbone with pinching of force and deformation, damage due to ductility and energy, and degraded unloading stiffness based on ductility. Five parameters are used to define hysteretic behaviour including pinching and stiffness degradation. The input parameter for *hysteretic* material is shown below-

uniaxialMaterial Hysteretic $matTag $s1p $e1p $s2p $e2p $s3p $e3p $s1n $e1n $s2n $e2n $s3n $e3n $pinchX $pinchY $damage1 $damage2 <$beta>

where :

$matTag integer tag identifying material

$s1p $e1p	force & deformation at first point of the envelope in the positive direction
$s2p $e2p	force & deformation at second point of the envelope in the positive direction
$s3p $e3p	force & deformation at third point of the envelope in the positive direction
$s1n $e1n	force & deformation at first point of the envelope in the negative direction
$s2n $e2n	force & deformation at second point of the envelope in the negative direction
$s3n $e3n	force & deformation at third point of the envelope in the negative direction
$pinchx	pinching factor for deformation during reloading
$pinchy	pinching factor for force during reloading
$damage1	damage due to ductility
$damage2	damage due to energy
$beta	power used to determine the degraded unloading stiffness based on ductility, mu-beta (optional, default=0.0)

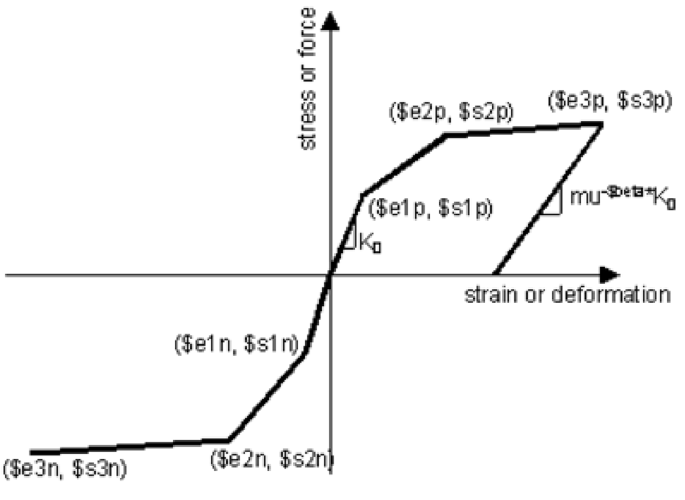

(a)

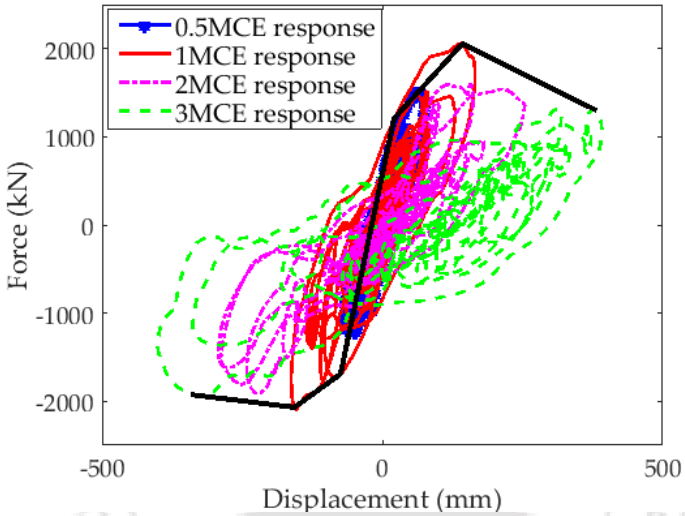

(b)

Figure 6.3. (a) Sample Hysteretic material model created using OpenSees platform (b) backbone curve developed from experimental force-displacement hysteretic response

The first, second and third points on the envelope curve in Figure 6.3 (a) are evaluated with series of hit and trial procedures from the backbone curve of experimental hysteresis loop corresponding to all the intensity level in Figure 6.3 (b). The parameters evaluated are used in defining the zero-length element, which is introduced at the base of bridge pier in the calibrated model framework.

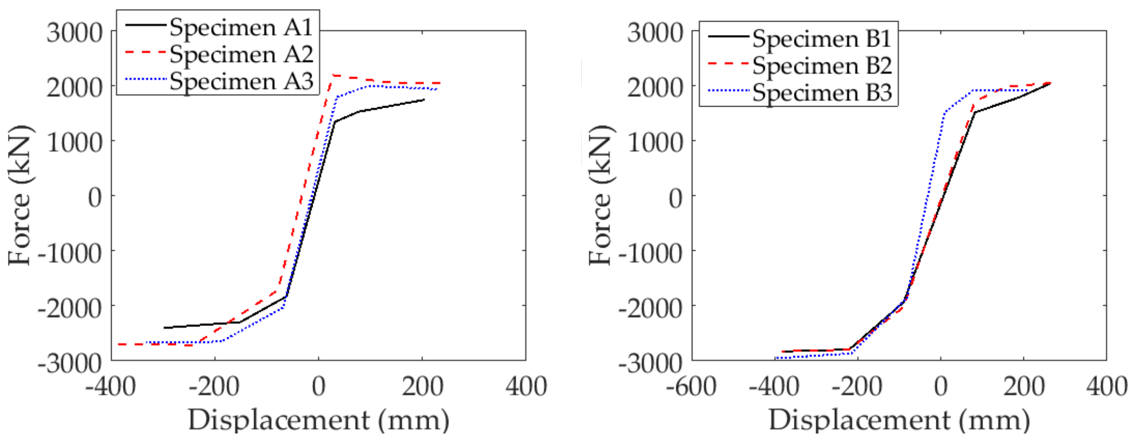

Figure 6.4. Back-bone curve for all the tested specimens

From Figure 6.4, it can be seen that there is not much difference in the pattern of back-bone curve for all the three specimens (Type 1, 2 and 3) cast with of a particular material type. So, back bone curve for specimen of Type 1 is studied in details for the model calibration in the present study.

Figure 6.5 and Figure 6.6 shows the improvements in the overall response for conventional concrete and HyFRC bridge piers following the implementation of the aforementioned calibration procedure. It is observed that addition of nonlinear translational spring at the base are highly effective in achieving the improved matching of both lateral displacement and force along with dissipated energy in the calibrated model.

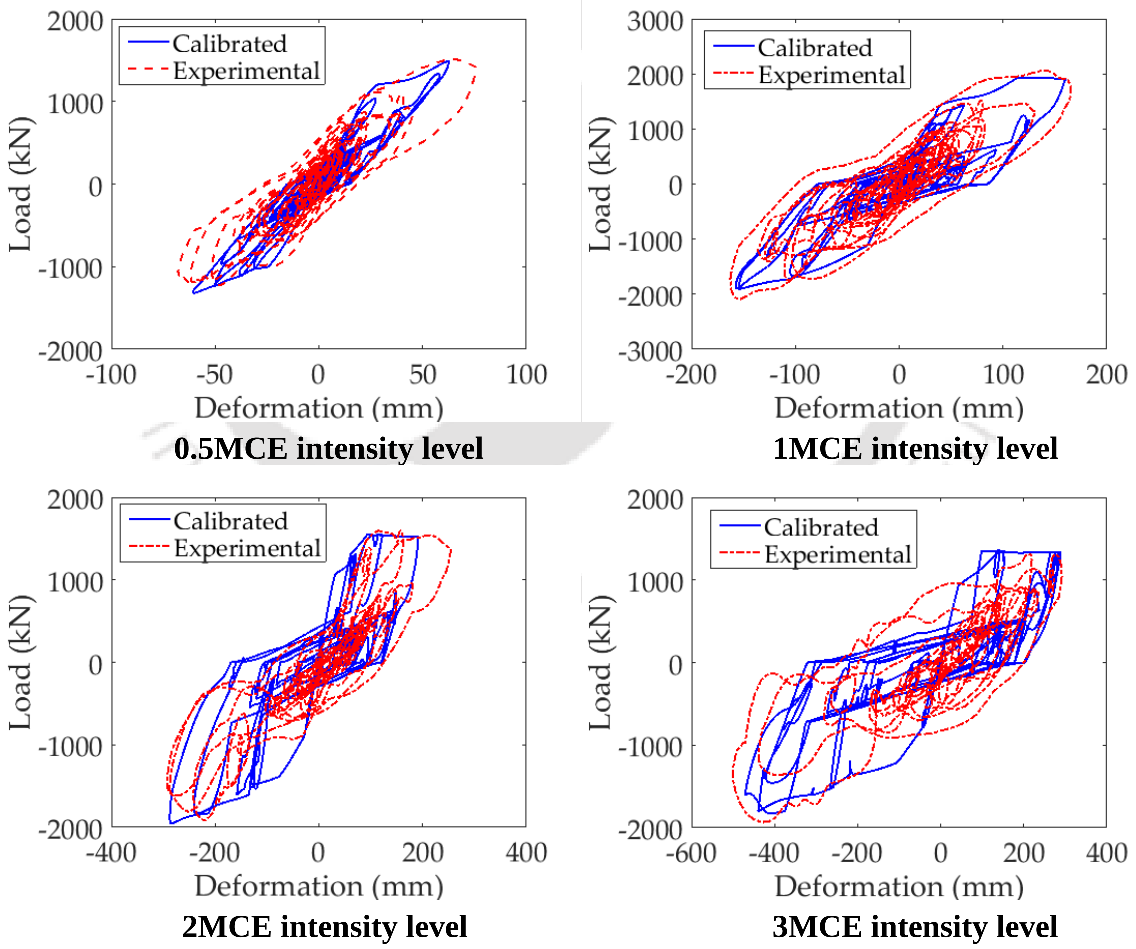

Figure 6.5. Comparison of the numerical results of conventional concrete bridge pier obtained from calibrated model with experimental results for different intensity levels

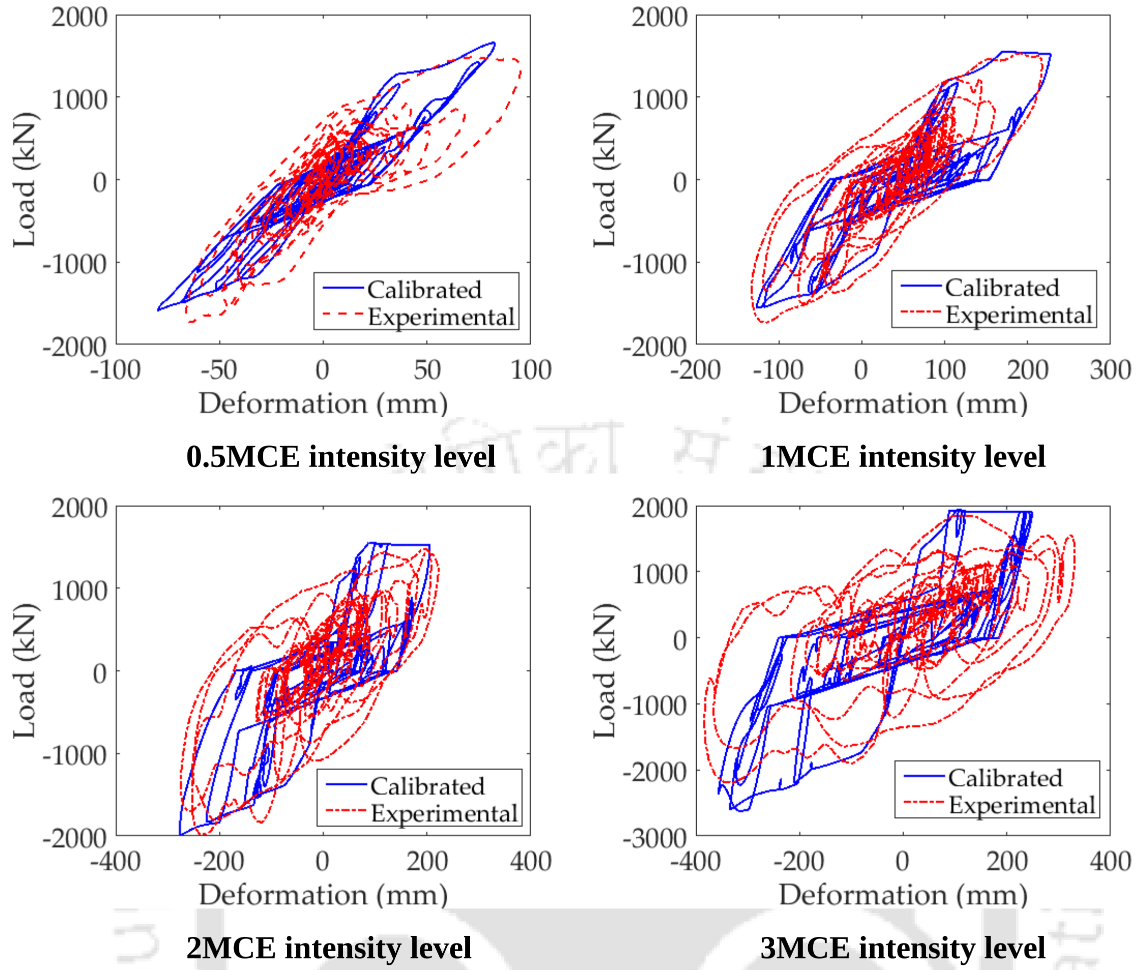

Figure 6.6. Comparison of the numerical results of HyFRC bridge pier obtained from calibrated model with experimental results for different intensity levels

6.4.1 Energy dissipation of calibrated results

Cumulative energy dissipation at a particular time step is calculated by summing the areas corresponding to preceding time step with energy dissipation of current time step and plot of cumulative energy dissipation with time is shown in Figure 6.7 and Figure 6.8. In all the cases with excitation of different MCE intensity levels, we see that energy dissipation capacity of calibrated model closely matches the experimental capacity for both conventional concrete and HyFRC specimen.

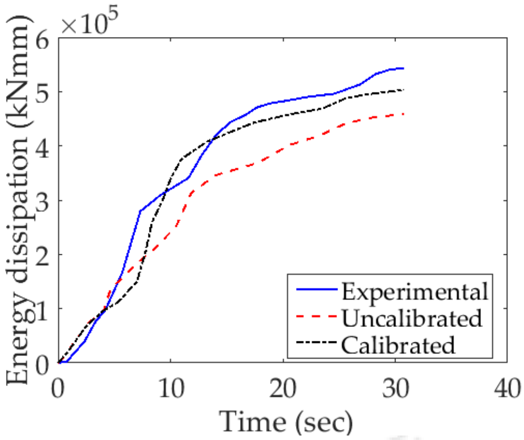

0.5 MCE intensity level

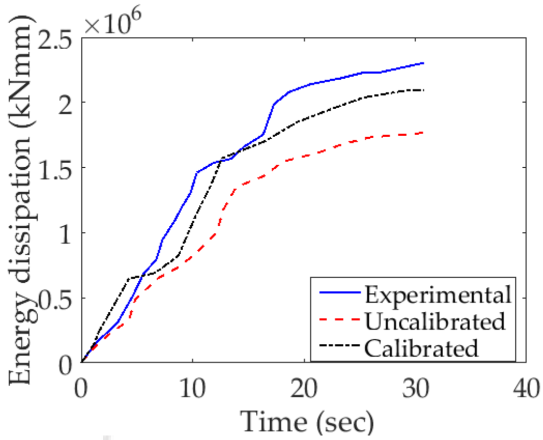

1MCE intensity level

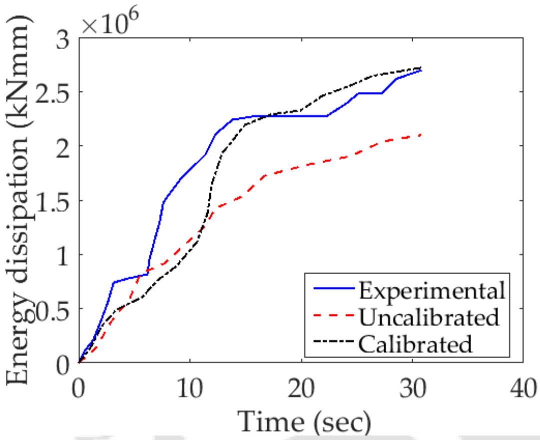

2 MCE intensity level

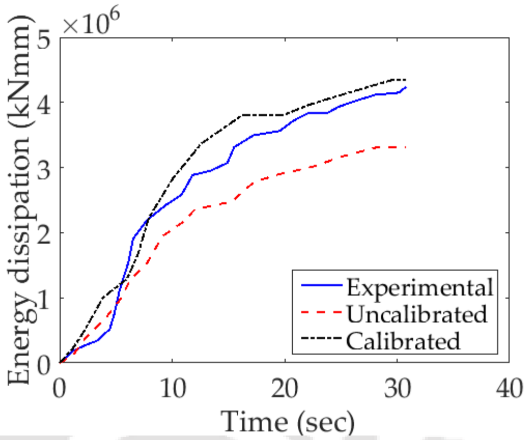

3 MCE intensity level

Figure 6.7. Comparison of the energy dissipation for all MCE levels for conventional concrete bridge pier

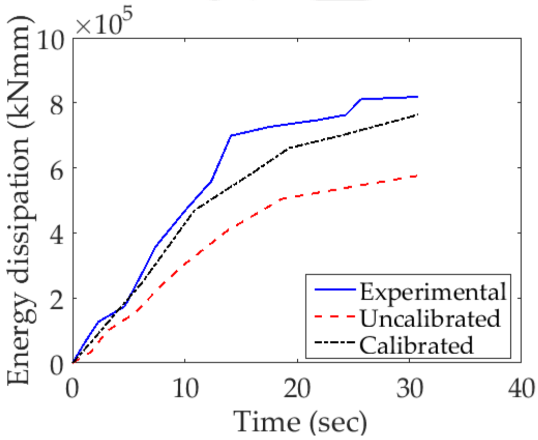

0.5 MCE intensity level

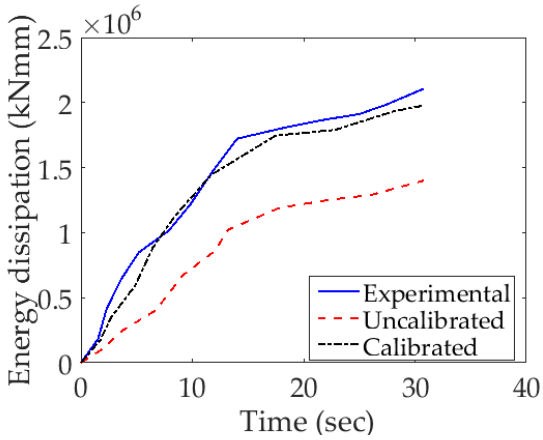

1MCE intensity level

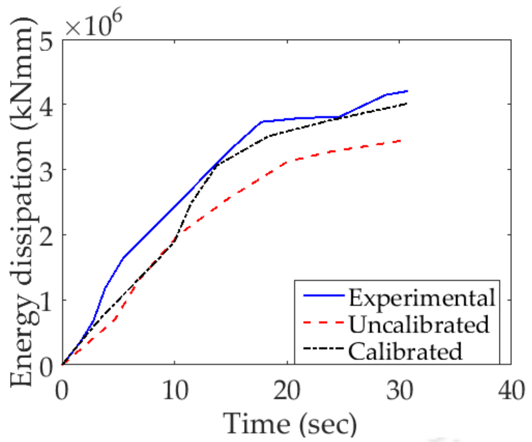

2 MCE intensity level

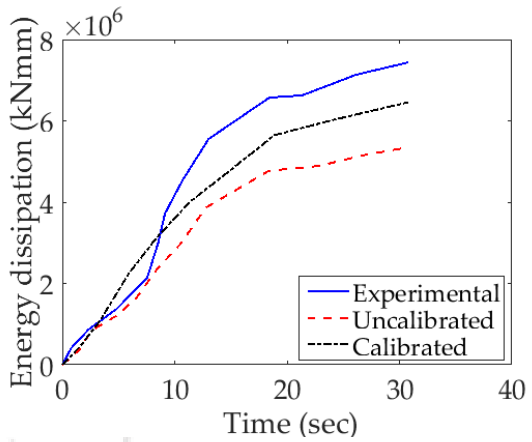

3 MCE intensity level

Figure 6.8. Comparison of the energy dissipation for all MCE levels for HyFRC bridge pier

6.5 CONCLUDING REMARKS

In this chapter, the numerical model discussed in chapter 4 is calibrated on the basis of results from hybrid simulations. Calibration is done by incorporation of spring at the base of the pier. Spring models are developed from the backbone curve of the force-deformation relationships. The resulting model is able to capture the stiffness and strength degradation effects at each intensity levels of loading. Peak load and peak deformation comparison as well as energy dissipation capacity of un-calibrated and calibrated model is carried out for verifying the result.

Chapter 7
SEISMIC VULNERABILITY ASSESSMENT OF THE BRIDGE

7.1 GENERAL

Precise evaluation of seismic demand on a structure and seismic vulnerability, which are crucial for seismic risk assessment, can be effectively studied with the help of seismic fragility curves. In recent decades, seismic fragility curves have emerged as a powerful tool to quantify the probability of exceedance of a certain level of damage for a given intensity level of ground motion. While researchers focussed on the development of these curves for conventional concrete bridges, very few studies are however found, where failure probabilities of FRC as well as conventional concrete bridge piers using fragility curves are compared (Zhang et al. 2016).

Several techniques/methodologies for generating seismic fragility curves for bridges were recently developed. These can be broadly classified into three groups: based on expert opinion (Applied Technology Council (ATC) 1991), empirically based (Mander and Basoz 1999, Shinozuka et al. 2000b), and based on analytical procedure (Nielson and DesRoches 2007, Farsangi et al. 2014). Due to limitations, such as inconsistency in damage observation, requirements of large amount of recorded damage data, etc. in expert-based and empirically based fragility curves, the analytical fragility curves have become more popular and are being extensively used to generate fragility curves for bridge structures. However, the results of analytical methods are highly influenced by definition of damage states and by the level of accuracy of analytical model in predicting seismic vulnerability of bridge. In the present study, more practical and precise bridge specific fragility curves are developed using hybrid method considering damage states derived from experimental observations and calibrated analytical model obtained from hybrid simulation.

A brief review of methodology adopted in this study to develop fragility curves is first presented and that is followed by identification of different damage states based on the observed damage pattern in the experimental element of hybrid simulation. The study on selection and scaling of ground motion used for the fragility analysis is carried out. Analytical fragility curve can be developed using two methods, namely, regression analysis and maximum likelihood estimation. Both the methods are used for generating fragility curves from incremental dynamic analysis (IDA) data and then compared. This chapter also provides comparison of fragility curves obtained from both calibrated and initial un-calibrated model, highlighting the importance of model calibration. This chapter ends with comparison of seismic fragility curves for bridge piers made of conventional concrete and HyFRC bridge pier using calibrated model in each case.

7.2 Methodology for Development of Analytical Fragility Curve

Over the last decade, IDA has emerged as a powerful tool for estimating the seismic demands on highway bridges and similar other structure. Several researchers (Billah et al. 2012, Mackie and Stojadinović 2005, Bhuiyan and Alam 2012, Zhang et al. 2009) used seismic demand estimated by IDA for seismic fragility analysis of highway bridges. IDA consists of series of nonlinear time history analysis (NLTHA) performed on a structure using suites of ground motions that are scaled up successively until collapse takes place. The method is similar to the way how an incremental pushover analysis is done. Incrementally scaled ground motions gradually drifts the structure from linear elastic behaviour to final global instability. IDA curves describing the relation between engineering demand parameter (EDP) and intensity measure (PGA, S_a *(T1)*) are then developed for every considered ground motion applied to the bridge. Component responses are obtained for each scaled ground motion by performing NLTHA and the results are compared to the respective limit state of damage. Ground motion scaling is stopped when the limit value associated with the complete damage state is exceeded by any one of the bridge components. Probability of failure can be calculated from multiple IDA data at each scaled intensity measure (IM) level by counting the number of IDA curves that cross the vertical line corresponding to the considered limit state. The ratio of these IDA curves to the total number of IDA curves is the probability of failure or fragility at that level of IM. In a similar way, probability of failure or fragility can be found for the considered limit state at other IM levels. The fragility values obtained using the multiple IDA curves are discrete fragility points. Moreover, it is preferable to express fragility as a continuous function of the intensity measure by applying probability based model on the IDA data using either regression method or maximum likelihood estimates. Subsequent subsection briefly describes these two methods used to develop seismic fragility curves of the bridge under consideration using incremental dynamic analysis, namely, a probabilistic seismic demand model (PSDM) based method suggested by Cornell and Jalayer (2002) and maximum likelihood method suggested by Shinozuka et al. (2000b).

7.2.1 Fragility analysis using PSDM and regression

If both the demand (D) and capacity (C) follow a lognormal distribution, then the bridge fragility is expressed as (Melchers 2001):

$$P\left[D > C / IM\right] = \Phi\left(\frac{\ln(\mathrm{S_D}/\mathrm{S_C})}{\sqrt{\beta_{D/IM}^2 + \beta_c^2}}\right) \tag{7.1}$$

where $\Phi[.]$ is the standard normal cumulative distribution function, S_D and $\beta_{D/IM}$ are the median and dispersion of log-normally distributed seismic demand, S_C and β_C are the median and dispersion of log-normally distributed seismic capacity. The limit state capacity for different damage states are derived either from experimental results or are derived analytically using pushover analysis by assuming variability in structural as well as material parameters.

In the present study, limit state capacity model is derived using the response data of experimental elements in hybrid simulation. The seismic demand is described through probabilistic seismic demand models (PSDMs), expressed in terms of an appropriate intensity measure. Cornell and Jalayer (2002) suggested that the estimate of the median demand (S_D) can be represented by a power model as:

$$S_D = aIM^b \tag{7.2}$$

where *IM* is the seismic intensity measure of choice (*PGA*, *PGV* or $S_{a\,(T1)}$) and both *a* as well as *b* are coefficients obtained using simple regression analysis after converting Equation 7.2 in logarithmic space. In literature, two approaches are available to develop PSDM: the cloud approach (Choi et al. 2004, Mackie and Stojadinović 2004, Nielson and DesRosches 2007) and scaling approach (Zhang and Huo 2009). In the cloud approach, un-scaled recorded earthquake ground motions are used in the nonlinear time-history analysis, whereas in the scaling approach, all the ground motions are scaled to specific intensity levels. IDA is used at each level of intensity and then a PSDM is developed based on the results of nonlinear time history analysis. In order to carry out cloud analysis, large number of ground motion data covering entire range of intensity levels are required so that structure experiences linear to nonlinear range of deformation, covering each of the considered damage states. Further, due to lesser number of ground motions selected in this study, the adopted procedure utilizes the scaling approach i.e. IDA based method following the guidelines of FEMA P695 (2009). IDA results are used to develop PSDM, which is then combined with the limit state capacity model to develop the seismic fragility curves for the considered bridge.

By substituting the formulation of median seismic demand S_D described in Equation 7.1, the fragility function is expressed as (Nielson 2005):

$$P\left[D > C / IM\right] = \Phi\left(\frac{\ln\left(IM\right) - \dfrac{\ln\left(S_c\right) - \ln\left(a\right)}{b}}{\dfrac{\sqrt{\beta_{D/IM}^2 + \beta_c^2}}{b}}\right) \tag{7.3}$$

This fragility function is lognormally distributed with a median $\lambda = \exp\left[\dfrac{\ln\left(S_c\right) - \ln\left(a\right)}{b}\right]$ and dispersion $\zeta = \dfrac{\sqrt{\beta_{D/IM}^2 + \beta_c^2}}{b}$ leading to following formulation:

$$P\left[D > C / IM\right] = \Phi\left(\frac{\ln\left(IM\right) - \ln\left(\lambda\right)}{\zeta}\right) \tag{7.4}$$

This method of fragility analysis is referred as ‘PSDM regressed’ method in this work.

7.2.2 Fragility analysis using maximum likelihood estimates

Shinozuka et al. (2000b) proposed fragility curve in the form of two parameter lognormal distribution function. The two parameters, namely median acceleration capacity (c_k) and lognormal standard deviation of the randomness (β_R) are estimated through a maximum likelihood method. The analytical form of fragility function $F_r\,(IM_i,\, c_k,\, \beta_R)$ for the damage state k using the above two parameters is defined as:

$$F_r = \Phi\left[\frac{\ln(IM_i / c_k)}{\beta_R}\right] \tag{7.5}$$

The likelihood function takes the form of Bernoulli distribution and is expressed as:

$$L = \prod_{i=1}^{n}\left[F_r\left(IM_i\right)\right]^{p_i}\left[1 - F_r\left(IM_i\right)\right]^{q_i} \tag{7.6}$$

where, $F_r\,(IM_i)$ represents the fragility at $IM = IM_i$ based on a specific damage state and is calculated using Equation 7.5. Total number of sample response points is designated by n which is total number of intensity level under which analysis is performed, p is 1 or 0 depending on whether the damage state k is exceeded or not and $q = 1 - p$. The two parameters c_k and β_R are evaluated by maximizing the likelihood function L:

$$\frac{\partial \ln L}{\partial c_k} = \frac{\partial \ln L}{\partial \beta_R} = 0 \tag{7.7}$$

This method of fragility analysis is referred as ‘Maximum likelihood’ method in this work.

7.3 Definition of Damage State using Experimental Results

Identification of damage state is one of the foremost steps in evaluating fragility curve. The considered bridge structure is analysed for four different intensity levels of earthquake excitation as discussed in Chapter 5. Each intensity level consists of 31 seconds of recorded data (Figure 4.8). Scaling to different intensity levels are done during hybrid simulation such that the bridge actually experiences different level of damage starting from minor crack to major damage as described in Chapter 5. The damages experienced by experimental elements during hybrid simulation are carefully studied and classified into four damage states viz. slight, moderate, severe and collapse. Limit state capacity values are used to define boundary of these damage states in terms of engineering demand parameter in the form of drift. These states are considered based on the actual damages monitored in the scaled pier specimen during hybrid simulation. The limit state corresponding to different damage states are correlated to the measured strain in concrete as well as reinforcement during the tests. The following parameters are utilized in order to define limit state capacity values of four considered damage states.

a) Slight damage: If measured maximum strain value in concrete exceeds the cracking strain of 138 μm/m for conventional concrete and 140 μm/m for HyFRC. These limiting values are obtained from four point bending test as per ASTM 1609 (1989) standard.

b) Moderate damage: If crack width exceeds 2mm. Frankie et al. (2013) reports a drift of 0.1% for flexural cracking. The pier height of scaled model for present research is 1800 mm, considering drift of 0.1%, crack width is found to be 1.8 mm (≈ 2 mm)

c) Extensive damage: If measured maximum strain value in reinforcement exceeds the yield strain of 2000 μm/m. The yield strains of reinforcement bars are available from laboratory test and strain results of specimens are reported in Appendix D.

d) Collapse: If maximum strain in concrete exceeds the crushing strain of concrete. The magnitude of crushing strain in concrete are in the range 3000 μm/m to 5000 μm/m according to Ni Choine (2014).

Careful visual observations from experimental elements of hybrid simulation reveals that cracking on surface of the specimens occurs during the test under 0.5 MCE intensity level. This is also evident from the distribution of strain as obtained from the strain gauges embedded in core of different specimens. Further, it is observed that widening of cracks occurs during 1MCE intensity level. Based on the data from strain gauges placed on the reinforcement (Figure 5.22), it is observed that yielding of reinforcement bar occurs during the test under 2MCE intensity level. Major concrete crushing is observed visually during 3MCE intensity level. However, in order to reduce computational time in fragility analysis, the limit state capacity are defined in terms of pier drift ratio instead of checking strains in each of the time history analysis (Frankie 2013). Table 7.1 shows the qualitative definition of various damage states in terms of structural parameters along with its quantitative description in terms of peak displacement and drift ratio for both conventional concrete and HyFRC specimen. In fragility analysis, the maximum drift ratio corresponding to damage state parameters for each time history analysis under different seismic excitations are monitored and is compared with the range of drift ratios indicated in Table 7.2.

Table 7.1. Damage state definition based on hybrid simulations under different intensity levels of excitations

Qualitative and quantitative description of damage state	**Damage states**			
	0.5MCE: Slight Damage	**1MCE: Moderate Damage**	**2MCE: Extensive Damage**	**3MCE : Collapse**
Affected Structural Parameters	Initiation of crack on the surface of the specimen	Widening up of crack in concrete	Yielding of reinforcement bars	Major crushing and spalling of concrete
Conventional Concrete Specimen				
Peak displacement (mm)	75.75	165.46	253.94	291.82
Drift ratio (%)	0.84	1.84	2.82	3.24
HyFRC Specimen				
Peak displacement (mm)	94.81	186.65	273.91	399.29
Drift ratio (%)	1.05	2.07	3.04	4.44

Table 7.2. Limit state capacity for each damage state in terms of Drift Ratio (Dr)

Drift Ratio (%) Conventional Concrete	**Drift Ratio (%) HyFRC**	**Damage Level**	**Definition**
$0.00 < Dr \leq 0.84$	$0.00 < Dr \leq 1.05$	I	No Damage
$0.84 < Dr \leq 1.84$	$1.05 < Dr \leq 2.07$	II	Slight Damage
$1.84 < Dr \leq 2.82$	$2.07 < Dr \leq 3.04$	III	Moderate Damage
$2.82 < Dr < 3.24$	$3.04 < Dr < 4.44$	IV	Extensive Damage
$Dr \geq 3.24$	$Dr \geq 4.44$	V	Collapse

7.4 Selection of Ground Motions

Selection of ground motion plays an important role in developing fragility curves. Several studies (Shome 1999, Kwon and Elnashai 2006) have shown that the record to record variability of ground motions is the primary contributor to the aleatory uncertainty. Aleatoric uncertainty is associated with the inherent randomness in the system. Therefore, structure must be subjected to more than one ground motion history with sufficient variability to reduce this uncertainty. There are three approaches available in literature (Cimellaro et al. 2009) to obtain earthquake records for the purpose of assessment of any structure:

- Select natural records from past strong motion database.
- Simulate synthetic ground motion from theoretical seismological models of seismic fault rupture.
- Simulate artificial accelerograms using stochastic or random vibration theory to match the target response spectra.

In this study, the record set belong to a bin of relatively larger magnitudes of 6.5-7.6 recorded on firm soil is used as per recommendation of FEMA P695 (2009). PGA is used as intensity measure of ground motion records because it can be obtained very easily from ground motion record without any information about structural properties. The provisions of FEMA P695 (2009) have been followed to select the ground motion and for sake of completeness it is quoted here in brief. The criterion followed to select the ground motions are:

a) Source Magnitude – Only large magnitude time-histories (M > 6.5) have been selected which result in strong shaking for longer durations and thus affect a large area on the surface.

b) Source Type – Seismic events based on strike slip or reverse type faults have been selected

c) Site Source Distance – The minimum site to source distance has been limited to 10 kilometres i.e. far field record sets have been selected.

d) Site Conditions – Ground motions recorded on soft rock or stiff soil have been selected.

e) Number of records per event – It has been limited to 2 to avoid any potential event based bias

f) Strongest Ground Motion Records – Limits of PGA > 0.2g and PGV > 15 cm/s have been arbitrarily applied, though they generally represent threshold structural damage.

g) Strong Motion Instrument Capability – Older instruments have limitations on their ability to record long period vibrations accurately. Records not valid upto at least 4 seconds have been excluded.

A total of twenty-two far field ground motions which meet the above criteria as given in FEMA P695 (2009) are selected for the current study from PEER NGA database. These records do not depend on any specific properties of structure and can be applied for excitation of variety of structures. Table 7.3 shows details of the selected ground motion for fragility analysis.

Table 7.3. Details of selected ground motions

S No.	PEER NGA Sequence No.	Event Name	Fault Mechanism	Earthquake Magnitude	Site Source Distance (km) Epicentral	PGA (g)
GM1	953	Northridge	Thrust	6.7	13.3	0.52
GM2	960	Northridge	Thrust	6.7	26.5	0.48
GM3	1602	Duzce, Turkey	Strike-slip	7.1	41.3	0.82
GM4	1787	Hector Mine	Strike-slip	7.1	26.5	0.34
GM5	169	Imperial Valley	Strike-slip	6.5	33.7	0.35
GM6	174	Imperial Valley	Strike-slip	6.5	29.4	0.38
GM7	1111	Kobe, Japan	Strike-slip	6.9	8.7	0.51
GM8	1116	Kobe, Japan	Strike-slip	6.9	46	0.24
GM9	1158	Kocaeli, Turkey	Strike-slip	7.5	98.2	0.36
GM10	1148	Kocaeli, Turkey	Strike-slip	7.5	53.7	0.22
GM11	900	Landers	Strike-slip	7.3	86	0.24
GM12	848	Landers	Strike-slip	7.3	82.1	0.42
GM13	752	Loma Prieta	Strike-slip	6.9	9.8	0.53
GM14	767	Loma Prieta	Strike-slip	6.9	31.4	0.56
GM15	1633	Manjil, Iran	Strike-slip	7.4	40.4	0.51
GM16	721	Superstition Hills	Strike-slip	6.5	35.8	0.36
GM17	725	Superstition Hills	Strike-slip	6.5	11.2	0.45
GM18	829	Cape Mendocino	Thrust	7.0	22.7	0.55
GM19	1244	Chi-Chi, Taiwan	Thrust	7.6	32	0.44
GM20	1485	Chi-Chi, Taiwan	Thrust	7.6	77.5	0.51
GM21	68	San Fernando	Thrust	6.6	39.5	0.21
GM22	125	Friuli, Italy	Thrust	6.5	20.2	0.35

7.4.1 Normalization method

FEMA P695 (2009) normalization procedure is used in the current study and for completeness of the study it is reproduced herein. As per this method, individual records of a given set are normalized by their peak ground velocities (PGV). Hence, some records are factored downwards and some factored upwards while maintaining the overall ground motion strength of the set. Normalisation by PGV is an easy and simple way to remove unwarranted variability between records due to inherent difference in event magnitude, source type and site condition, distance to source while still maintaining the inherent record to record variability necessary for accurately predicting fragility.

As per FEMA P695 (2009) guidelines, normalization is done with respect to the geometric mean of PGV of the two horizontal components. Normalization factor for the i^{th} record and normalized horizontal component of the i^{th} record can be obtained by using following equations:

$$NM_i = \frac{Median(PGV_{PEER,i})}{PGV_{PEER,i}} \tag{7.8}$$

$$\begin{aligned} NTH_{1,i} &= NM_i \times TH_{1,i} \\ NTH_{2,i} &= NM_i \times TH_{2,i} \end{aligned} \tag{7.9}$$

where, NM_i is the normalization factor of both horizontal components of the i^{th} record

$PGV_{PEER,\,i}$ is the Peak ground velocity of the i^{th} record

Median ($PGV_{PEER,i}$) is the median of $PGV_{PEER,i}$ values of records in the set,

$NTH_{1,i}$, $NTH_{2,\,i}$ are the normalized i^{th} record of horizontal component 1 and 2 respectively

$TH_{1,\,i}$, $TH_{2,\,i}$ are the i^{th} record of horizontal component 1 and 2 respectively

7.4.2 Scaling procedure

As mentioned in FEMA P695 (2009) that scaling of earthquake records is necessary if the selected natural records are not strong enough to force the structure to entire range of nonlinear behaviour i.e. the various limit states which is necessary for the generation of fragility curve. In general, three types of scaling procedures are available in literature-

- Recorded ground motions are scaled to match the PGA of target spectrum (Parool and Rai 2013).
- Recorded ground motion are scaled to match spectral acceleration value at fundamental time period of the structure $S_{a\,(T1)}$ (FEMA P695 2009, Vamvatsikos and Cornell 2002).
- Recorded ground motion are scaled to match the target spectrum by minimizing the misfit over the range of periods (Bommer and Acevedo 2004, ASCE 43).

Figure 7.1 shows the graphical representation of above procedure.

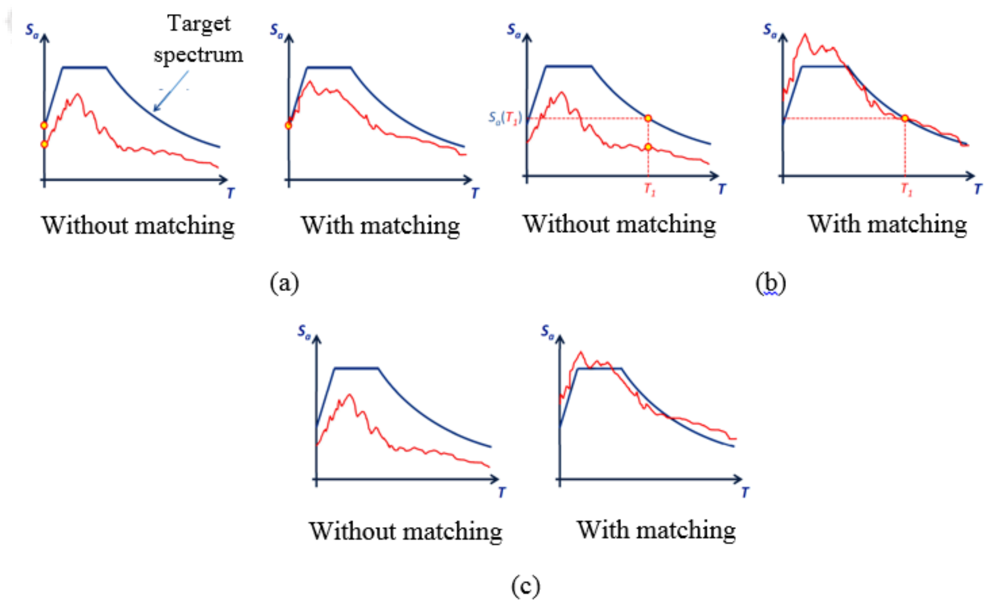

Figure 7.1. Scaling procedures: (a) target spectra based on PGA (b) target spectra based on S_a(T1) (c) target spectra by minimizing misfit over range of periods

In the present study, mean response spectrum of major components of ground motion is scaled to match PGA of standard response spectrum in order to attain statistical stability. The design response spectrum prescribed in IS: 1893 (2002) corresponding to Zone V (0.36g) is taken as standard response spectrum. This scale factor is termed as global scale factor (GS). In this study, IDA is chosen as the method to compute the maximum response. One factor termed as hazard factor (HF) is used (ranging from 0.1g to 1.5g) to represent hazard level to which structure is subjected. This range of hazard level covers entire range of PGA value corresponding to all the seismic zones of India (Vamvatsikos and Cornell 2002). Therefore, the raw ground motion data is scaled using total three factors. The relationship is described as:

$$GM_{scaled} = GM_{raw} \times NM \times GS \times HF \tag{7.10}$$

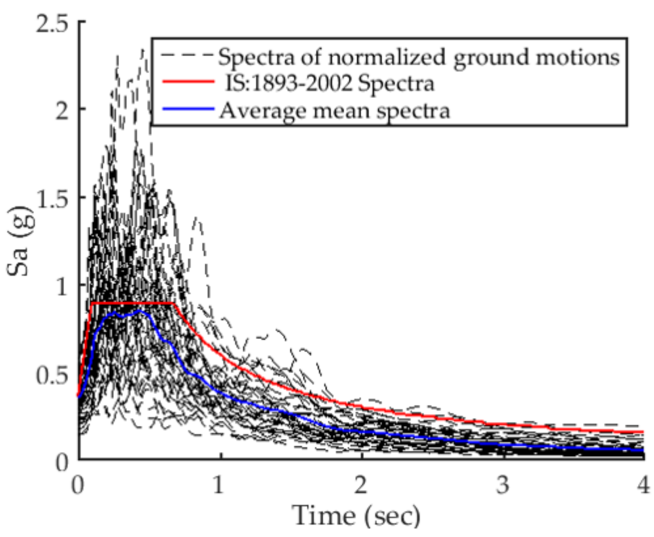

Figure 7.2. Comparison between IS 1893 (2002) design spectrum with mean spectrum of 22 selected ground motions

Thus each ground motion is multiplied with normalization factor, global factor and hazard level ranging from 0.1g to 1.5g. Figure 7.2 shows comparison between IS 1893

(2002) design spectrum with mean spectrum of 22 selected ground motions normalized and scaled to Zone V (0.36g) hazard level.

7.5 Seismic Fragility Curves

This section presents the results of the fragility analysis from three perspectives. First, in section 7.6.1, the two fragility analysis method viz. 'PSDM regressed' and 'Maximum likelihood' methods are compared in terms of their closeness to the direct fragility estimates i.e. fragility obtained directly using multiple IDA plots. Mandal et al. (2016) have carried out similar comparison of two methods for nuclear power plant. Here, for comparison of the two methods, results obtained from calibrated model of pier made of conventional concrete is used. Secondly, the importance of model calibration based on experimental results is highlighted by comparing seismic fragility obtained from un-calibrated and calibrated model for conventional concrete. Lastly, the seismic fragility curves for conventional concrete bridge and HyFRC bridge is compared in section 7.6.1 using calibrated numerical model. This results highlights the effectiveness of HyFRC in improving performance of the bridge pier.

7.5.1 Comparisons of two fragility analysis methods

'PSDM regressed' and 'Maximum likelihood' methods are compared in terms of how close each fragility curve is to the fragility obtained directly using multiple IDA plots. As stated earlier, IDA based fragility gives discrete data points at each IM level which is calculated by counting the number of IDA curves that cross the vertical line corresponding to considered limit state as shown in Figure 7.3. The ratio of these IDA curves to the total number of IDA curves is the probability of failure or fragility at that level of IM.

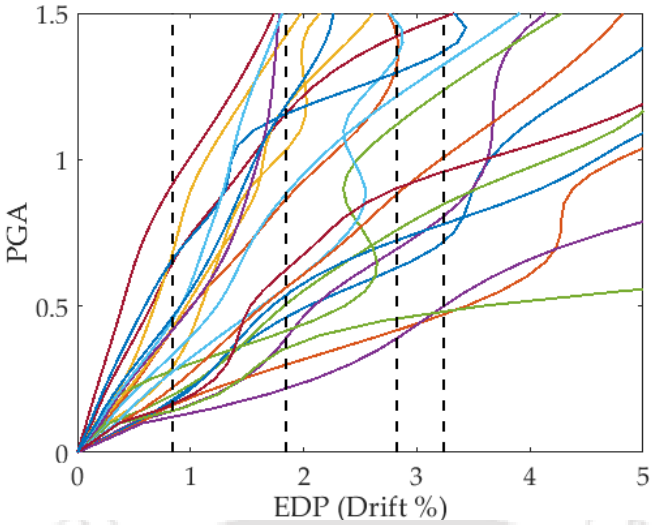

Figure 7.3. IDA curves along with limit state capacity for conventional concrete bridge pier

To make the comparison, the two methods are bought to the same level in terms of uncertainty consideration by ignoring randomness/uncertainty in capacity parameters, which means the fragility analysis are carried out by considering ground motion uncertainty only. Therefore, β_C in Equation 7.3, which indicate dispersion in limit state capacity in PSDM regressed method, is not considered. Figure 7.4 shows fragility curves obtained for conventional concrete bridge pier using calibrated model for four different limit states using two methods. It is observed that at low probability around 5% both methods give similar result which are in close argument with fragility obtained from IDA data. However at higher probability level, difference is observed in the results of these two methods. Considering discrete fragility obtained at each IM level from IDA data as benchmark, numerical comparison is performed by calculating coefficient of determination (R^2) and root mean square error (RMSE).

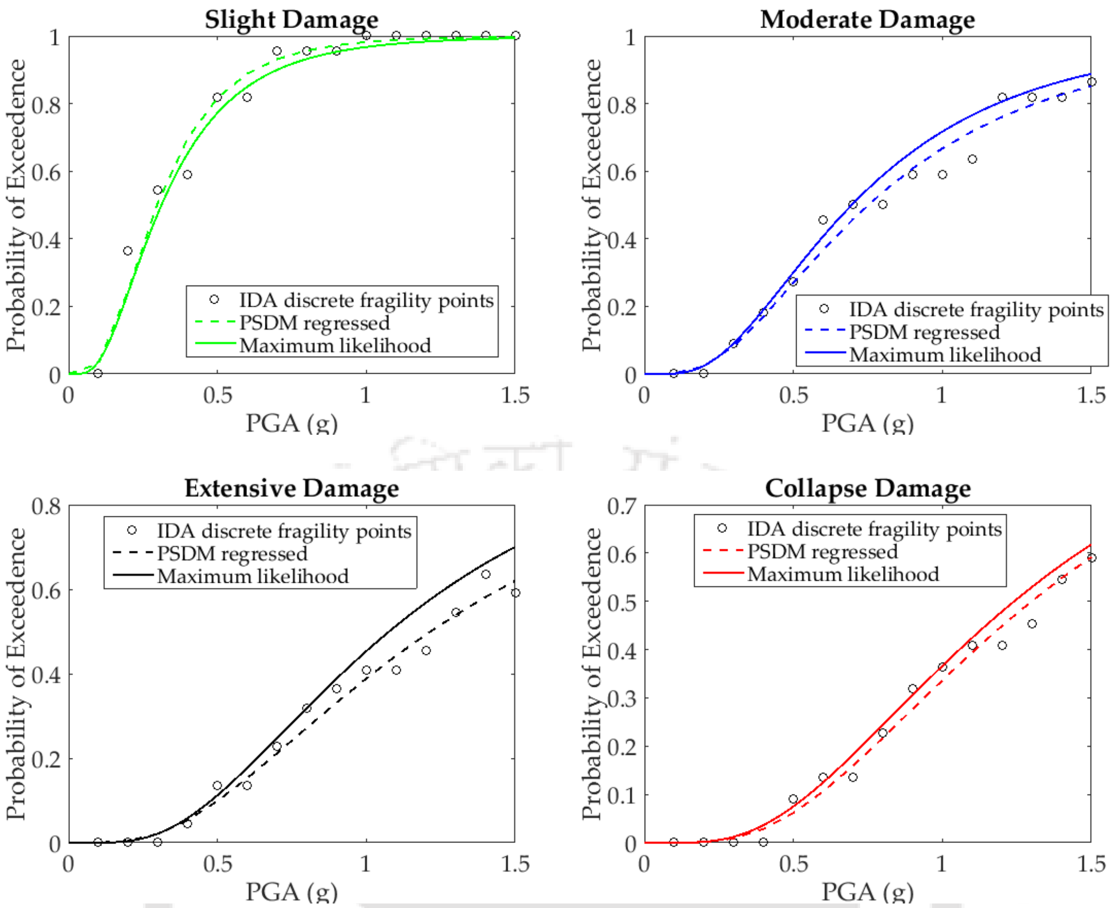

Figure 7.4. Comparison of fragility curves obtained using two methods for conventional concrete bridge pier

Table 7.4 summarized this comparison for each limit state. A slightly higher R^2 value and lower RMSE indicate that Maximum likelihood method gives better results as compared to PSDM regressed method for all limit states. However, Maximum likelihood method is more calculation intensive as it require calculation of new set of parameters (c_k and β_R) at each limit state. In PSDM regressed method, parameters (a, b, $\beta_{D/IM}$) are calculated only once during regression. Taking this into account, for further analysis only PSDM regressed method is used to develop fragility curves.

Table 7.4. Comparison of PSDM regressed and maximum likelihood fragility method

Limit State	Methods			
	PSDM regressed		Maximum likelihood	
	R^2	RMSE (%)	R^2	RMSE (%)
Slight	0.9729	5.95	0.9731	5.92
Moderate	0.9595	12.38	0.9779	9.14
Extensive	0.9322	19.75	0.9821	10.15
Collapse	0.9727	13.62	0.9843	10.35

7.6 COMPARISONS OF FRAGILITY CURVES OBTAINED USING CALIBRATED AND UN-CALIBRATED MODEL FOR CONVENTIONAL CONCRETE BRIDGE

In chapter 6, it is shown that there is significant difference in the response obtained from initial numerical model and response observed from experimental results. This is mainly due to the assumption made in the numerical model as stated in the chapter 6. It is also shown that how calibration of initial model with experimental results helps in getting the response in line with the response observed during experiment. Taking this into account, it is meaningful to show how model calibration affect the results of probabilities of failure i.e. fragility. Figure 7.5 shows comparison of fragility curves obtained from calibrated and un-calibrated model for conventional concrete pier. It can be seen that the probability of exceeding a particular damage state obtained using calibrated model is much higher than that obtained using uncalibrated model. This results clearly highlights the importance of using calibrated model in the seismic fragility analysis of the considered bridge.

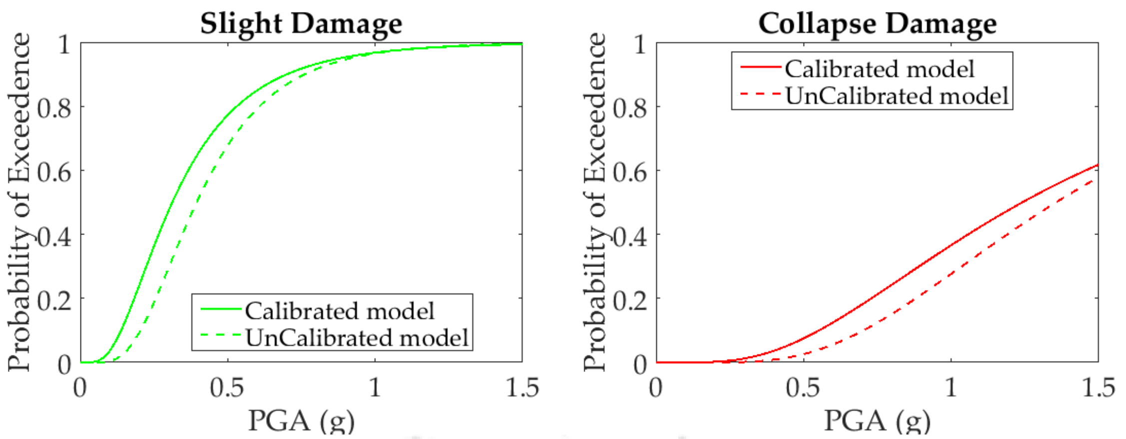

Figure 7.5. Comparison of fragility curves obtained from calibrated and un-calibrated model for conventional concrete bridge pier

Table 7.5 shows that the difference in dispersion and median value of the fragility at all damage states for both un-calibrated and calibrated model for conventional concrete bridge pier. It is observed that un-calibrated model overestimates the median value of fragility or in other words, it underestimates the failure probabilities across all the considered damage state. For example, there is 21% difference observed in the median value of fragility for slight damage between un-calibrated and calibrated model. In terms of probability of failure, it is observed that for a PGA of 0.36g (design PGA of the sample bridge), the failure probability obtained from un-calibrated model comes out to be 42.89%, 5.07%, 0.87% and 0.49% for slight, moderate, extensive and collapse damage state. On the other hand failure probability obtained from calibrated model as 58.9%, 14.85%, 4.14% and 2.5% for slight, moderate, extensive and collapse damage state. Therefore, use of un-calibrated model is erroneous in prediction of failure probabilities.

The calibrated numerical model along with damage states observed from experiments is used next to compare the seismic fragility of conventional concrete and HyFRC bridge pier.

Table 7.5. Difference in median value and dispersion of the fragility obtained from un-calibrated and calibrated model

Damage state	**Un-calibrated model**		**Calibrated model**		**Percentage change in median value**
	λ	ζ	λ	ζ	
Slight	0.395	0.68	0.312	0.62	21.01
Moderate	0.834	0.68	0.696	0.62	16.55
Extensive	1.220	0.68	1.077	0.62	11.72
Collapse	1.356	0.68	1.241	0.62	8.48

7.6.1 Comparisons of fragility curves for conventional concrete and HyFRC bridge

In order to assess the impact of use of HyFRC in seismic vulnerability of bridges, seismic fragilities are evaluated for both conventional and HyFRC bridge which are shown in Figure 7.6. It is worthwhile to note again here that development of bridge fragility damage states are obtained from the experimental hybrid simulation results. Also, response of analytical model is calibrated with the response of hybrid simulation, therefore, it closely represent response of the real structure which is essential for derivation of high-fidelity fragility curves.

A complete list of the dispersion and median value of the bridge fragility at all damage states is provided in Table 7.6 for both conventional and HyFRC bridge. An increase in median value of fragility for different damage states for HyFRC bridge is further a direct indication of the decrease in seismic vulnerability with the use of HyFRC in bridge pier. Results shows that use of HyFRC in bridge pier leads to 45 % increase in median PGA for collapse damage state as compared to that of conventional concrete bridge pier

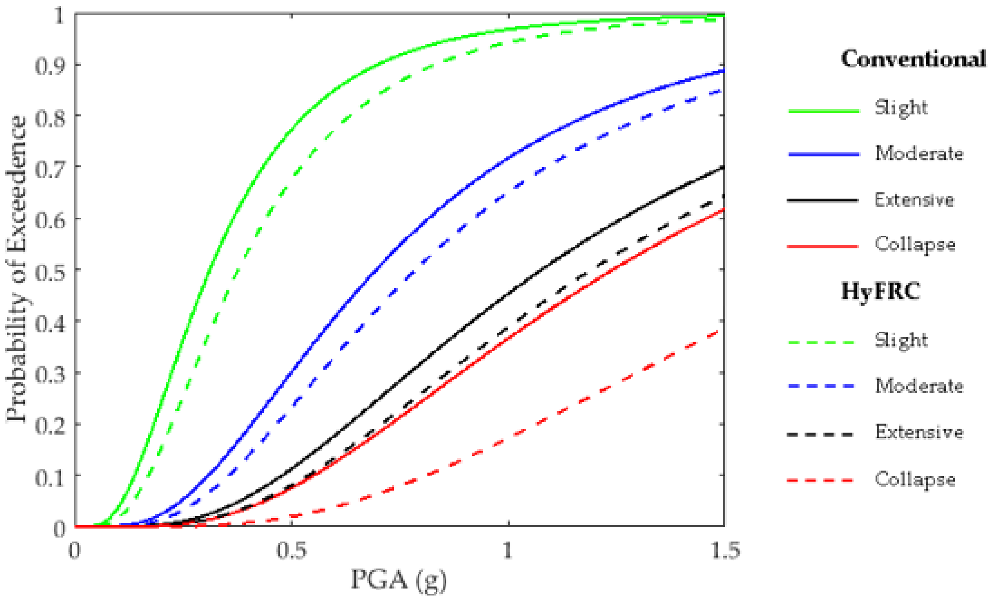

Figure 7.6. Comparison of fragility curves of bridge piers made of conventional concrete and HyFRC developed using calibrated model

Table 7.6. Median and dispersion values of fragilities for all damage states for both conventional and HyFRC bridge pier

Damage state	Conventional concrete bridge		HyFRC bridge	
	λ	ζ	λ	ζ
Slight	0.312	0.62	0.380	0.57
Moderate	0.696	0.62	0.787	0.57
Extensive	1.077	0.62	1.200	0.57
Collapse	1.241	0.62	1.796	0.57

7.7 Concluding remarks

This chapter compares the seismic performance of conventional concrete and HyFRC bridge pier using fragility curves where limit state capacity are obtained using observed result of experimental hybrid simulation and demand is obtained using calibrated analytical model. The demand and capacity are then compared to develop seismic fragility curves. It may be mentioned that no studies in the past used experimentally derived limit states and calibrated analytical model validated using hybrid simulation for development of fragility curves.

The chapter starts with brief description of methodology used to develop fragility curve followed by identification of damage states using experimental results. Selection of ground motion based on FEMA P695 procedure is provided next. Using the selected ground motions, fragility analysis is carried out using IDA procedures. Comparison of two methodology, namely, 'PSDM regressed' and 'Maximum likelihood' is carried out in terms of their closeness to the direct fragility estimates i.e. fragility obtained directly using multiple IDA plots. PSDM regressed method is less computing intensive and so it is used in all further analysis. The importance of model calibration through experimental results is also highlighted by comparing seismic fragility obtained from un-calibrated and calibrated model for conventional concrete and the results establishes the importance of model calibration. For instance, there is 21% difference observed in the median value of fragility for slight damage state condition for un-calibrated and calibrated models. Further, the seismic fragility analysis using experimentally observed damage state and calibrated numerical model show that the HyFRC piers to be less vulnerable as compared to conventional concrete piers across all damage states. These results justifies the importance for use of HyFRC in bridge pier.

Chapter 8

CONCLUSIONS AND RECOMMENDATION FOR FUTURE RESEARCH

8.1 OVERVIEW

Bridges are the most important components of transportation infrastructure, and their continued safe performance after a seismic event is vital to human and economic activities. In the present study, use of HyFRC and additional detailing features in pier-foundation interface is studied in details for evaluation for improved seismic performance of bridge pier. Prior to usage of HyFRC in bridge pier, material level characterization of HyFRC is carried out in details. The performance of HyFRC bridge piers under different intensity levels of seismic excitation and also under cyclic load are evaluated. The detailed test results are documented in terms of various parameters related to seismic performance such as load carrying capacity, stiffness degradation, energy dissipation, displacement ductility, vulnerability etc.

8.2 SUMMARY

The major motivation of the present research work is prompted from the fact that use of HyFRC in place of conventional concrete can lead to increase in ductility. The best possible combinations of selected fibres for improving ductility of concrete specimens is first evaluated. It is also observed from literature that the HyFRC has superior shear resistance as compared to conventional concrete. Kumar et al. (2011) studied HyFRC specimens with 50% lesser transverse reinforcement as compared to conventional RC bridge pier and reported comparable seismic performance. Shear capacity of standard prisms are evaluated with 50% reduction in shear reinforcement.

An existing bridge is considered for the study. It is known that damage in a bridge pier is mostly localized at the column-foundation interface region. Post-earthquake rehabilitation works of bridge piers become easier if the crack location is shifted away from the pier-foundation interface zone. This is likely to be achieved by incorporation of some additional features at column-foundation interface. Three different detailing strategies are considered at pier-foundation interface region. While normal reinforcement details are followed for specimen type 1, additional reinforcing bars (dowels) are used in the interface region for specimen type 2 and corrugated sheet duct is used below interface region in specimen type 3. It is necessary to perform an advanced level of experimental investigation in order to evaluate the seismic performance of the bridge with pier made of high performance material. In the present research, performance of all the types of pier specimens with different detailing are evaluated using hybrid simulation.

Hybrid simulation technique can integrate efficiently the seismic behaviour of entire bridge including structural elements with behavioural uncertainties. For this reason, hybrid simulation is considered to observe behaviour of pier-foundation interface zone in the present study. Four input excitations corresponding to different intensity levels are used in the hybrid simulation, which is followed by the quasi-static cyclic test to take the specimens to the ultimate failure level. Hybrid simulation is carried out by physically testing critical elements of a structure (such as bridge piers), while the remaining elements are concurrently simulated numerically. The numerical model is developed in OpenSees platform and the elements of the numerical model are suitably chosen for simulating appropriate behaviour of different components of the sample bridge. The hybrid simulation is performed using a step-by-step numerical solution of the governing equations of motion for a model that is formulated considering both numerical and physical portions of the structure. The OpenFresco framework, which is used to define the experimental elements, provides a useful and effective set of modules for performing hybrid simulations. It further helps to connect the numerical module developed in OpenSees platform to the experimental elements in the laboratory. The effect of HyFRC for enhancing seismic induced damage resistance is investigated by hybrid simulation of the entire bridge structure.

The results obtained from hybrid simulation of six different scaled pier specimens and subsequent testing under cyclic loading are examined to explore the effectiveness of use of fibres as well as additional detailing features at pier-foundation interface region. Comparison of measured and observed responses of specimens made of two types of materials are made to highlight changes in damage pattern, displacement ductility and energy dissipation capacities of specimens. Extent of damage at the end of test is significantly lesser in all the three HyFRC specimens than the corresponding three conventional concrete specimens. HyFRC specimen with dowel bar shows least damage amongst all the specimens, while all HyFRC piers shows consistently higher energy dissipation capacity in comparison to corresponding conventional concrete piers.

The use of HyFRC leads to delay in crack formation and crack growth, which in turn reduce strain level in reinforcing bars. Strain gauges are used to measure strain in concrete as well as in reinforcement to explore the relative merits and demerits of both HyFRC and conventional concrete. Strains are monitored at the critical pier locations to correlate the growth of strain with damage in specimens. The strains in reinforcement of HyFRC piers are found to be considerably reduced at all stages of loadings and displacement ductility of HyFRC specimens got improved compared to those of the conventional concrete piers. The lower growth rate of strain in HyFRC bridge piers in turn can be related to the improvement in basic seismic design parameters.

In order to accurately predict the response of the initial numerical model in line with experimental results, modification are made in the model which includes addition of translational spring at the pier-foundation interface and adjustments in damping ratio to capture hysteretic damping effects. The calibrated model is able to capture the stiffness and strength degradation effects at each intensity levels of loading.

Fragility function for the entire bridge system is developed considering the results of current experimental studies. Incremental dynamic analysis (IDA) is used in the procedure for development of fragility curves. In this study, the provisions of FEMA P695 (FEMA, 2009) are followed to select the ground motion. Finally, the seismic demand and failure probabilities of HyFRC bridge piers and conventional concrete bridge piers are compared using these fragility curves.

8.3 Conclusions

The major contributions and conclusions ascribed to the present study may be summarized as follows:

- Fibres greatly contribute in controlling degradation of concrete in a structural element. Damage experienced by different HyFRC specimens at different stages of loading with varying intensity levels and their comparison with those of corresponding conventional concrete specimens clearly establishes this observation. Comparison between the envelope curves along with stiffness degradation further reinforces the aforesaid observation.
- Performance of HyFRC in structural elements are superior compared to conventional concrete under the action of seismic excitations. HyFRC specimens are observed to consistently exhibit higher energy dissipation capacity than that of the corresponding concrete specimen at different intensity levels of excitation.

- On the basis of strain measurement, it is established that the growth of strain and hence crack initiation is delayed in HyFRC specimens compared to that of conventional concrete specimens. Further, it is also observed that the presence of additional components like dowel bars, corrugated sheets in the vicinity of pier-foundation interface zone shift the damage zone away from the interface region. This may facilitate ease of rehabilitation, if required after any high intensity earthquake event.
- High confinement steel requirement in seismic resistant design procedure may be reduced by the use of HyFRC, without compromising displacement ductility. This would help in reduction of congestion due to reinforcement, particularly at the junction region and would thus reduce the possibility of formation of void, honeycomb in concrete.
- Dowel reinforcements in bridge pier are effective in shifting of damage away from pier-foundation interface zone. Piers with dowel reinforcement are capable of showing higher energy dissipation capacity than that of the corresponding bridge piers with conventional reinforcement detailing.
- Use of corrugated sheet also has the potential for crack relocation from the interface zone. The effectiveness is likely to be improved by appropriate selection of gauge size of the sheet.
- The extent of damage at the end of cyclic test in the pier-foundation interface in the HyFRC specimens is significantly lesser than that of the corresponding conventional concrete specimens and hence rehabilitation of such specimen would be easier.
- The experimental investigation using hybrid simulation is an efficient technique for the evaluation of seismic performance of a complete structural system.

- The use of nonlinear spring at the pier base is found to be quite effective in terms of attaining close agreement between results of obtained from calibrated model and those of hybrid simulation.
- Seismic fragility analysis using experimentally observed damage state and calibrated numerical model distinctly establishes HyFRC piers are less vulnerable as compared to conventional concrete piers across all damage states.

8.4 RECOMMENDATION FOR FUTURE RESEARCH

Additional work may be undertaken in the following areas:

- Real time hybrid simulation can be performed to bring forth inertial effect and actual damping effect due to the action of an earthquake on the structure.
- The present study initiated use of corrugated steel duct up to the pier-foundation interface level. The gauge size of the duct can be further increased to have visible influence of corrugated sheet on relocation of crack away from the interface zone.
- Different types of fibre combinations can be tried for HyFRC bridge piers.
- Large experimental data are required to develop more reliable fragility functions. This requires additional testing of scaled bridge pier specimens.
- Multiple span bridge can be considered for similar study. Distributed hybrid simulation can also be carried out for such multiple span bridge.

Appendix A
MIX DESIGN ACCORDING TO IS 10262-1982

A.1 MATERIAL TESTING

Cement

Specific gravity of Cement by Le Chatelier Flask Apparatus:

Wt of Cement taken=64 gm

Initial Reading=0.2 ml

Final Reading=22.6 ml

Volume of Liquid Displacement= Final-Initial

Density of Cement (γ)= Mass of Cement in gm/ Displacement Volume in cm^3

Specific Gravity= Density of cement (γ)

γ =64/ (22.6-0.2) = 2.86

Coarse aggregates (CA)

The coarse aggregates used were of size 1o mm (down) by sieve analysis and were mostly angular in shape.

Specific gravity test result

Sr. No.	**Description**	**Weight (gm)**
1	Weight of empty Pycnometer + water	W_1 = 1328
2	Weight of empty Pycnometer + aggregates + water	W_2 = 1660
3	Weight of Pycnometer	W_3 = 462
4	Pycnometer + dry surface aggregates	W_4 = 986

Specific gravity = $(W_4 - W_3)/ [(W_4 - W_3) - (W_2 - W_1)]$

= 524/(524-332) =2.73

Fine aggregate (FA)

Sieve analysis result confirms fine aggregate to be of Zone III

Specific gravity test result

Sl. No.	Description	Weight (gm)
1	Weight of empty Pycnometer + water	W_1 = 1238
2	Weight of Pycnometer + sand + water	W_2 = 1559
3	Weight of Pycnometer	W_3=150
4	Pycnometer + dry surface sand	W_4 = 672

Specific gravity = $(W_4 - W_3)/ [(W_4 - W_3) - (W_2 - W_1)]$ = 522/ (522-321) =2.59

A.2 IS METHOD OF MIX DESIGN

The Indian Standards Institution (ISI) has recommended guidelines for concrete mix design based on cement and other material locally available in India. These guidelines are applicable for normal concrete (less than 60 MPa) mix design.

Step 1: Design Stipulations

Characteristic compressive strength = 25 N/mm^2

Maximum size of aggregate = 10mm

Degree of workability = 0.8

Degree of quality control = Good

Step 2: Collection of Data

1. Cement: Type PCC of Brand 'Ultratech'

Specific gravity of cement = 2.86

2. Coarse Aggregate: Source- Meghalaya

Specific gravity of coarse aggregate = 2.73

Water absorption (coarse aggregate) = Nil

3. Fine Aggregate: Source-Saigaon, Kukurmara

Specific gravity of fine aggregate = 2.59

Water absorption (fine aggregate) = Nil

Surface moisture (fine aggregate) = Nil

Step 3: Target mean strength

$f_{ck}' = f_{ck} + 1.65\ S$ (As per Clause 3.2 IS:10262:2009)

S=4.0 (As per IS:456 Table no.8,Page-23)

Target mean strength, $f_{ck}' = 25 + (1.65 \times 4.0) = 31.6$ MPa

Step 4: Selection of water/cement ratio –

W/C ratio = 0.5

Water + surface moisture = 186 kg/m^3

Sand as percentage of total aggregate = 35% × vol. of aggregate

Adjustments are required in water content sand percentage for other conditions ::

		Water	Sand
Decrease in w/c ratio of (by mass)	0.6 – 0.5 = 0.1	0	-2%
Increase in Compacting factor	0.8 – 0.8 = 0	0	-
Sand zone	Confirming Zone III	0	-1.5%
Total		0%	-3.5%

Required water content = 186 lit/m^3

Required sand content = 35 – 3.5 = 31.5%

Required cement content = 186/0.5 = 372 kg/m^3

Step 5: Determination of amount of coarse and fine aggregate

Entrapped air = 2% (from IS 10262 table 3, page 9)

CA content and FA content clause 3.5.1

V = [W + (C/Sc) + (fa/(p × Sfa)] × 1/1000

=>(1 – 0.02) = [186+ (372/2.86) + (1/0.315).(fa/2.59)]×(1/1000)

=>fa=541.67 kg

V= [W + (C/Sc) + Ca/ (1 – p)×(Sca)]× 1/1000

=>0.98 = [186+ (372/2.86) + (1/(1-.315))(Ca/2.73)]1/1000

=>ca=1241.58 kg

Step 6: Final Mix Proportion:

Content	Water	Cement	F.A.	C.A.
Ratio	0.5	1.0	1.46	3.34

Appendix B
DESIGN OF BEAM FOR SHEAR REINFORCEMENT TEST PROGRAM

B.1 LOAD CARRYING CAPACITY OF BEAM WITH FOUR 10 mm Ø LONGITUDINAL REINFORCEMENT

This appendix provides the calculation of shear reinforcement for the prism specimen as mentioned earlier in Section 3.3. The dimension of the prism specimen is 150 × 150 × 700 mm and is reinforced with 4-10 mm diameter longitudinal reinforcement as shown in Figure 3.11. The detail calculation of load carrying capacity and design of shear reinforcement as per IS 456 are shown below:

Assuming the prism section as singly reinforced section, the neutral axis depth x_u can be calculated as below:

Limiting depth of neutral axis for Fe 500 is given as

$$x_{u,\max} = 0.48d$$

where, d is the effective depth of the section and given as

$$d = D - \mathrm{cover} - \phi_s - \frac{\phi_l}{2} = 150 - 20 - 8 - 10/2 = 117 \text{ mm}$$

$$x_{u,\max} = 0.48 \times 117 = 56.16 \text{ mm}$$

Assuming $x_u \le x_{u,\max}$ and applying the force equilibrium, i.e.

Compression force, C_u = Tension force, T_u

$$0.362 f_{ck} b x_u = 0.87 f_y A_{st}$$

$x_u = \frac{0.87 f_y A_{st}}{0.362 f_{ck} b}$, where f_y is the yield strength of steel = 500 Mpa, A_{st} is the area of longitudinal reinforcement on tension side $= 2\times(\pi/4)\times 10^2$ = 157 mm^2, f_{ck} is the characteristic strength of concrete = 35 MPa and b is the width of section = 150 mm

$x_u = \frac{0.87\times 500\times 157}{0.362\times 35\times 150}$ = 35.93 mm $\leq x_{u,\max}$, therefore the section is singly reinforced section.

The ultimate moment of resistance M_{uR} of the considered prism section is given as:

$$\begin{aligned} M_{uR} &= 0.87\, f_y A_{st}\left(d - 0.416 x_u\right) \\ &= 0.87\times 500\times 157\times\left(117 - 0.416\times 35.93\right) \\ &= 6.9\times 10^6\, N\text{-}mm \end{aligned}$$

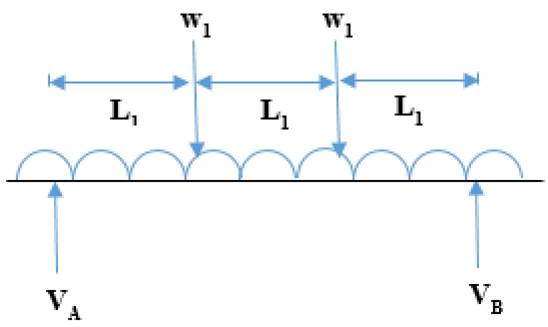

Figure B.1. Free body diagram for four point bending test

For the four point bending test (Figure B.1.), the maximum moment M occurs at the midpoint and is given as:

$$M = \frac{wl^2}{8} + w_1\times\left(l_1 + \frac{l_1}{2}\right) - w_1\times\frac{l_1}{2}$$

where, l is the length between supports = 600 mm, w_1 is the factored point load, w is the factored self-weight of the beam $= (1.5\times 25)\frac{kN}{m^3}\times 0.15\times 0.15 = 0.845\frac{kN}{m} = 0.845\frac{N}{mm}$

By substituting maximum moment carrying capacity $M = M_{uR}$, the factored point load w_1 that can be taken by the beam without failure is calculated as:

$$6.9\times10^{6}=\frac{0.845\times600^{2}}{8}+w_{1}\times\left(200+\frac{200}{2}\right)-w_{1}\times\frac{200}{2}$$

$$\Rightarrow w_{1}=34.3\times10^{3}N=34.3kN$$

Design of transverse reinforcement:

The factored shear force V_u at support is given as:

$$\begin{aligned}V_{u}&=\frac{wl}{2}+w_{1}\\&=\frac{0.845\times600}{2}+34300\\&=34553.5N=34.6kN\end{aligned}$$

The shear force resisted by concrete is given as:

$$\begin{aligned}V_{uc}&=\tau_{c}bd\\&=0.63\times150\times117\\&=11.06\times10^{3}N=11.06kN\end{aligned}$$

where, $\tau_c=0.63$ is the design shear strength of the concrete obtained from Table 19 IS 456. Since, the factored shear force V_u is greater than the shear strength resisted by concrete V_{uc}, the section must be design for shear reinforcement. The shear resistance V_{us} that must be provided by vertical stirrups is given as:

$$V_{us}=\frac{0.87f_{y}A_{sv}d}{s}$$

where, $V_{us}=V_{u}-V_{uc}=23kN$, A_{sv} is the area of two-legged stirrups and s is the spacing of stirrups.

For two-legged 8 mm diameter stirrups, the minimum spacing required

$$\begin{aligned}s&=\frac{0.87f_{y}A_{sv}d}{V_{us}}\\&=\frac{0.87\times500\times2\times(\pi/4)\times8^{2}\times117}{23\times10^{3}}\\&=222.3mm\end{aligned}$$

However, the minimum spacing provided must be less than the spacing required as per Clause 26.5 of IS: 456. The minimum spacing required is given as:

$$s \le \begin{Bmatrix} 0.75d \\ or \\ \dfrac{0.87 f_y A_{sv}}{0.4b} \\ or \\ 300mm \end{Bmatrix}$$

Therefore, as per this clause the minimum spacing provided is 90 mm.

Appendix C
TENSILE TEST RESULTS OF REINFORCEMENT BAR

C.1 STEEL FOR LONGITUDINAL REINFORCEMENT

The longitudinal reinforcement used in the pier specimen consist of bars of size 16 mm diameter and Fe 500 grade steel. Before specimen caging, bars were randomly selected and tested in tension as per IS: 432(I)-1982 and IS: 1608-1995 code by using a 1000 KN Universal Testing Machine to determine the yield and ultimate strengths. Typical monotonic stress-strain curves for the tested 16mm diameter bar is shown in Figure C.1. The yield strength is found to be 547MPa and ultimate strength as 635MPa.

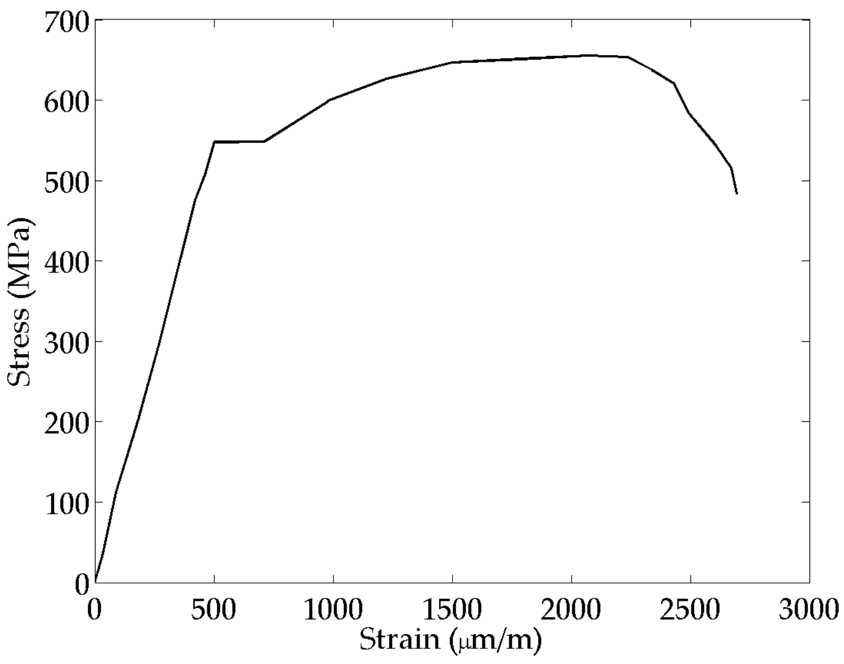

Figure C.1. Typical stress strain diagram for steel sample of 16 mm diameter

C.2 STEEL FOR TRANSVERSE REINFORCEMENT

Transverse reinforcement used in the pier specimen is of 8 mm diameter and Fe 500 grade. IS: 432(I)-1982 and IS: 1608-1995 code was used for the testing procedure. Typical monotonic stress-strain curves for tested bar is shown in Figure C.2. The yield strength is found to be 578MPa and ultimate strength as 689MPa.

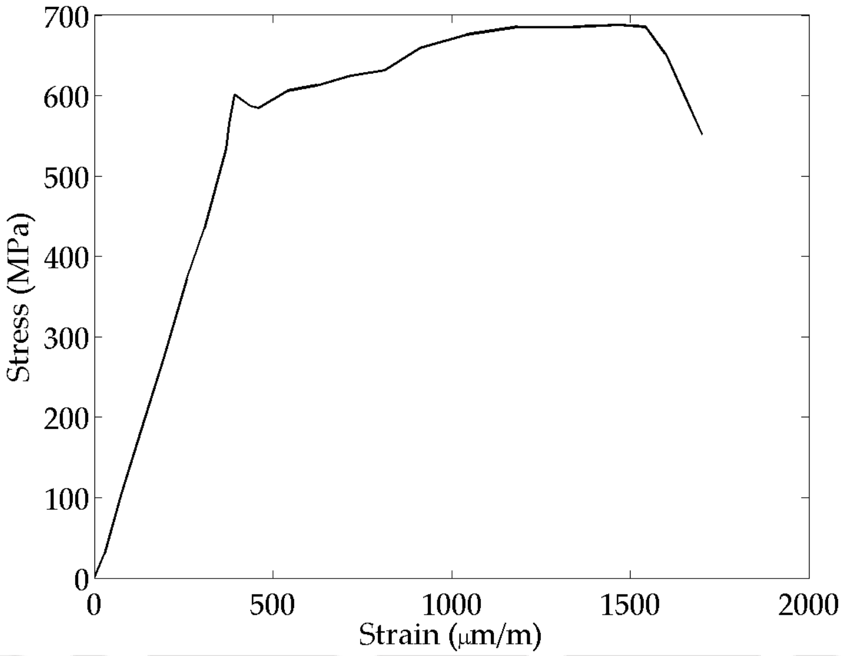

Figure C.2. Typical stress strain diagram for steel sample of 8 mm diameter

Appendix D

RESPONSE HISTORY OF STRAIN GAUGES IN LONGITUDINAL REINFORCEMENT

Strain history of strain gauges at C1 are shown in the following figures.

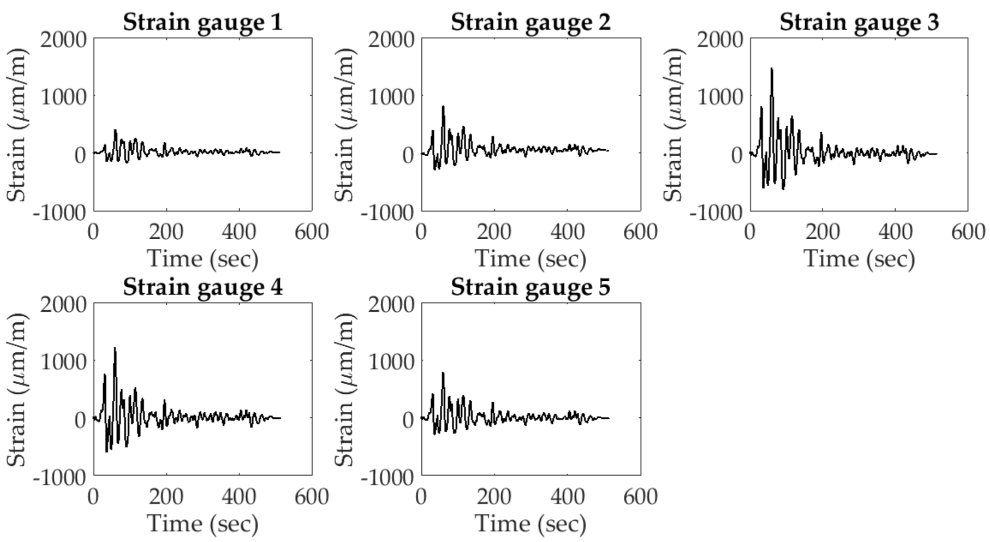

Figure D.1. Measured response history of specimen type A-1 at 0.5MCE intensity level

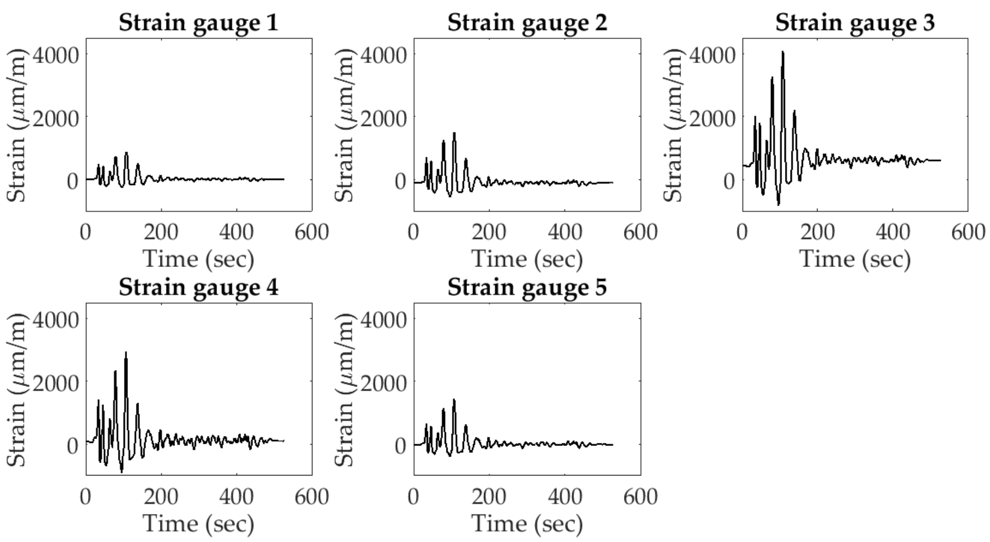

Figure D.2.. Measured response history of specimen type A-1 at 1MCE intensity level

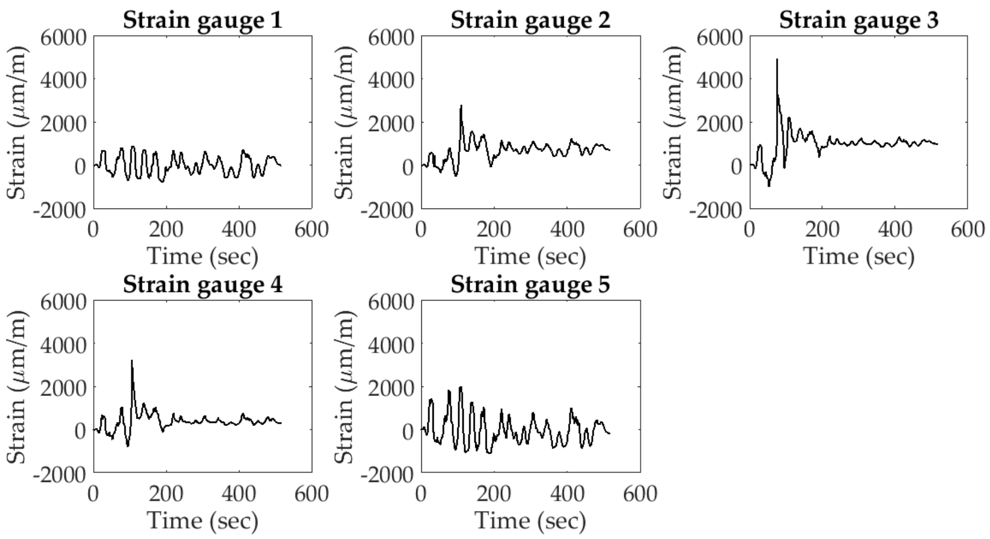

Figure D.3. Measured response history of specimen type A-1 at 2MCE intensity level

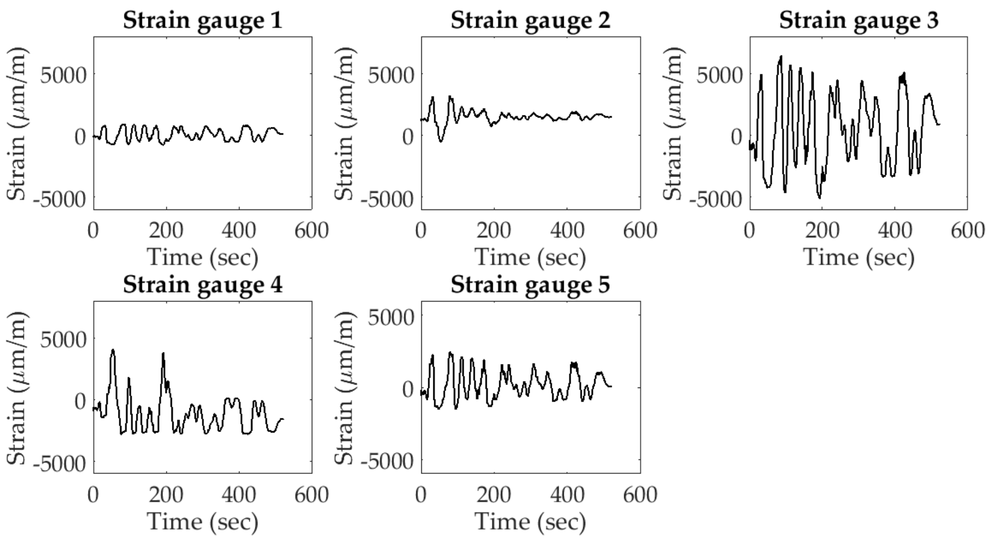

Figure D.4. Measured response history of specimen type A-1 at 3MCE intensity level

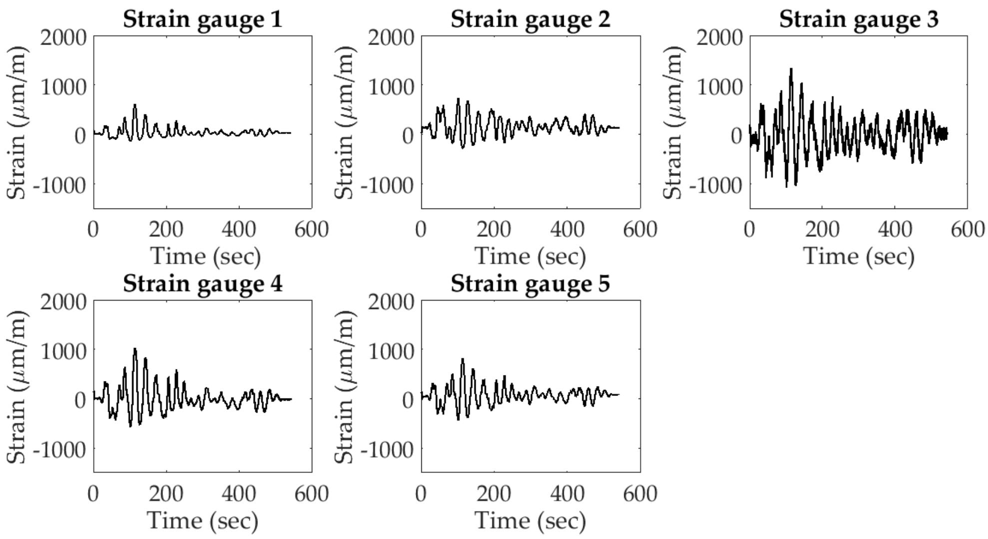

Figure D.5. Measured response history of specimen type B-1 at 0.5MCE intensity level

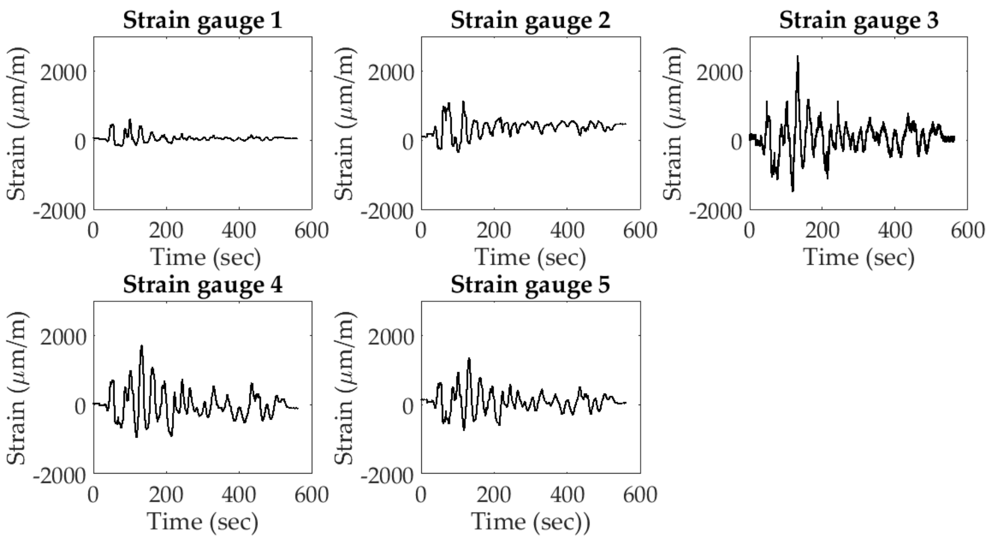

Figure D.6. Measured response history of specimen type B-1 at 1MCE intensity level

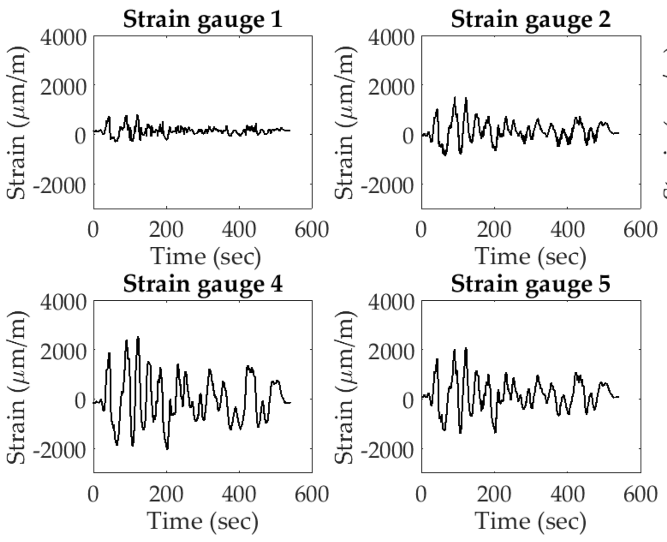

Figure D.7. Measured response history of specimen type B-1 at 2MCE intensity level

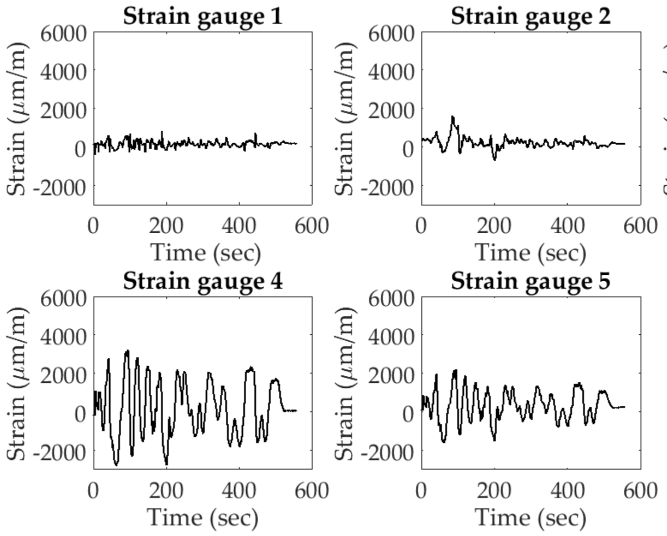

Figure D.8. Measured response history of specimen type B-1 at 3MCE intensity level

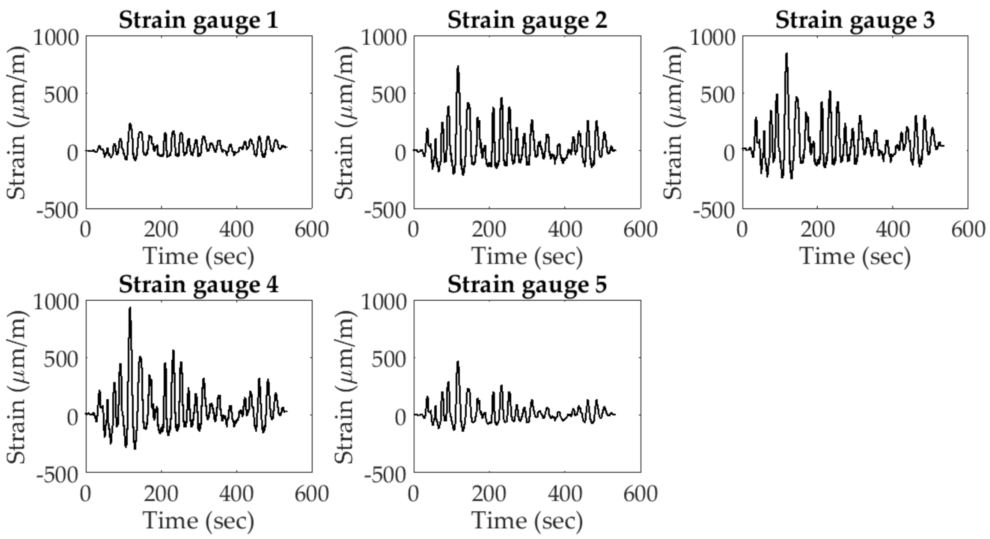

Figure D.9. Measured response history of specimen type A-2 at 0.5MCE intensity level

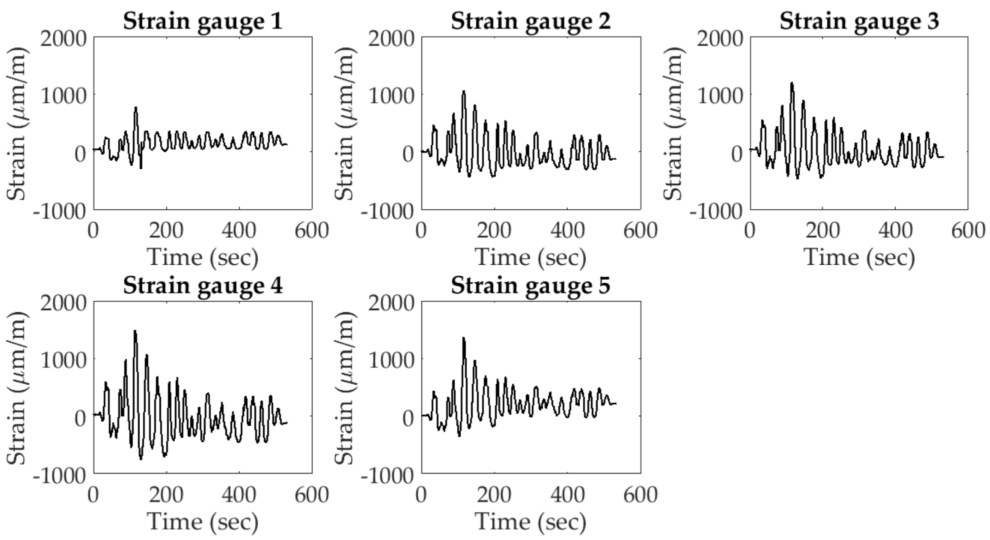

Figure D.10. Measured response history of specimen type A-2 at 1MCE intensity level

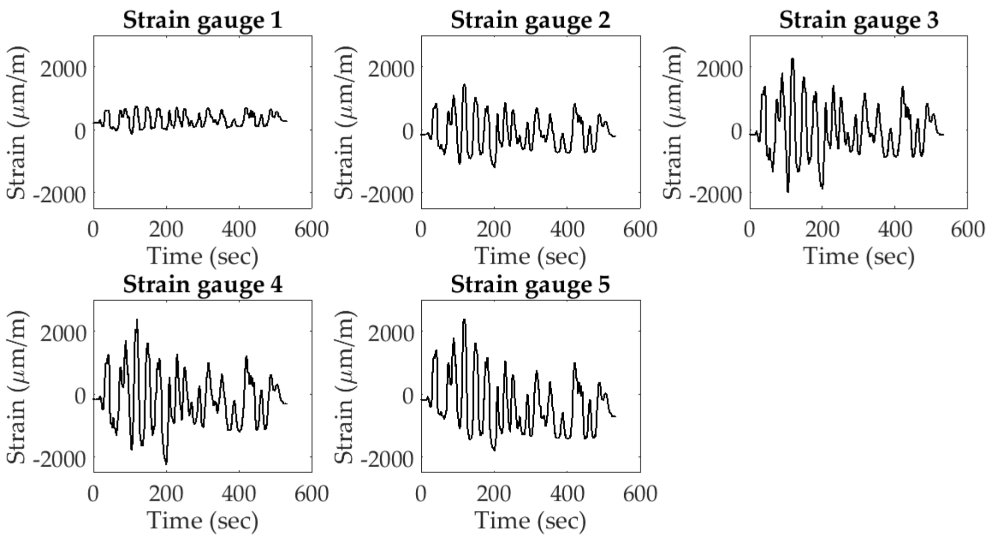

Figure D.11. Measured response history of specimen type A-2 at 2MCE intensity level

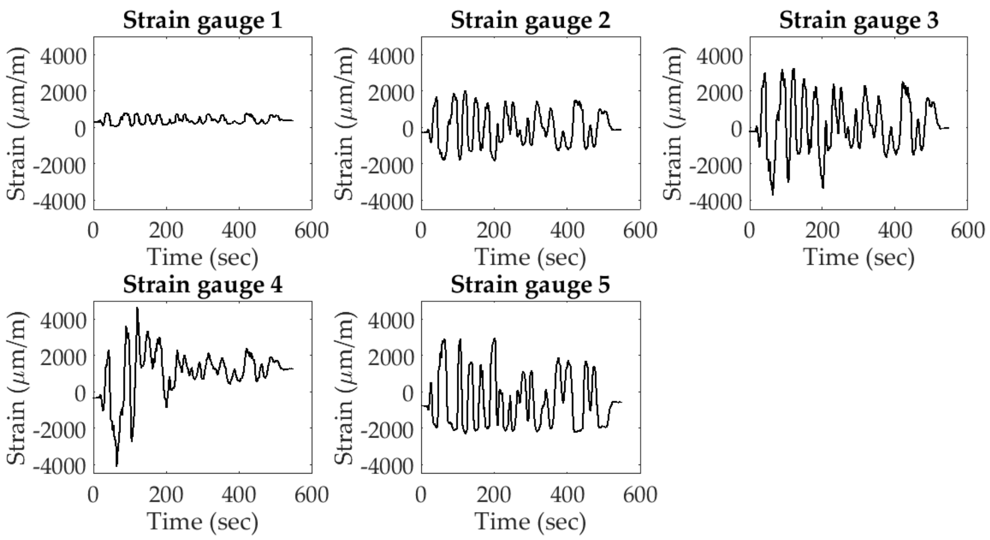

Figure D.12. Measured response history of specimen type A-2 at 3MCE intensity level

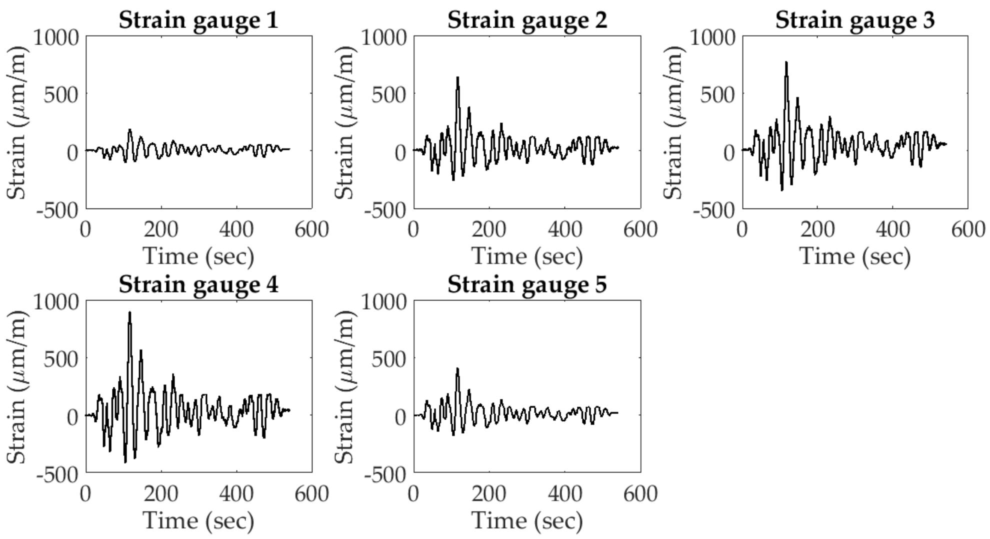

Figure D.13. Measured response history of specimen type B-2 at 0.5MCE intensity level

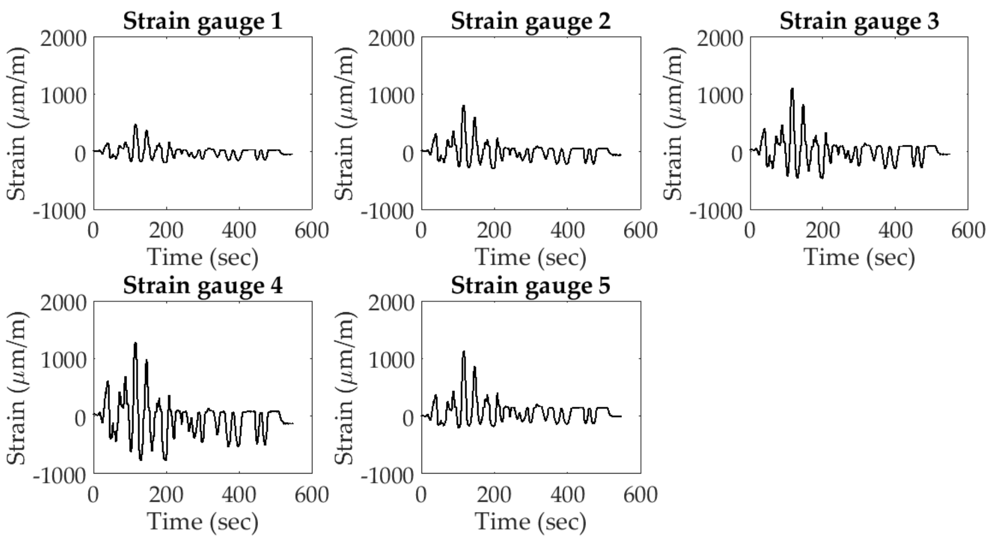

Figure D.14. Measured response history of specimen type B-2 at 1MCE intensity level

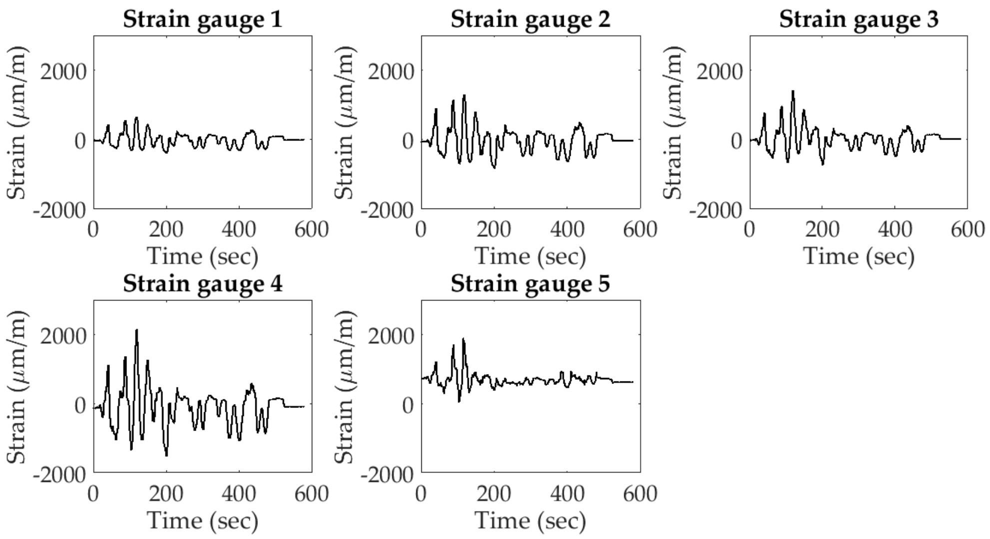

Figure D.15. Measured response history of specimen type B-2 at 2MCE intensity level

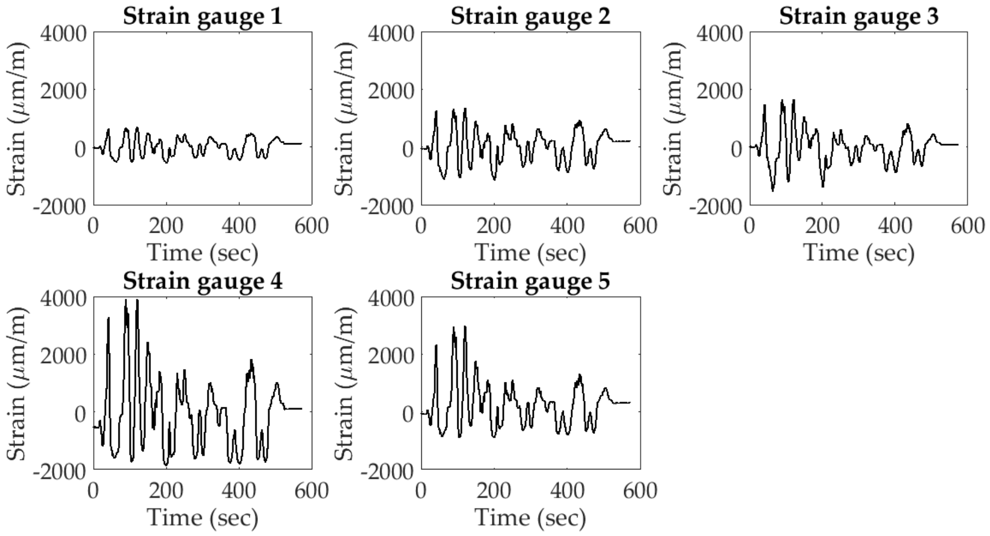

Figure D.16. Measured response history of specimen type B-2 at 3MCE intensity level

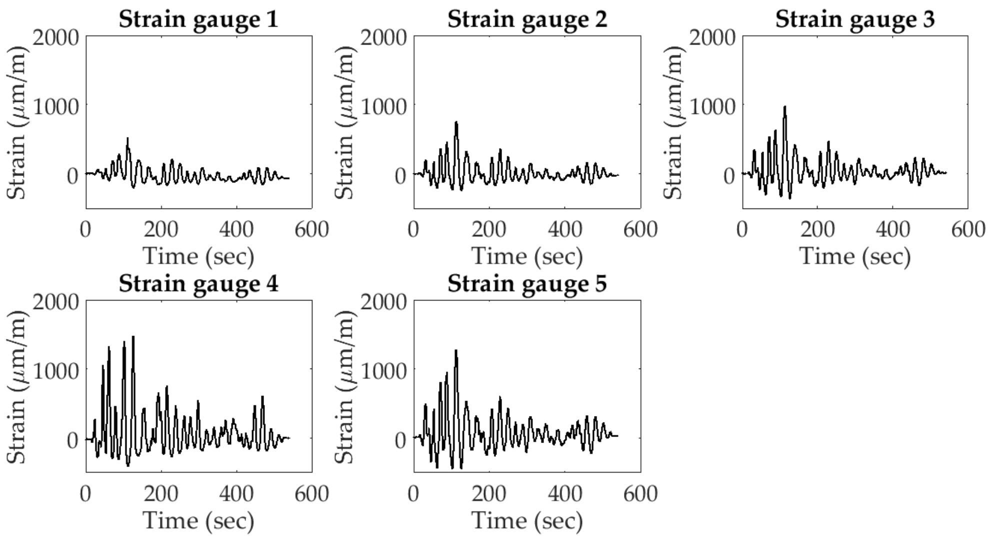

Figure D.17. Measured response history of specimen type A-3 at 0.5MCE intensity level

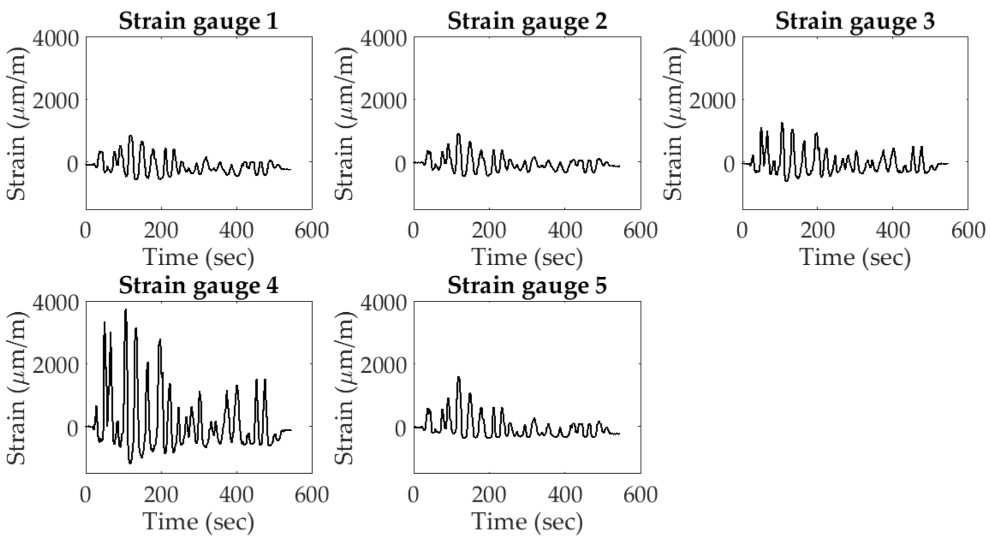

Figure D.18. Measured response history of specimen type A-3 at 1MCE intensity level

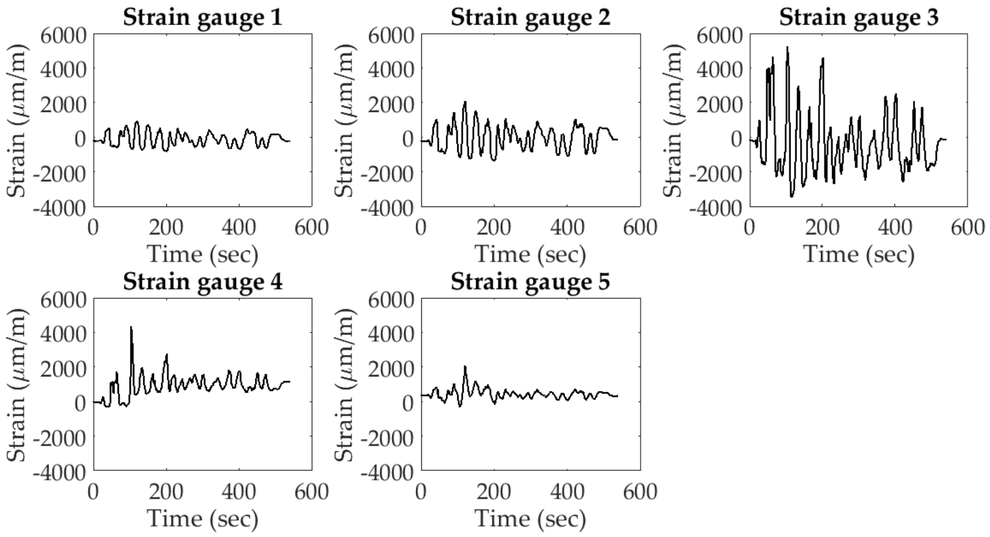

Figure D.19. Measured response history of specimen type A-3 at 2MCE intensity level

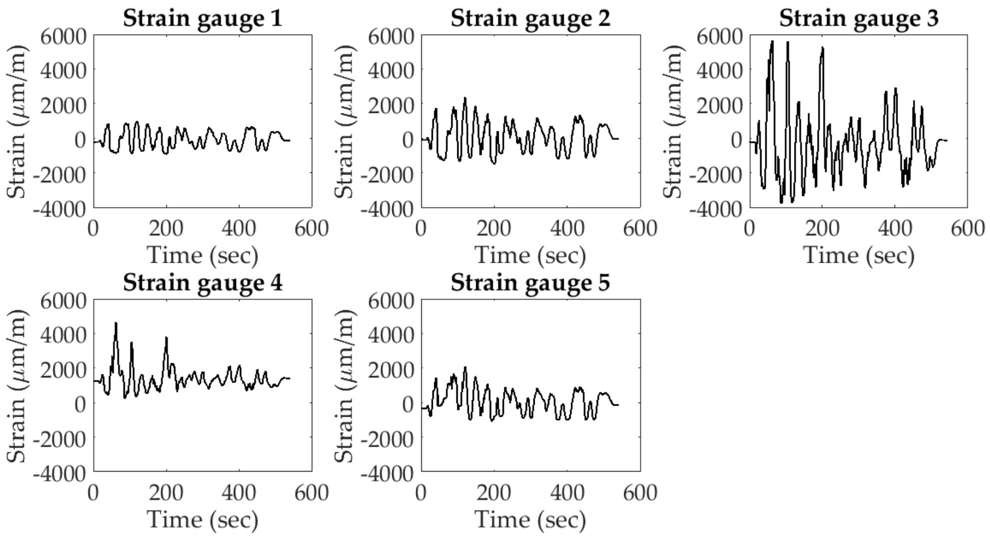

Figure D.20. Measured response history of specimen type A-3 at 3MCE intensity level

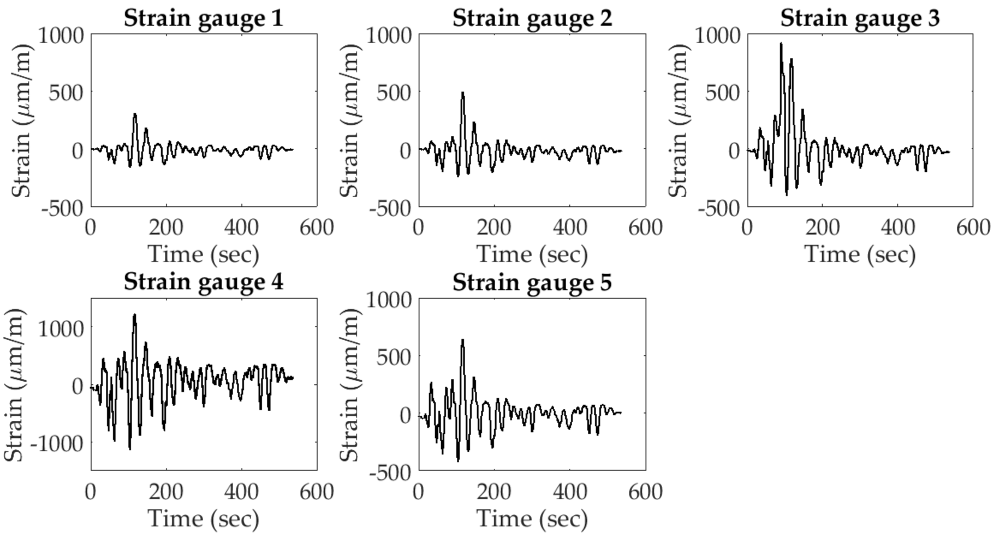

Figure D.21. Measured response history of specimen type B-3 at 0.5MCE intensity level

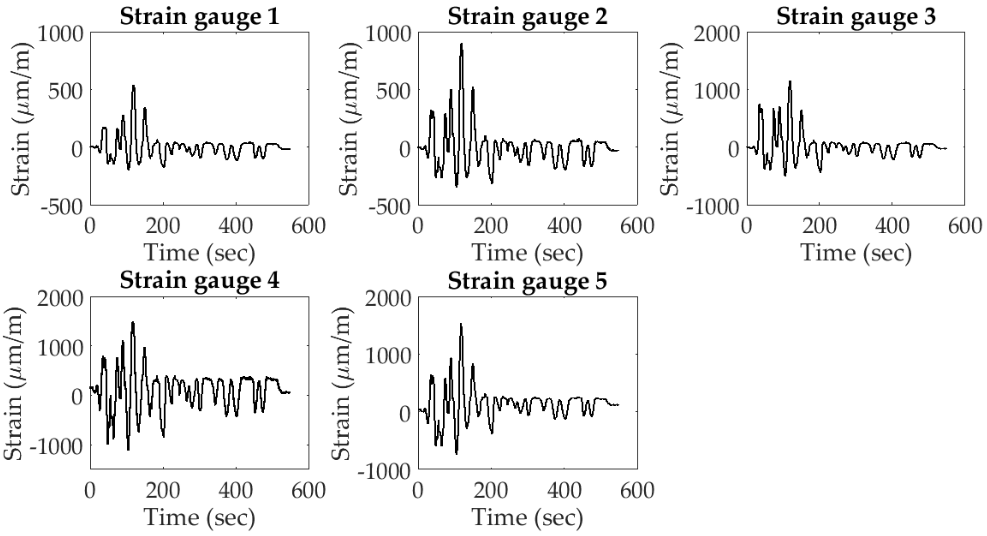

Figure D.22. Measured response history of specimen type B-3 at 1MCE intensity level

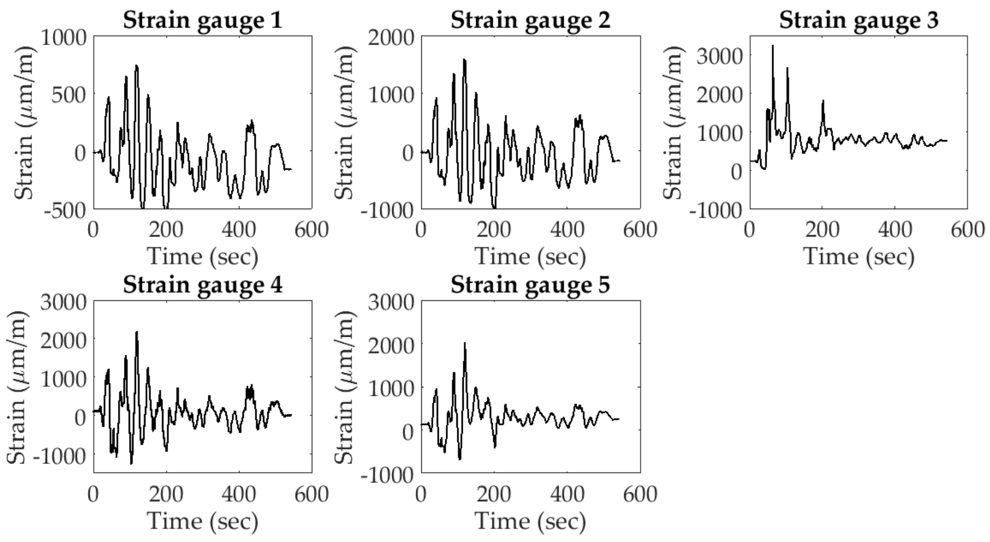

Figure D.23. Measured response history of specimen type B-3 at 2MCE intensity level

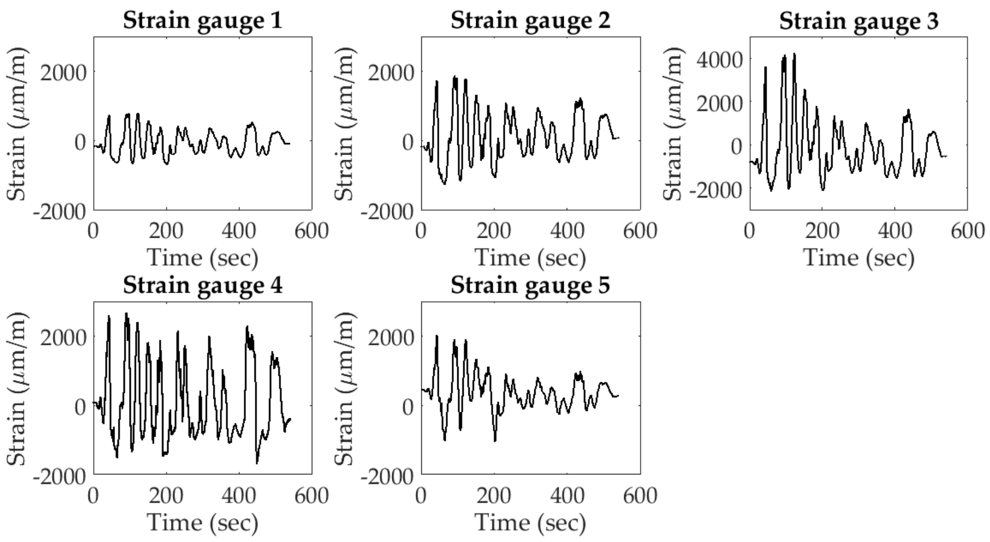

Figure D.24. Measured response history of specimen type B-3 at 3MCE intensity level

REFERENCES

Abdelnaby, A. E., Frankie, T. M., Elnashai, A. S., Spencer, B. F., Kuchma, D. A., Silva, P., & Chang, C. M. (2014). Numerical and hybrid analysis of a curved bridge and methods of numerical model calibration. *Engineering Structures*, *70*, 234-245.

ACI 318 (1989). *Building Code Requirements for Reinforced Concrete and Commentary*. ACI 318-89/ACI 318R-89) American Concrete Institute, Detroit, Michigan.

ACI 544.1R-96 (2002). *State-of-the-Art Report on Fiber Reinforced Concrete*. American Concrete Institute.

Alemdar, Z.F (2010). *Plastic Hinging Behavior of Reinforced Concrete Bridge Columns* (Ph.D. Dissertation). University of Kansas, KS 66045, US

American Society for Testing and Materials. (2011). *Standard Test Method for Flexural Performance of Fiber-Reinforced Concrete (Using Beam with Third-Point Loading).* American Society of Testing Materials, Standard Designation C1609.

ASCE 43 (2005). *Seismic design criteria for structural systems, and components in nuclear facilities*. ASCE/SEI 43-05 American Society of Civil Engineers, Reston, USA.

ASTM, C. “1018” (1989). *Standard Test Method for Flexural Toughness and First-Crack Strength of Fiber Reinforced Concrete (Using Beam with Third Point Loading).* American Society of Testing Materials, ASTM Standards for Concrete and Aggregates, Vol. 04.02, Standard Designation C1018, 499-505

ATC (1985). *Earthquake damage evaluation data for California*. Report No. ATC-13, Applied Technology Council, Redwood City, CA.

ATC (1991). *Seismic vulnerability and impact of disruption of lifelines in the Coterminous United States*. Report No. ATC-25, Applied Technology Council, Redwood City, CA.

Aviram, A., Stojadinovic, B., & Parra-Montesinos, G. J. (2014). High-performance fiber-reinforced concrete bridge columns under bidirectional cyclic loading. *ACI Structural Journal*, *111*(2), 303.

Banerjee, S., & Chi, C. (2013). State-dependent fragility curves of bridges based on vibration measurements. *Probabilistic Engineering Mechanics*, *33*, 116-125.

Banthia, N., & Gupta, R. (2004). Hybrid fiber reinforced concrete (HyFRC): fiber synergy in high strength matrices. *Materials and Structures*, *37*(10), 707-716.

Banthia, N., & Nandakumar, N. (2003). Crack growth resistance of hybrid fiber reinforced cement composites. *Cement and Concrete Composites*, *25*(1), 3-9.

Banthia, N., & Sappakittipakorn, M. (2007). Toughness enhancement in steel fiber reinforced concrete through fiber hybridization. *Cement and Concrete Research*, 37(9), 1366-1372.

Banthia, N., & Soleimani, S. M. (2005). Flexural response of hybrid fiber-reinforced cementitious composites. *Materials Journal*, *102*(6), 382-389.

Banthia, N., & Trottier, J.F. (1995). Test methods for flexural toughness characterization of fiber reinforced concrete: some concerns and a propositionShino. *ACI Materials Journal*, *92* (1), 48-57.

Basoz, N., & Kiremidjian, A. S. (1998). *Evaluation of bridge damage data from the Loma Prieta and Northridge, California earthquakes*. Multidisciplinary Center for Earthquake Engineering Research (MCEER), Report No. MCEER-98-0004.

Bentur, A., & Mindess, S. (2006). *Fibre reinforced cementitious composites*. CRC Press.

Bhuiyan, M. A., & Alam, M. S. (2012). Seismic vulnerability assessment of a multi-span continuous highway bridge fitted with shape memory alloy bars and laminated rubber bearings. *Earthquake Spectra*, *28*(4), 1379-1404.

Billah, A. M., Alam, M. S., & Bhuiyan, M. R. (2012). Fragility analysis of retrofitted multicolumn bridge bent subjected to near-fault and far-field ground motion. *Journal of Bridge Engineering*, *18*(10), 992-1004.

Bommer, J. J., & Acevedo, A. B. (2004). The use of real earthquake accelerograms as input to dynamic analysis. *Journal of Earthquake Engineering*, 8(spec01), 43-91.

Carrion, J. E. (2007). *Model-based strategies for real-time hybrid testing*. NSEL Report Series, Report No. NSEL-006, University of Illinois at Urbana-Champaign.

Chen, Y., Feng, M. Q., & Soyoz, S. (2008). Large-scale shake table test verification of bridge condition assessment methods. *Journal of Structural Engineering*, *134*(7), 1235-1245.

Choi, E., DesRoches, R., & Nielson, B. (2004). Seismic fragility of typical bridges in moderate seismic zones. *Engineering Structures*, *26*(2), 187-199.

Chopra, A.K. (2001). *Dynamics of Structures - Theory and Applications to Earthquake Engineering*, Prentice-hall, NewJersey 07458, US.

Chung, J., & Hulbert, G. M. (1993). A time integration algorithm for structural dynamics with improved numerical dissipation: the generalized-α method. *Journal of applied mechanics*, *60*(2), 371-375.

Cimellaro, G. P., Reinhorn, A. M., D'Ambrisi, A., & De Stefano, M. (2009). Fragility analysis and seismic record selection. *Journal of Structural Engineering*, *137*(3), 379-390.

Combescure, D., & Pegon, P. (1997). α - Operator Splitting time integration technique for pseudodynamic testing Error propagation analysis. *Soil Dynamics and Earthquake Engineering*, 16, 427-443

Cornell, C., & Jalayer, F. (2002). Probabilistic basis for 2000 SAC federal emergency management agency steel moment frame guidelines. *Journal of Structural Engineering*, 128(4), 526–533.

Cruz Noguez, C. A., & Saiidi, M. S. (2012). Performance of advanced materials during earthquake loading tests of a bridge system. *Journal of Structural Engineering*, 139(1), 144-154.

Dodd L.L. (1992). *The Dynamic Behavior of Reinforced Concrete Bridge Piers Subjected to New Zealand Seismicity* (Ph.D. Dissertation). The University of Canterbury, Christchurch, New Zealand.

Eswari, S., Raghunath, P. N., & Suguna, K. (2008). Ductility performance of hybrid fibre reinforced concrete. *American Journal of Applied Sciences*, *5*(9), 1257-1262.

Farsangi, E. N., Rezvani, F. H., Talebi, M., & Hashemi, S. A. H. (2014). Seismic risk analysis of steel-MRFs by means of fragility curves in high seismic zones. *Advances in Structural Engineering*, *17*(9), 1227-1240.

FEMA P695. (2009). *Quantification of Building Seismic Performance Factors*. Applied Technology Council, Redwood City, California for the Federal Emergency Management Agency, Washington, D.C.

Fischer, G., & Li, V. C. (2002). Effect of matrix ductility on deformation behavior of steel-reinforced ECC flexural members under reversed cyclic loading conditions. *ACI Structural Journal*, *99*(6), 781-790.

Frankie, T. M. (2013). *Impact of complex system behavior on seismic assessment of RC bridges.* (Ph.D. dissertation), University of Illinois at Urbana-Champaign.

Fukuyama, H., Matsuzaki, Y., Nakano, K., & Sato, Y. (1999). Structural performance of beam elements with PVA-ECC. In *Proceedings of High Performance Fiber Reinforced Cement Composites 3 (HPFRCC 3)*, 531-542.

Ganesan, N., Indira, P.V., & Sabeena, M.V. (2014). Behaviour of hybrid fibre reinforced concrete beam–column joints under reverse cyclic loads. *Materials and Design*, *54*, 686–693

Ghobarah, A., Aziz, T.S., & Biddah, A. (1996). Rehabilitation of reinforced concrete beam-column joints. *In Eleventh World Conference on Earthquake Engineering*, Acapulco, Mexico, Paper No. 1394, p. 8.

Griezic, A., Cook, W. D., & Mitchell, D. (1996). Seismic retrofit of bridge column-footing connections. In *Proc., 11th World Conf. on Earthquake Engineering (CD-ROM), Paper No. 508*, *1* (Vol. 8).

Hachem M. M., Mahin, S.A., & Moehle J.P. (2003). *Performance of Circular Reinforced Concrete Bridge Columns under Bidirectional Earthquake Loading*. Report No. PEER

2003/06, Pacific Earthquake Engineering Research Center, University of California, Berkeley.

Hughes, T. J., Pister, K. S., & Taylor, R. L. (1979). Implicit-explicit finite elements in nonlinear transient analysis. *Computer Methods in Applied Mechanics and Engineering*, *17*, 159-182.

Hung, C. C. (2010). *Computational and hybrid simulation of high performance fiber reinforced concrete coupled wall systems* (Ph.D. dissertation), University of Michigan, Michigan.

Hwang, H., Liu, J., & Chiu, Y. (2001). *Seismic fragility analysis of highway bridges*. Mid-America Earthquake Center Technical Report CD Release.

IS: 1893-Part 1. (2002). *Indian Standard Criteria for Earthquake Resistant Design of Structures: Part 1 General Provisions and Buildings*. Bureau of Indian Standards (BIS), New Delhi.

IS: 456 (2000). *Plain and Reinforced Concrete - Code of Practice*. Bureau of Indian Standards (BIS), New Delhi.

Jain, K., & Singh, B. (2014). Investigation of steel fibres as minimum shear reinforcement. *Proceedings of the Institution of Civil Engineers-Structures and Buildings*, *167*(5), 285-299.

Jiang, Z., & Banthia, N. (2010). Size effects in flexural toughness of fiber reinforced concrete. *Journal of Testing and Evaluation*, *38*(3), 332-338.

Johnson, N., Saiidi, M. S., & Sanders, D. (2009). Nonlinear earthquake response modeling of a large-scale two-span concrete bridge. *Journal of Bridge Engineering*, 14(6), 460-471.

JSCE (1984). *Method of tests for flexural strength and flexural toughness of steel fiber reinforced concrete*, JSCE Japan Society Civil Engineering, 3, 58-61.

Kappos, A. J., & Panagopoulos, G. (2010). Fragility curves for reinforced concrete buildings in Greece. *Structure and Infrastructure Engineering*, *6*(1-2), 39-53.

Kappos, A. J., Panagopoulos, G., Panagiotopoulos, C., & Penelis, G. (2006). A hybrid method for the vulnerability assessment of R/C and URM buildings. *Bulletin of Earthquake Engineering*, *4*(4), 391-413.

Kappos, A. J., Stylianidis, K. C., & Pitilakis, K. (1998). Development of seismic risk scenarios based on a hybrid method of vulnerability assessment. *Natural Hazards*, *17*(2), 177-192.

Kawashima, K., Zafra, R., Sasaki, T., Kajiwara, K., & Nakayama, M. (2011). Effect of polypropylene fiber reinforced cement composite and steel fiber reinforced concrete for enhancing the seismic performance of bridge columns. *Journal of Earthquake Engineering*, *15*(8), 1194-1211.

Kheni, D., Scott, R.H., Deb, S.K., & Dutta, A. (2015). Ductility enhancement in beam-column connection using hybrid fibre-reinforced concrete. *ACI Structural Journal*, *112* (2), 167-179.

Kim, S. J., Holub, C. J., & Elnashai, A. S. (2011). Experimental investigation of the behavior of RC bridge piers subjected to horizontal and vertical earthquake motion. *Engineering Structures*, *33*(7), 2221-2235.

Kumar, P., Jen, G., Trono, W., Lallemant, D., Panagiotou, M., & Ostertag, C. P. (2011). *Self-compacting hybrid fiber reinforced concrete composites for bridge columns*. Pacific Earthquake Engineering Research Center (PEER), Report No. 106.

Kwon, O. S., & Elnashai, A. (2006). The effect of material and ground motion uncertainty on the seismic vulnerability curves of RC structure. *Engineering Structures*, *28*(2), 289-303.

Lavorato, D. (2009). *Pseudo-dynamic tests on reinforced concrete bridge piers repaired and/or retrofitted by means of techniques based on innovative materials*. (Ph.D. dissertation), University of Roma Tre, Rome.

Li, V. C. (2003). On engineered cementitious composites (ECC). *Journal of advanced concrete technology*, *1*(3), 215-230.

Lin, S. L., Li, J., Elnashai, A. S., & Spencer, B. F. (2012). NEES integrated seismic risk assessment framework (NISRAF). *Soil Dynamics and Earthquake Engineering*, *42*, 219-228.

Mackie, K. R., & Stojadinović, B. (2005). *Fragility basis for California highway overpass bridge seismic decision making*. PEER Report No. 2005/02, Pacific Earthquake Engineering Research Center, University of California, Berkeley, CA.

Mandal, T. K., Ghosh, S., & Pujari, N. N. (2016). Seismic fragility analysis of a typical Indian PHWR containment: comparison of fragility models. *Structural Safety*, *58*, 11-19.

Mander, J.B., & Basoz, N. (1999). Seismic fragility curves theory for highway bridges. In *Proceedings of the 5th US Conference on Lifeline Earthquake Engineering*, Seattle, USA.

McKenna, F.T. (1997). *Object-Oriented finite element programming: Frameworks for analysis, algorithms and parallel computing*, (Ph.D. Dissertation). University of California, Berkeley.

Melchers, R. E. (2001). *Structural Reliability Analysis and Prediction*, 2nd Edition, John Wiley & Sons.

Mondo, E. (2011). *Shear Capacity of Steel Fibre Reinforced Concrete Beams without Conventional Shear Reinforcement* (Master Thesis). Royal Institute of Technology (KTH), Stockholm, Sweden.

Mukherjee, S., and Gupta, V.K. (2002). Wavelet-based generation of spectrum-compatible time-histories, Soil Dynamics and Earthquake Engineering 22, 9: 799–804.

Ni Choine, M. (2014). *Seismic reliability assessment of aging integral bridges* (Ph.D. Dissertation). Trinity College, Dublin.

Nielson, B. G. (2005). *Analytical fragility curves for highway bridges in moderate seismic zones* (Ph.D. Dissertation). Georgia Institute of Technology, Atlanta, GA.

Nielson, B. G., & DesRoches, R. (2007). Analytical seismic fragility curves for typical bridges in the central and southeastern United States. *Earthquake Spectra*, *23*(3), 615-633.

Okada, T., & Unjoh, S. (2008). Shake table tests for bridge model using structural response control devices. *In Proceedings of 14th World Conference on Earthquake Engineering*, Beijing, China.

Pan, Y., Agrawal, A. K., Ghosn, M., & Alampalli, S. (2009). Seismic fragility of multispan simply supported steel highway bridges in New York State. I: Bridge modeling, parametric analysis, and retrofit design. *Journal of Bridge Engineering*, *15*(5), 448-461.

Parool, N., & Rai, D. C. (2015). Seismic fragility of multispan simply supported bridge with drop spans and steel bearings. *Journal of Bridge Engineering, 20*(12), 04015021.

Parra-Montesinos, G. J. (2006). Shear strength of beams with deformed steel fibers. *Concrete International*, *28*(11), 57-66.

Paulay T., & Priestley M. J. N. (1992). *Seismic Design of Reinforced Concrete and Masonry Structures*. John Wiley & Sons.

Penelis, G. G., Sarigiannis, D., Stavrakakis, E., & Stylianidis, K. C. (1988). A statistical evaluation of damage to buildings in the Thessaloniki, Greece, earthquake of June, 20, 1978. In *9th World Conference on Earthquake Engineering, Kyoto-Tokyo* (Vol. 7, pp. 187-192).

Pinto, A. V., Pegon, P., Magonette, G., & Tsionis, G. (2004). Pseudo-dynamic testing of bridges using non-linear substructuring. *Earthquake Engineering & Structural Dynamics*, *33*(11), 1125-1146.

Priestley, M. J. N., Seible, F., & MacRae, G. (1995). *The Kobe Earthquake of January 17, 1995: Initial Impressions from a Quick Reconnaissance*. University of California, San Diego, Structural Systems Research Project, Report No. SSRP-95/03, University of California, San Diego.

Qian, C. X., & Stroeven, P. (2000a). Development of hybrid polypropylene-steel fibre-reinforced concrete. *Cement and Concrete Research*, *30*(1), 63-69.

Qian, C., & Stroeven, P. (2000b). Fracture properties of concrete reinforced with steel–polypropylene hybrid fibres. *Cement and Concrete Composites*, *22*(5), 343-351.

Ramanathan, K., DesRoches, R., & Padgett, J. (2010). Analytical fragility curves for multispan continuous steel girder bridges in moderate seismic zones. *Transportation Research Record: Journal of the Transportation Research Board*, (2202), 173-182.

Saiidi, M. S., Vosooghi, A., & Nelson, R. B. (2012). Shake-table studies of a four-span reinforced concrete bridge. *Journal of Structural Engineering*, 139(8), 1352-1361.

Saiidi, M. S., Vosooghi, A., Choi, H., & Somerville, P. (2013). Shake table studies and analysis of a two-span RC bridge model subjected to a fault rupture. Journal of Bridge Engineering, 19(8), A4014003.

Saiidi, M., Cruz, C., & Hillis, D. (2010). Multi-shake table seismic studies of a 33-meter railway concrete bridge with high-performance materials. *International Journal of Civil Engineering*, 8(1), 13-18.

Sasaki, T., Zafra, R., & Kawashima, K. (2012). Effect of polypropylene fiber reinforced concrete for enhancing the seismic performance of bridge columns. In *Proceedings of 15th World Conference on Earthquake Engineering,* Paper No. 2064, Lisboa.

Schellenberg, A., & Mahin, S. (2006a). Integration of hybrid simulation within the general-purpose computational framework OpenSees. In *Eighth US National Conference on Earthquake Engineering*.

Schellenberg, A., & Mahin, S. (2006b). Application of an experimental software framework to hybrid simulation of structures through collapse. In *1st European Conference on Earthquake Engineering and Seismology*.

Schellenberg, A., Yang, T. Y., Mahin, S. A., & Stojadinovic, B. (2008, October). Hybrid simulation of structural collapse. In *Proceedings of the 14th World Conference on Earthquake Engineering,* Beijing, China.

Schellenberg, A.H., Mahin, S.A., & Fenves, G.L. (2009). *Advanced Implementation of Hybrid Simulation*. PEER Report, no. 104.

Shannag, M. J., & Alhassan, M. A. (2005). Seismic upgrade of interior beam-column subassemblages with high-performance fiber-reinforced concrete jackets. *ACI Structural Journal*, *102*(1), 131.

Shinozuka, M., Feng, M. Q., Kim, H. K., & Kim, S. H. (2000a). Nonlinear static procedure for fragility curve development. *Journal of Engineering Mechanics*, *126*(12), 1287-1295.

Shinozuka, M., Feng, M. Q., Kim, H., Uzawa, T. & Ueda, T. (2000b). *Statistical analysis of fragility curves*. Technical Report MCEER.

Shome, N. (1999). *Probabilistic seismic demand analysis of nonlinear structures*. (PhD Thesis) Stanford University, USA.

Sivakumar, A. & Santhanam, M. (2007). Mechanical properties of high strength concrete reinforced with metallic and non-metallic fibres. *Cement & Concrete Composites 29*(8), 603–608

Skazlić, M. (2010). Development and application of hybrid fibre reinforced concrete. In *Second International Conference on Sustainable Construction Materials and Technologies*.

Soleimani, S. M. (2005). *Flexural response of hybrid fiber reinforced cementitious composites* (Master Thesis). The University of British Columbia, Vancouver.

Sun, W., Chen, H., Luo, X., & Qian, H. (2001). The effect of hybrid fibers and expansive agent on the shrinkage and permeability of high-performance concrete. *Cement and Concrete Research*, *31*(4), 595-601.

Susetyo, J., Gauvreau, P., & Vecchio, F. J. (2011). Effectiveness of steel fiber as minimum shear reinforcement. *ACI Structural Journal*, *108*(4), 488.

Takanashi, K., (1975). Non-linear earthquake response analysis of structures by a computer-actuator online system-Part 1: Detail of the system. *Transactions of the Architectural Institute of Japan* (229): 77-83.

Tsai, M. H., Wu, S. Y., Chang, K. C., & Lee, G. C. (2007). Shaking table tests of a scaled bridge model with rolling-type seismic isolation bearings. *Engineering structures*, *29*(5), 694-702.

Vamvatsikos, D., & Cornell, C. A. (2002). Incremental dynamic analysis. *Earthquake Engineering & Structural Dynamics*, *31*(3), 491–514.

Vosooghi, A., & Saiidi, M. S. (2012). Experimental fragility curves for seismic response of reinforced concrete bridge columns. *ACI Structural Journal*, *109*(6), 825.

Walton, P. L., & Majumdar, A. J. (1975). Cement-based composites with mixtures of different types of fibres. *Composites*, *6*(5), 209-216.

Whyte, C., Scacchioli, A., Bayen, A. & Stojadinovic, B. (2008). Assessment of quality of hybrid simulation using reachability analysis. In *Proceedings of the 14th World Conference on Earthquake Engineering*, Beijing, China.

Yamazaki, F., Motomura, H., & Hamada, T. (2000). Damage assessment of expressway networks in Japan based on seismic monitoring. In *Proceedings of the 12th world Conference on Earthquake Engineering*. Auckland, New Zealand.

Yang, T. Y., Mosqueda, G., & Stojadinovic, B. (2008). Evaluating the quality of hybrid simulation test using an energy-based approach. In *Proceedings of the 14th World Conference on Earthquake Engineering*, Beijing, China.

Yang, Y. S., Tsai, K. C., Elnashai, A. S., & Hsieh, T. J. (2012). An online optimization method for bridge dynamic hybrid simulations. *Simulation Modelling Practice and Theory*, *28*, 42-54.

Zhang, J., & Huo, Y. (2008). Optimum isolation design for highway bridges using fragility function method. In *Proceedings of 14th World Conference on Earthquake Engineering*. Beijing, China.

Zhang, J., & Huo, Y. (2009). Evaluating effectiveness and optimum design of isolation devices for highway bridges using the fragility function method. *Engineering Structures*, *31*(8), 1648-1660.

Zhang, Y., Fan, J., & Fan, W. (2016). Seismic fragility analysis of concrete bridge piers reinforced by steel fibers. *Advances in Structural Engineering*, *19*(5), 837-848.

This page is intentionally left blank

List of Publications

Journals

- Kotoky, N., Deb, S.K. & Dutta, A. "Experimental studies on HyFRC bridge piers with different detailings at pier-foundation interface", under review in Journal of Bridge Engineering, ASCE
- Kotoky, N., Dutta, A. & Deb, S.K. "Seismic performance evaluation of HyFRC piers by hybrid simulation", under review in Composite Structures
- Kotoky, N., Dutta, A. & Deb, S.K. "Comparative study on seismic vulnerablity of highway bridge with RC and HyFRC piers", under review in Bulletin of Earthquake Engineering
- Singh, T., Kotoky, N., Unnikrishnan, B.M. & Dutta, A. "Flexural crack simulation in Hybrid fibre reinforced concrete specimen", Computer and Structures, to be communicated

Conferences

- Kotoky, N., Dutta, A. & Deb, S.K. "Hybrid Simulation of Structural System", Proceedings of 15th Symposium on Earthquake Engineering, IIT Roorkee, India, Paper no. A131, pp. 827-835, 2014
- Kotoky, N., Dutta, A. & Deb, S.K. "Hybrid testing of concrete bridge piers with different detailing at column-foundation interface", Proceedings of 10th Structural Engineering Convention, CSIR-SERC Chennai, 2016
- Kotoky, N., Dutta, A. & Deb, S.K. "Enhancement of seismic performance of structures using HyFRC", Proceedings of Thirty-third National Convention of Civil Engineers on Recent Advances in Structural Engineering, Institute of Engineers, Ahmedabad, 2017.